Simulation of the Construction Process of Roller Compacted Concrete Dams. II: Stress and Damage

Miguel Cervera,* Javier Oliver† and Tomás Prato‡

ABSTRACT

In this work a numerical procedure for the simulation of the construction process of Roller Compacted Concrete (RCC) dams is described. The basis of the work is a coupled thermo-chemo-mechanical model for the behaviour of concrete at early ages that allows to simulate the observed phenomena of hydration, aging, creep and damage. In this second part the formulation and assessment of the mechanical aspects of the model are presented. Long term effects are included by incorporating a creep model inspired in the Microprestress-Solidification Theory, which naturally accounts for the aging effects. Tensile damage is also considered, via a damage model formulated in a normalized format, so that the phenomenon of aging is included. This allows to obtain the stress field inside the dam at any time during the construction and the following years, in order to assess the risk of occurrence of tensile damage. Results from a real case study are compared to alternative studies considering different construction schedules.

*Asst. Prof. Struc. Anal., ETS Ingenieros de Caminos, 08034 Barcelona, Spain.
†Prof. Cont. Mech., ETS Ingenieros de Caminos, 08034 Barcelona, Spain.
‡Grad. Res. Asst., ETS Ingenieros de Caminos, 08034 Barcelona, Spain.

INTRODUCTION AND MOTIVATION

The basic design requirement for concrete dams in to ensure their integrity, watertighness and durability. Therefore, any new procedure for dam construction must contemplate and adopt measures against the risk of cracking, and particularly, against thermally induced cracking. This is also the case for RCC dams, where to achieve the high production rates that make them economically profitable, longitudinal joints are totally avoided, pipe cooling is not suitable, and even transverse joints must be reduced to the minimum. Because of this, the technological specifications for massive concrete dams differ from those used for slim structures in one essential point: heat generation and the resulting thermal stresses are decisive, rather than attaining a high initial strength.

One of the main features of RCC is that its low cement content makes its hydration heat be considerably low, down to three times smaller than for conventional concretes. Nevertheless, the high concreting rate used in RCC dams may lead to significant temperature rises (see Part I). This increase in temperature occurs during the first days after placing, when the stiffness of concrete is still quite low and creep (viscous) effects are significant; therefore, it usually leads to moderate, and mainly compressive, stresses. This means that, in general, the temperature distribution at the moment of completion of the dam may be considered as virtually free from thermally induced tensile stresses.

However, months later, when the hydration process has finished, no more hydration heat is produced and the stiffness has significantly increased, the concrete starts to cool down. The temperature in the body of the dam drops from the (almost) maximum values attained at the completion of the construction process, to a finally stable distribution that will consist of seasonal oscillations around the mean annual temperature.

The drop in the temperature at a point is inevitably accompanied by a volume reduction. If this volume change is restricted by the surrounding concrete or the foundation rock, thermally induced stresses will develop and may lead to cracking. Therefore, the cause of thermal stresses and cracking is not the temperature change in itself, but the spatial restriction for free thermal shrinkage.

The main causes for volume change restriction are:

(a) the non uniform temperature distribution due to the evolutionary construction process,

(b) thermal gradients near the faces of the dam due to convection phenomena with the enviroment,

(c) external geometrical and thermal restraints such as the foundation rock.

(d) design geometrical aspects such as the distance between transverse joints, and

Therefore, the investigation of the risk of cracking due to thermal variation must distinguish two main different patterns:

(a) Cracking in the interior of the dam body due to the cooling process from the non uniform distribution of maximum temperatures down to

the mean annual temperature. This cooling process may take several years after the completion of the dam;

(b) Cracking near the surface as a consequence of the thermal gradient in concrete. This gradient increases, for instance, with the fast cooling of the ambient temperature. This process may become the critical problem during the first weeks after concreting.

Internal cracks due to the long term cooling process must be carefully considered during the design and construction process. For RCC dams the qualitative and quantitative assessment of the influence of major factors such as the composition of the mix, the ambient temperature, the placing temperature, placing speed (lift thickness and placement interval) and time for starting placement must be established.

On the other hand, surface cracks are difficult to avoid without the use of, for instance, heat-insulating formwork. They are usually only several milimeters deep, but they have an influence on the watertightness and durability of the concrete surface and specific measures against water penetration, such as the inclusion of PVC membranes, have to be considered. Moreover, they may progress later into deeper temperature cracks due to long term temperature drop, affecting the stability of the dam, and they should be prevented.

This paper presents a numerical procedure for the simulation of the construction process of Roller Compacted Concrete (RCC) dams.

Firstly, a mechanical model is proposed to predict the evolution of the thermally induced stresses in concrete at early ages. The reference model is based on the theory of Continuum Damage Mechanics and it incorporates two separate scalar internal variables to represent damage both under tension and compression conditions. The damage model is reformulated in a suitable normalized format so that it can incorporate the phenomenon of aging. Long term mechanical behaviour is considered by incorporating a creep model inspired in the recently proposed Microprestress-Solidification Theory.

Secondly, the case study of Urugua-í RCC Dam in Argentina is discussed. The dam is a straight RCC gravity structure, 76 m high and 676 m long. Crest elevation is 203 m. The actual conditions and concreting schedule that ocurred during the construction of the dam between January 1988 and March 1989 are considered as the reference case. The stress analysis during the construction and the first eleven years of service life of the dam is carried out. Results concerning the short term, long term and stable regime are shown to assess the safety of the design and the risk of tensile cracking.

Thirdly, alternative studies considering different construction schedules are performed to their effect on the safety assessment of the dam. An interruption of the construction process during the winter months due, for instance, to inadequate weather conditions or flooding of the construction site, is considered. Also, a slower placing speed taking two years instead of one to complete the dam is also discussed. It is concluded that any of these two eventualities would increase the risk of tensile cracking, and full section transverse contraction joints should be provided to ensure the same level of safety as for the reference case.

NUMERICAL MODEL

The mechanical model used in this work is described in detail in Cervera et al. (1999), and it will only be sketched here. The assessment of the model and numerical simulations of available experiments regarding the mechanical behaviour of concrete at early ages can also be found in that reference.

Microprestress-Solidification Theory

Figure 1 shows a schematic representation of the viscoelastic rheological model used to represent the long term mechanical behaviour of concrete; it consists of a Maxwell chain model that can be described in terms of the elastic moduli, E^i, and the dashpot viscosities, η^i, of the $i = 1, ..., N$ Maxwell elements of the chain. It is also helpful to consider the elastic moduli, E^i, and the relaxation times of the dashpots, defined as $\tau^i = \eta^i / E^i$, as an alternative characterization of the chain. It is convenient to take $\tau^1 = \infty$ in the series expansion, so that E^1 can be considered as the *asymptotic* elastic modulus of concrete.

In the framework of aging models the general case of such a rheological model would consist of independently varying elastic moduli and dashpot viscosities. However, it is usual to restrict the model to the consideration of proportional varying elastic moduli and constant relaxation times [Carol and Bazant 1993]. In the following we will assume that during the aging process all the elastic moduli vary proportionally to the aging function defined by the aging model (see Part I), $E^i(\kappa) = \lambda_E(\kappa)\, E^i_\infty$ (where κ is the aging degree, E^i_∞ are values at the end of the hydration process, and $E_\infty = \sum_{i=1}^N E^i_\infty$), and that the relaxation times, τ^i, remain constant. It was shown in Carol and Bazant (1993) that this is equivalent to the model arising from Solidification Theory [Bazant and Prasannan 1989] with a non-aging Maxwell chain for the basic constituent. The total stress sustained by the Maxwell chain is easily computed as

$$\sigma = \sum_{i=1}^{N} \sigma^i \tag{1}$$

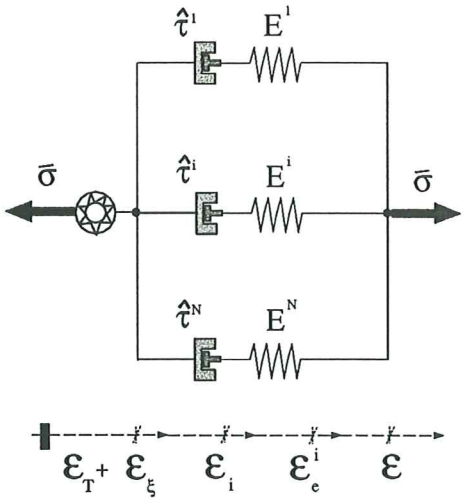

Figure 1: Rheological model for long term behaviour.

Choosing the stress in each Maxwell element of the chain, $\boldsymbol{\sigma}^i$, as internal variables, it was shown there that the first order differential equations governing the evolution of these variables are

$$\dot{\boldsymbol{\sigma}}^i + \frac{\boldsymbol{\sigma}^i}{\tau^i} = \lambda_E(\kappa) E^i_\infty \, \overline{\boldsymbol{D}} \, \dot{\boldsymbol{\varepsilon}} \quad \text{for} \quad i = 1, ..., N \tag{2}$$

where tensor entities are used as the multidimensional counterparts of the scalar ones used for uniaxial models; $\boldsymbol{\varepsilon}$ is the total strain tensor and the non-dimensional tensor $\overline{\boldsymbol{D}} = (1/E)\boldsymbol{D}$ has been used, being $\boldsymbol{D}$ the usual linear–elastic constitutive tensor.

The proposed model (and the underlying Solidification Theory) cannot be the final solution of the long term aging because the duration of creep for a fixed load decreases significantly with an increasing age at loading even after many years, while the hydration degree essentially stops before one year of age. In Bazant et al. (1997) a physical model is formulated to obtain the viscosity of the flow dashpot as a function of the tensile micro-prestress carried by the bonds and bridges crossing the gel pores in the hardened cement gel. The long term creep is assumed to originate from viscous shear slips between the opposite walls of micropores in which the bonds that transmit the micro-prestress break and reform. Let us define μ as a variable that can be regarded as the normalized value of the micro-prestress. If humidity effects are not considered the evolution of this normalized micro-prestress can be defined as

$$\mu(t) = \frac{1}{1 + c_{\mu 0} \, t} \tag{3}$$

Let us *define* the relaxation time of the flow term as

$$\tau_\mu = \frac{\tau_{\mu 0}}{\lambda_E(\kappa) \, \mu(t)} \tag{4}$$

where $\tau_{\mu 0}$ is a material property. Note that as time increases, the micro-prestress decreases, and so the viscosity of the flow term increases. Eventually, the micro-prestress will vanish, the viscosity will tend to infinity and the flow term will become inactive.

Now, Eq. (2) has to be modified to include the effect of the nonlinear flow term:

$$\dot{\boldsymbol{\sigma}}^i + \Big(\frac{1}{\tau^i} + \frac{1}{\tau_\mu}\Big) \boldsymbol{\sigma}^i = E^i(\kappa) \, \overline{\boldsymbol{D}} \, \dot{\boldsymbol{\varepsilon}} \quad \text{for} \quad i = 1, ..., N \tag{5}$$

Alternatively, the viscous strain in each Maxwell element, $\boldsymbol{\varepsilon^i}$, rather than the stress, $\boldsymbol{\sigma^i}$, can be selected as internal variables. The relationship between them is

$$\boldsymbol{\sigma}^i = E^i(\kappa) \, \overline{\boldsymbol{D}} : (\boldsymbol{\varepsilon} - \boldsymbol{\varepsilon}^i) \tag{6}$$

Substitution of Eq. (6) into Eq. (5) leads to the obtention of the evolution law for the viscous strains in the form

$$\dot{\boldsymbol{\varepsilon}}^i = \Big(\frac{1}{\tau^i} + \frac{1}{\tau_\mu} + \frac{1}{\tau_a}\Big)(\boldsymbol{\varepsilon} - \boldsymbol{\varepsilon}^i) = \frac{1}{\hat{\tau}^i}(\boldsymbol{\varepsilon} - \boldsymbol{\varepsilon}^i) \qquad \text{for} \quad i = 1, ..., N \tag{7}$$

with $\tau_a(\kappa) = \lambda_E / \dot{\lambda}_E$ representing the aging effect on the elastic modulus. Details on the numerical integration of Eq. (7) are given in Cervera and al.

(1992) and Galindo (1993). Note that even if τ^i and τ_μ are sufficiently large, there would be some viscous straining as long as the aging progresses and the elastic modulus varies ($\dot{\lambda}_E \neq 0$). As time increases, the rate of hydration decreases, and so the viscosity due to aging increases. Eventually, $\tau_a(t = \infty) = \infty$ and the model would revert to a standard Maxwell viscoelastic arrangement.

Aging Viscoelasticity and Damage

Finally, let us consider the coupling of the viscoelastic model described above with the aging damage model described in Cervera et al (1999), as well as including the relevant thermal and chemical couplings.

The basic hypothesis is that the stress sustained by the Maxwell chain is the effective (undamaged) stress, rather than the total stress. This idea is based on the concept that it is the effective stress the one acting on the effective (undamaged) solid concrete, while the total stress acts on the whole (damaged) solid.

Let us begin by defining the effective stresses and the elastic strains for one element of the Maxwell chain as:

$$\overline{\boldsymbol{\sigma}}^i \left(\boldsymbol{\varepsilon}_e^i, \kappa \right) = E^i(\kappa)\, \overline{\boldsymbol{D}} : \boldsymbol{\varepsilon}_e^i \tag{8}$$

with

$$\boldsymbol{\varepsilon}_e^i(\boldsymbol{\varepsilon}, \boldsymbol{\varepsilon}^i, T, \xi) = \boldsymbol{\varepsilon} - \boldsymbol{\varepsilon}_T - \boldsymbol{\varepsilon}_\xi - \boldsymbol{\varepsilon}^i \tag{9}$$

where T is the temperature and ξ is the hydration degree. Note that the thermal, $\boldsymbol{\varepsilon}_T = \alpha_T \left(T - T_{ref}\right) \mathbf{1}$, and chemical, $\boldsymbol{\varepsilon}_\xi = \alpha_\xi \xi \mathbf{1}$, volumetric strains affect all the elements in the same way, but the viscous strain tensor, $\boldsymbol{\varepsilon}^i$, is different for each Maxwell element. The reference temperature T_{ref} can be taken as equal to the temperature reached at the end of the setting phase (when the hydration degree reaches the percolation threshold, $\xi = \xi_{set}$), so that the thermal stressing initiates then.

Let us also define the stress split for each element, as

$$\overline{\boldsymbol{\sigma}}^{i+} = \sum_{j=1}^{3} < \overline{\sigma}_j^i > \boldsymbol{p}_j^i \otimes \boldsymbol{p}_j^i \qquad \text{and} \qquad \overline{\boldsymbol{\sigma}}^{i-} = \overline{\boldsymbol{\sigma}}^i - \overline{\boldsymbol{\sigma}}^{i+} \tag{10}$$

where $\overline{\sigma}_j^i$ denotes the j–th principal stress value from tensor $\overline{\boldsymbol{\sigma}}^i$, $\boldsymbol{p}_j^i$ represents the unit vector associated with its respective principal direction and the symbol $\otimes$ denotes the tensorial product. The symbols $< \, . \, >$ are the Macaulay brackets.

The total stress sustained by the Maxwell chain is obtained in the form:

$$\begin{aligned} \boldsymbol{\sigma} &= (1 - d^+) \sum_{i=1}^{N} \overline{\boldsymbol{\sigma}}^{i+} + (1 - d^-) \sum_{i=1}^{N} \overline{\boldsymbol{\sigma}}^{i-} \\ &= (1 - d^+)\, \overline{\boldsymbol{\sigma}}^+ + (1 - d^-)\, \overline{\boldsymbol{\sigma}}^- \end{aligned} \tag{11}$$

where the damage indices under tension and compression, d^+ and d^- respectively, have been introduced. These indices are monotonically increasing functions of the corresponding tensile and compressive effective stresses such that they vary in the range $0 \leq d^+(\overline{\boldsymbol{\sigma}}^+)\,, d^-(\overline{\boldsymbol{\sigma}}^-) \leq 1$.

The detailed description of the procedures followed for the characterization and evolution of the damage indices is given in Cervera et al. (1999).

URUGUA-Í DAM

The Urugua-í Hydroelectric Project is located in the Province of Misiones, North East of Argentina. The main dam is a straight RCC gravity structure, 76 m high and 676 m long. Maximum width at the base is 57 m. Crest elevation is 203 m. Details about the design and location of the joints are given in Part I and in Giobambattista (1995), Buchas and Buchas (1991) and Lorenzo and Calivari (1991).

Four different types of concrete were used in the dam:

- the foundation was built in CPC with a cement content of 180 kg/m^3 (H180),
- the upstream facing and the spillway crest was built in CPC with a cement content of 220 kg/m^3 (H220),
- the body of the dam was built in RCC with a cement content of 60 kg/m^3 (RCC60), but
- the interface between the dam and the foundation (0.80 m high) was builtin RCC with a cement content of 90 kg/m^3 (RCC90).

All RCC and CPC were made with Portland cement similar to Type II ASTM, without pozzolanic admixtures. Table 1 summarizes the relevant material properties for the four types of concrete.

STRESS ANALYSIS

In this Section, results from thermally induced stress analyses performed on a numerical model of Urugua-í RCC Dam are presented. Firstly, results from the reference case study, simulating the real construction process of the dam are discussed. This will provide an accurate assessment of the dam design and the actual short and long term safety conditions of the construction. Secondly, the analysis is repeated simulating a three months interruption of the construction process during the winter. The impact of such eventuality is studied and the comparison with the reference case is described. Thirdly, the analysis is repeated under the hypothesis that the placement interval is doubled and, therefore, the construction process is completed in two years. Again, results are compared to those from the reference case.

Properties	H180	H220	RCC60	RCC90	Rock
w/c	0.50	0.50	1.60	1.00	—
$\rho\ [Kg/m^3]$	2,440	2,400	2,500	2,500	2,700
$C\ [10^{-6} J/m^3\,{}^oC]$	2.35	1.95	2.49	2.44	2.37
$k_T\ [J/m\,hs\,{}^oC]$	6,807	6,807	6,987	6,109	7,740
$\alpha_T\ [10^6]$	6.0	8.0	7.40	8.33	—
$Q_\xi\ [10^{-7} J/m^3]$	7.79	9.50	2.57	3.97	—
$f_\infty^-\,[MPa]$	18.0	22.0	9.0	13.6	50.0
$f_\infty^+\,[MPa]$	2.0	2.2	0.875	1.36	5.0
$E_\infty\,[GPa]$	31.0	38.0	14.0	22.0	30.0

Table 1: Material Properties for Urugua-í Dam.

Numerical Model

The numerical model used for the stress analyses is identical to the one used in Part I for the 2D thermal analyses; it consists of a finite element discretization of the central cross section of the dam. The mesh represents the body of the dam (from elevation 125 to elevation 189), plus the foundation (from elevation 115 to elevation 125) and some surrounding foundation rock (down to elevation 90). The dam is formed by 157 RCC lifts 0.40 m thick. The upstream facing and the spillway crest, both cast in H220 concrete are also included in the model. In the 2D model, every lift is discretized into 25 elements across and 2 elements thick, thus resulting in 7,850 elements in the dam body. The mesh is finer near the up and dowstream faces to represent the CPC facing and to capture the boundary thermal effects. The total number of elements in the mesh is 9,500 including the foundation.

The material properties used to simulate the hydration and aging processes were listed in Part I. Table 2 summarizes the additional mechanical material properties used for in the numerical simulation for the stress analyses. They refer to the constitutive modelling of creep and tensile damage.

Properties	H180	H220	RCC60	RCC90
w/c	0.50	0.50	1.60	1.00
N	2	2	2	2
$E^1 : E^2$	3:1	3:1	3:1	3:1
$\tau^1\,[hs]$	∞	∞	∞	∞
$\tau^2\,[hs]$	15	15	75	75
$\tau_{\mu 0}\,[hs]$	600	700	1,000	1,000
$c_{\mu 0}\,[x10^{-3}1/hs]$	5.0	6.0	2.0	2.0
r_e^+	1.0	1.0	1.0	1.0
r_p^+	1.0	1.0	1.0	1.0
$G_{f\infty}^+\,[N/m]$	300	300	300	300

Table 2: Material Properties for Numerical Simulations.

The numerical model used allows to simulate the actual evolutionary construction process of the dam. To this end, the finite elements corresponding to the different concrete lifts are progressively activated at the times corresponding to their respective placing in the dam.

The initial temperature of the activated elements is automatically set equal to the corresponding placing temperature. For the reference simulation case the placing temperature of each lift is taken as equal to the ambient temperature corresponding to the placing date + 5 ^{o}C. The initial temperature of the foundation rock is assumed to vary linearly from the ambient temperature at the surface (elevation 125) to 10 ^{o}C at the bottom of the model (elevation 90). During the construction of the dam, temperature at the boundaries in contact with the air is automatically set equal to the ambient temperature at the corresponding date. After the completion of the dam, the analysis is continued for the subsequent eleven years, to be able to follow the evolution on the stresses during the cooling process. To this end, the ambient temperature is automatically adjusted to follow the average cyclic seasonal thermal variation in the area. The reservoir was

filled in July 1990, and from that time on the temperature in the water and therefore, at the upstream wall, is assumed to vary linearly between the ambient temperature at the surface and the upper layer of rock at the bottom of the reservoir.

Reference case study

The reference case study corresponds to the real concreting programme followed in the construction process of the Urugua-í RCC Dam. Concreting of the foundation began in January 1988 and was completed in March of the same year. RCC placing began in April 1988 and finished in March 1989. Therefore, it can be considered that the constrution of the body of the dam took one year, approximately. The dam was built with 40 cm thick lifts. The placement interval between lifts was 48 hs, approximately (up to elevation 191). Therefore, the placing speed can be estimated as $V = 20$ cm/day. The relative placing speed is $\bar{V} = V/H = 2.63$ x 10^{-3} 1/day = 0.96 1/year, where H is the dam height.

Figure 2 shows the short term longitudinal stress evolution for interior points corresponding to lifts placed with 2 months interval between them. The corresponding (placing month) elevations are: (4) 130 m, (6) 141 m, (8) 153 m, (10) 165 m and (12) 177 m. As the placing temperature is assumed above the ambient temperature (+ 5 ^{o}C), the lifts start to cool after being placed and they go into tension because of the restriction to deform imposed by the lifts below. However, the stress turns into compresion shortly afterwards, as the concrete starts to warm because of the release of the hydration heat and the heat flux coming from the surrounding concrete. This lasts until the concrete begins to cool again after the hydration process is finished and the heat in the dam is released towards the enviroment and the foundation rock. Note that lifts placed at the bottom of the dam begin to cool fairly early after their placement, and they are subjected to tension almost from the beginning (self-weight not considered).

Figure 3 shows a detail of the short term stress evolution for lifts 5, 6, 7 and 8 just after their placement (during the end of April and the beginning of May). Note how immediately after being placed the lifts are under tension because of the difference between the placing and the ambient temperatures (+ 5 ^{o}C) and heat is lost through the upper surface. Shortly after, a peak in the stress is reached as soon as the upper lift is placed and the temperature begins to rise again due to vertical heat conduction; as heat continues to be released through the upper surface a second peak is reached, now in compression; with the placing of a new lift, the cycle is repeated, every time with a smaller amplitude due to the increasing distance of the concrete to the upper exterior surface. It must be noted that this very short term oscillations in the stress would be amplified for thinner lifts or larger placing intervals, that is, for lower production rates; on the contrary, they would be reduced for thicker lifts or shorter placing intervals, that is, for higher production rates. Eight days after the placing of a lift, the stresses are clearly on the compression side as can be seen both in figures 2 and 3.

Figure 4 shows the short term evolution of the tensile strength for lifts 5, 6, 7 and 8. Note how the strength develops faster than the tensile stresses and, therefore, there is no risk of tensile cracking at this very early stage.

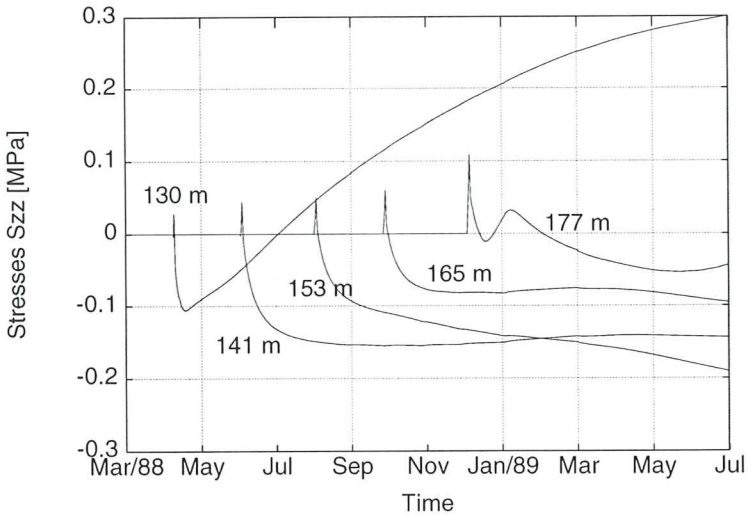

Figure 2: Short term stress evolution for different elevations.

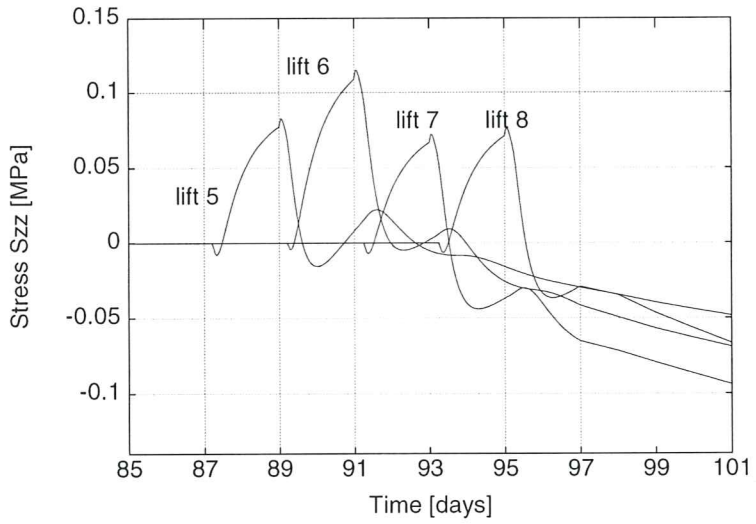

Figure 3: Short term stress evolution for four consecutive lifts.

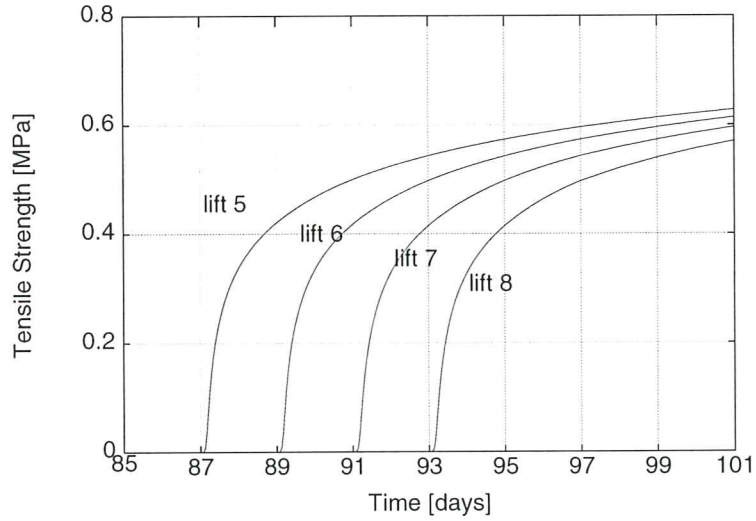

Figure 4: Short term strength evolution for four consecutive lifts.

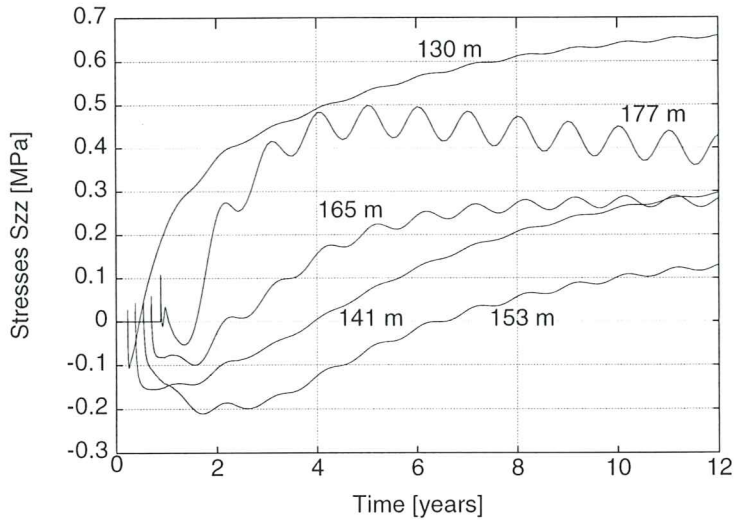

Figure 5: Long term stress evolution for different elevations.

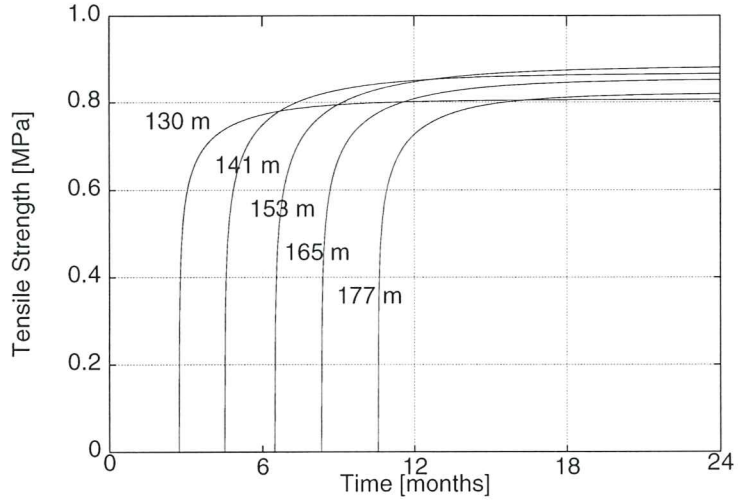

Figure 6: Long term strength evolution for different elevations.

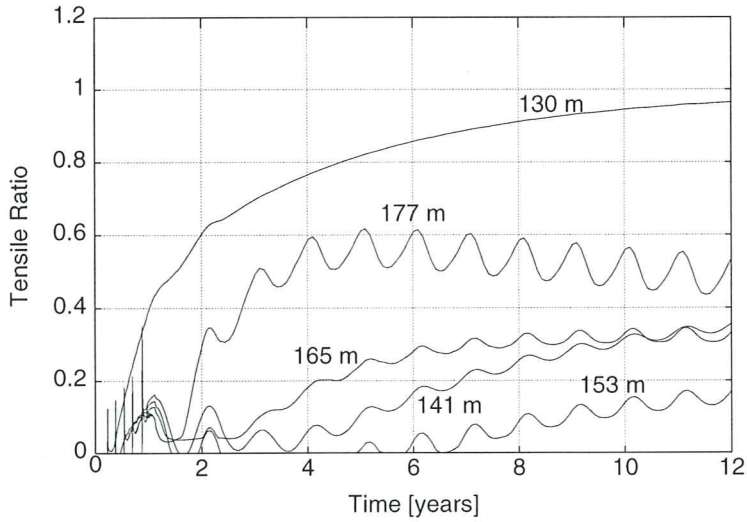

Figure 7: Long term tensile ratio evolution for different elevations.

Figure 5 shows the long term stress evolution for the same interior points described in figure 2. The stress analysis is run now for 11 years after the dam completion. During this period the temperature in the interior of the dam decreases progressively, as the heat generated during the hydration process is released through the up and downstream faces. The final stable temperature in the interior of the dam will be approximately equal to the mean annual temperature (20 ^{o}C). As the temperature drops, the longitudinal stress in concrete turns progresively from compression to tension. This phenomenon is faster for the upper elevations, both because they were placed in summer and because they are more exposed to the ambient temperature. However, the bottom lifts also go into tension very quickly because of the loss of heat towards the foundation rock. Note also that the seasonal oscillation of the ambient temperature is only noted in the stresses for the points located at higher elevations, while the bottom part of the dam body is virtually unaffected by it.

The evolution of the long term tensile stresses must be compared with the development of the tensile strength, depicted in figure 6, in order to assess the risk of cracking. Note that different tensile strengths are attained at the different elevations, due to the influence of temperature in the aging process. Figure 7 combines both results by showing the evolution of the tensile ratio, defined as the ratio of (the norm of) the tensile stresses over the current tensile strength. The closer this value is to unity, the greater is the risk of the onset of tensile damage. In general, it can be concluded from the analysis that the higher the location, the greater the risk of tensile damage. This was correctly evaluated by the designers of Urugua-í Dam, and they provided transverse contraction joints from elevation 182 up every 70-90 m. However, the present analysis also shows significant risk of tensile cracking in the long term in the contact area between the dam and the foundation. This risk is well recognised in the literature and it is usually referred to as *cracking by external restraint*. In fact, the stress analysis performed for Miyagase RCC Dam, reported by Hirose et al. (1988), found that the maximum risk of cracking occurred when the concrete just above the foundation rock was placed in summer. Nevertheless, it must be remarked that, due to Poisson's effect, the compressive vertical stresses due to self-weight, will also lead to compressive longitudinal stresses that largely reduce the risk of tensile cracking in this bottom area.

Figure 8 shows contour plots for the evolution of the tensile ratio in the body of the dam during the construction process (1 year). The corresponding month–elevations are: (a) June/88 146 m, (b) August/88 157 m, (c) November/88 175 m, (d) February/89 187 m and (e) June/89 196 m. As mentioned above, the developed stresses in the dam interior are initially compressive because they are due to the increase of temperature due to the hydration heat; they turn into tension some months after the concrete is placed, when the release of heat is completed and the concrete has started to cool. During this first year tensile stresses develop mainly in the lower part of the dam, because of external restraint caused by the foundation, and at the upstream and downstream faces, because of the enviromental thermal variations. Due to the low thermal conductivity of concrete, temperature gradients due to the difference between the ambient and inside temperatures are limited to a distance of about 2 m from the exterior faces. In

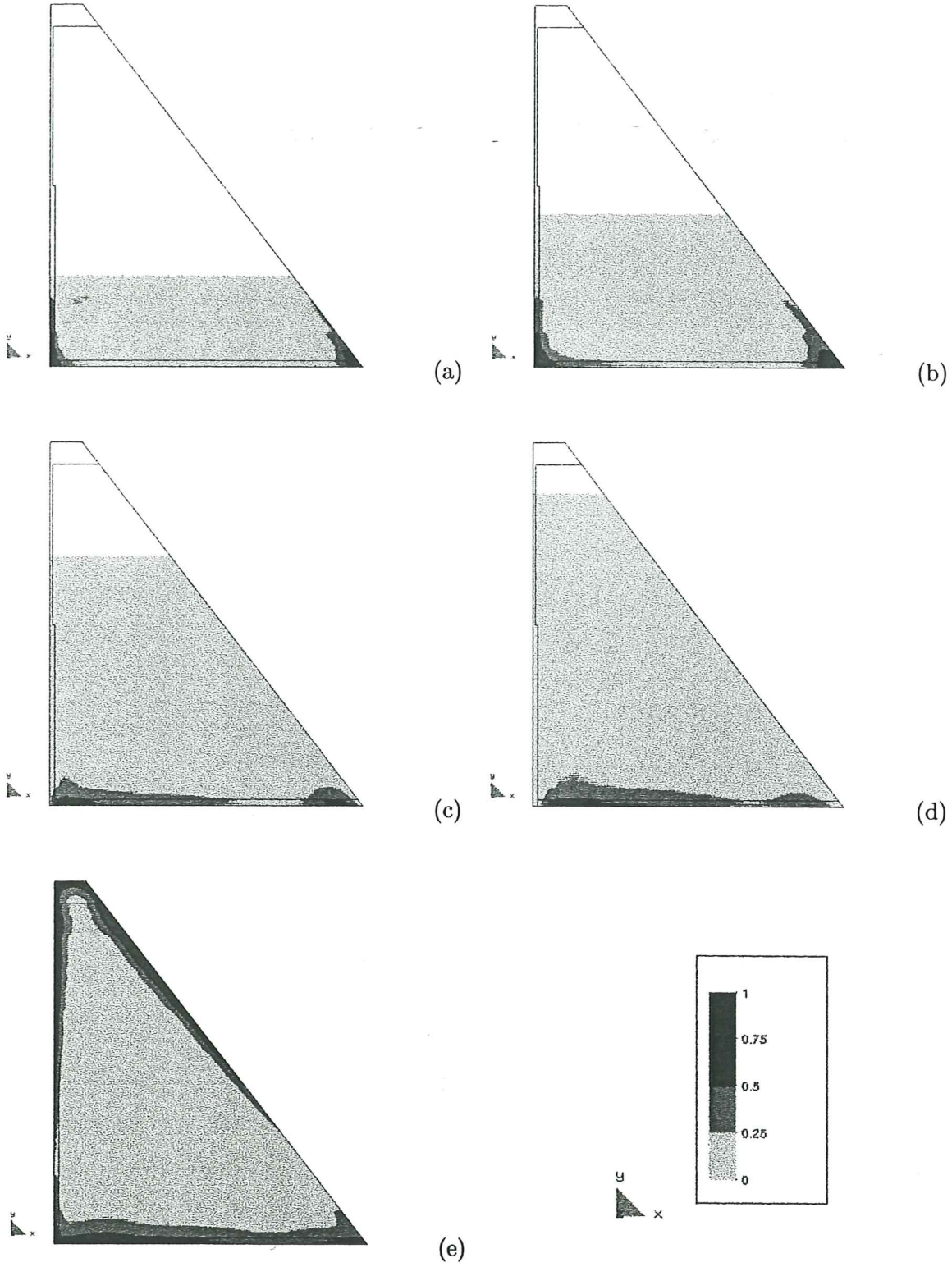

Figure 8: Short term evolution of tensile ratio.

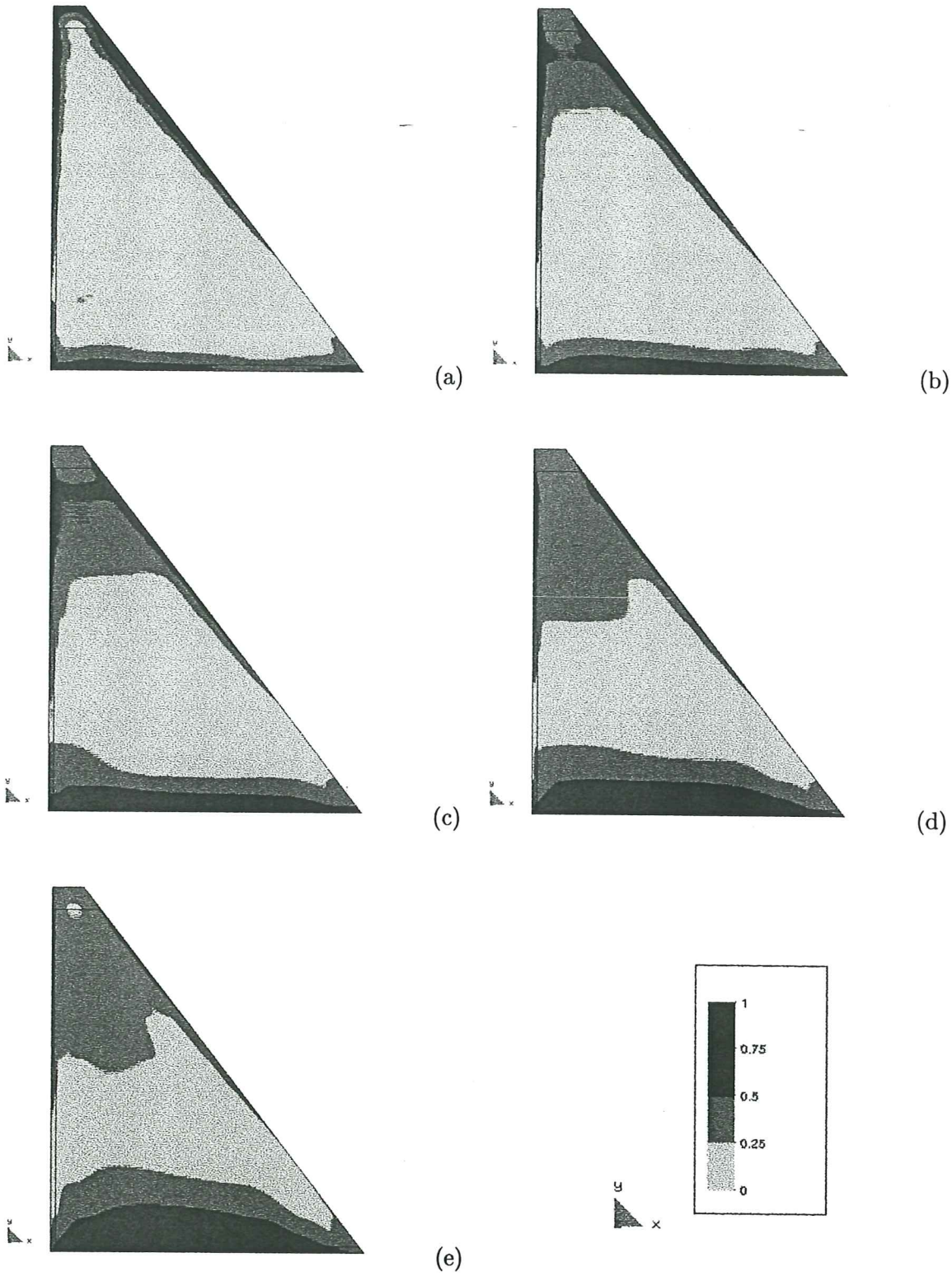

Figure 9: Long term evolution of tensile ratio.

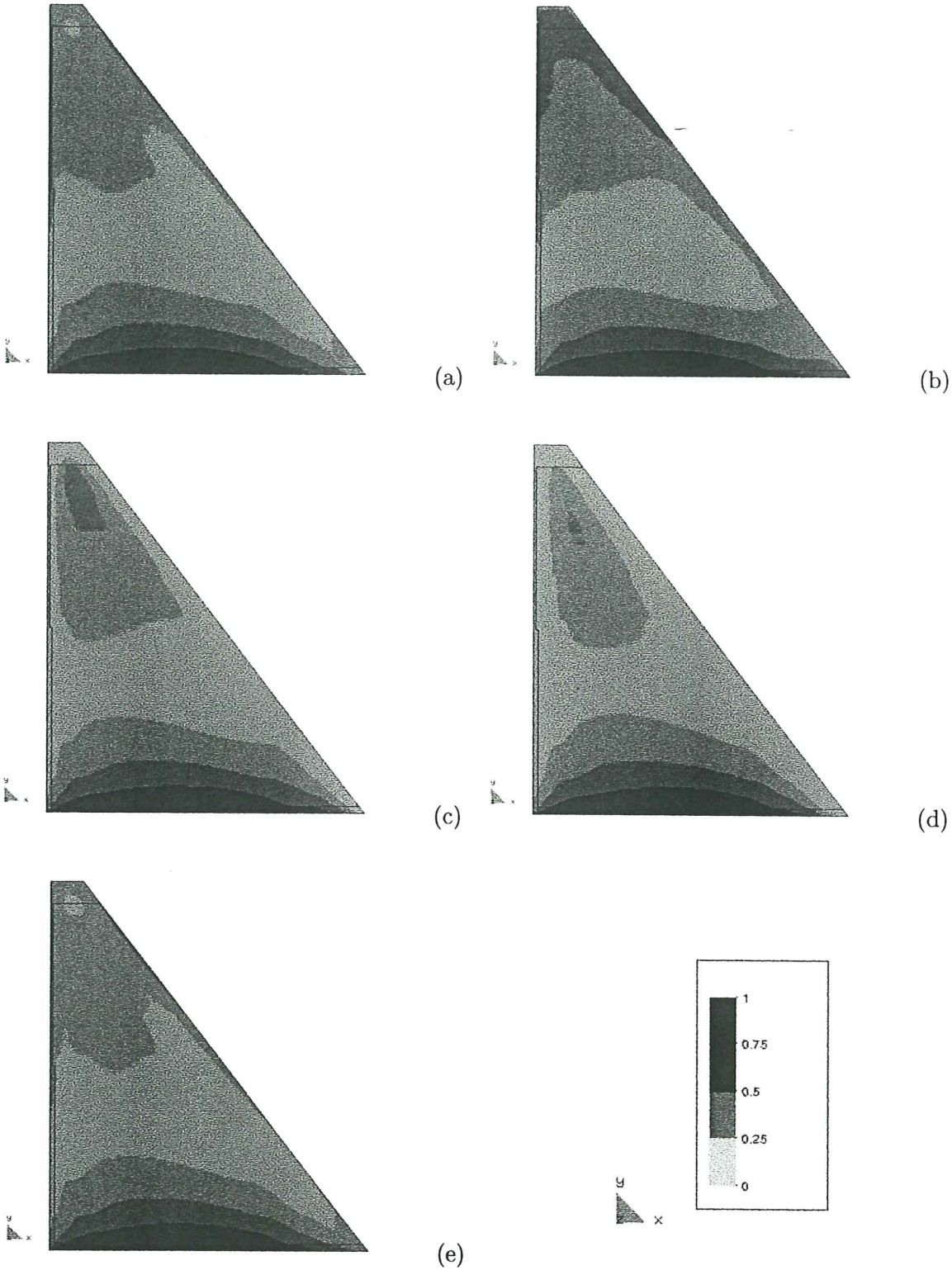

Figure 10: Seasonal evolution of the tensile ratio.

order to avoid superficial cracking induced by these temperature gradients transverse contraction joints are cut in the facing of the dam every 14.24 m, 1.20 m deep and running inside the RCC.

Figure 9 shows contour plots for the evolution of the tensile ratio in the body of the dam during the 10 first years after dam completion. All the snapshots correspond to the temperature distribution in winter (June). The corresponding years are: (a) 1989, (b) 1990, (c) 1991, (d) 1994 and (e) 1999. Note how as the overall temperature in the dam decreases, thermally induced tensile stresses progressively develop. In the upper part of the dam they are due to the internal restraint provided by the warmer concrete below; in the lower part of the dam free volume changes are restricted both by the warmer concrete above and the cooler foundation rock below. It is clear in the figure that the risk of cracking in the upper part of the dam develops in the first two years after completion.

After 10 years the heat 'stored' during the construction process has virtually disappeared. The dam is then in a thermally stable regime, subjected only to the cyclic seasonal oscillations. Figure 10 shows contour plots for the evolution of the tensile ratio in the body of the dam for the eleventh year after dam completion, once the cooling process is completed. The snapshots corresponding month/year are: (a) June/2000, (b) September/2000, (c) December/2000, (d) March/2001 and (e) June/2001. The stress distribution in June is typical of winter, while that in December is typical of summer. The September (spring) and March (autumn) distributions are typical transition distribution between the former. Due to the thermal inertia of the concrete maximum tensile stresses in the upper part of the dam appear in spring, after the cold winter conditions.

Interruption of the construction process

The complete stress analysis is repeated now considering that an interruption of the construction process during the winter months due, for instance, to inadequate weather conditions or flooding of the construction site, occurs. Thus, the concreting schedule from January 1988 until the end of June is followed as for the reference case, then it is stopped during July, August and September and resumed at the same placing speed from the beginning of October until the end of June 1999.

Figure 11 shows the temperature evolution for interior points corresponding to lifts placed with 1 month interval between them. The corresponding (placing month) elevations are: (4) 130 m, (5) 135 m, (6) 141 m, (10) 147 m, (11) 153 m, (12) 159 m, (1) 165 m, (2) 171 m, (3) 177 m, (4) 181 m and (5) 185 m. Higher temperature rises appear at the bottom lifts (April to June), because of the heat coming from the hydration of the H180 concrete in the foundation and in the lifts placed during the austral summer (December to February). The temperature is still rising in most of the dam after completion, particularly in those lifts placed immediatety before and after the winter interruption (June and October). The bottom layers, however, start to cool shortly after being placed because of the heat conduction towards the founding rock. Compared to the short term temperature evolution for the reference case, it can be observed that higher temperatures are attained in the middle part of the dam, between eleva-

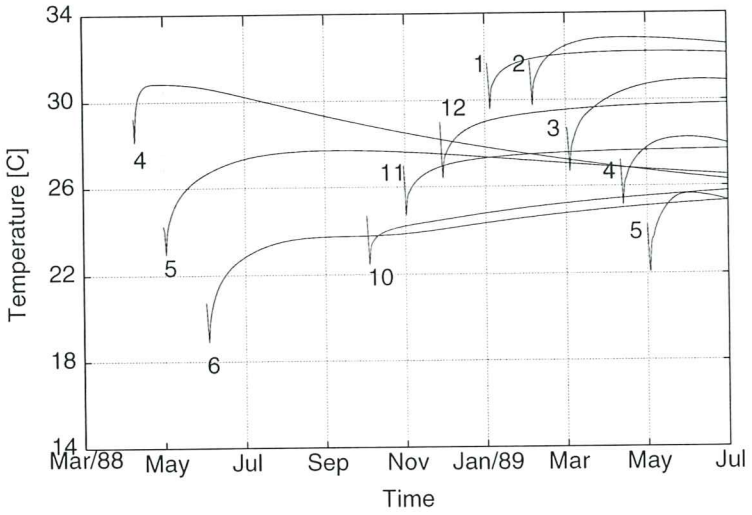

Figure 11: Temperature evolution for different elevations with 3 months interruption.

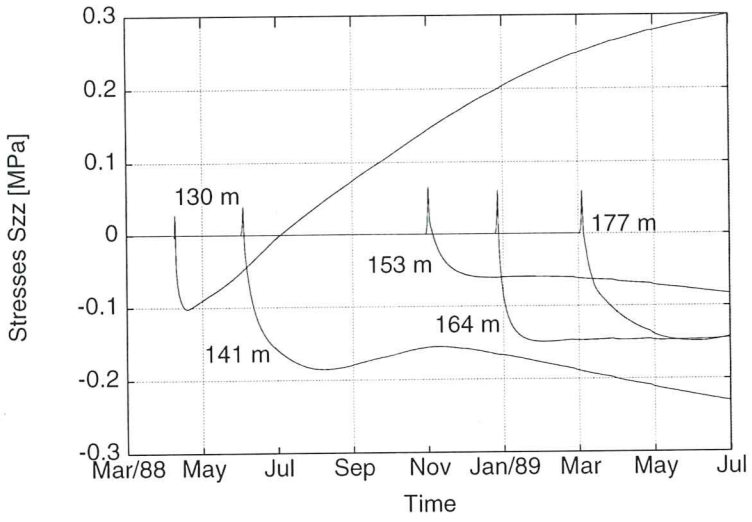

Figure 12: Short term stress evolution for different elevations with 3 months interruption.

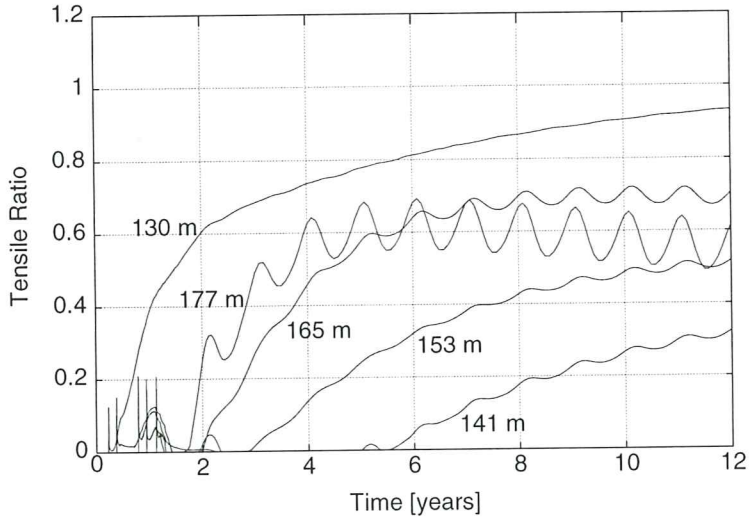

Figure 13: Long term tensile ratio evolution for different elevations with 3 months interruption.

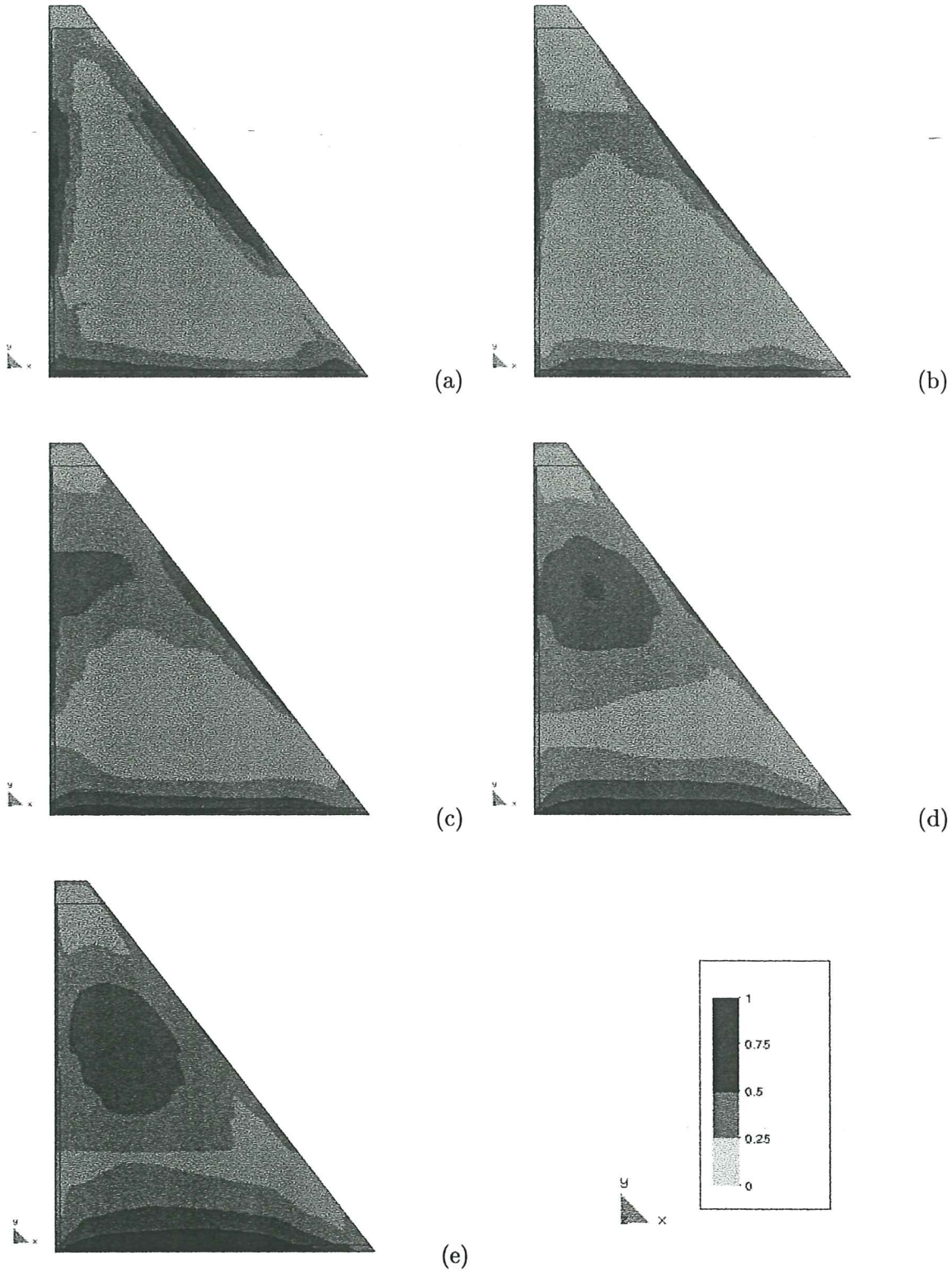

Figure 14: Long term evolution of tensile ratio with 3 months interruption.

tions 150 m. and 170 m., while lower temperatures arise above the latter elevation.

Figure 12 shows the short term longitudinal stress evolution for interior points corresponding to lifts placed with 2 months interval between them. The corresponding (placing month) elevations are: (4) 130 m, (6) 141 m, (11) 153 m, (1) 165 m and (3) 177 m. This has to be compared with Figure 2 to evaluate the influence of the interruption in the construction programme. As most of the concrete in dam is still warming at this early age, most of the longitudinal stresses are still compressive. Only at the bottom the thermally induced stresses turn rapidly into tension, very much in the same fashion as for the reference case. Note the effect of the three months interruption in the evolution of the stress at elevation 141 m: a peak is reached in compression because of the heat lost through the upper surface during the interruption, but compressive stresses continue to grow after the construction is resumed and heat continues to flow downwards from the new lifts placed above.

Figure 13 shows the long term evolution of the tensile ratio for the same elevations. This has to be compared with Figure 7 to evaluate the influence of the interruption in the construction programme. It is quite evident that the risk of cracking has increased significantly, particularly for elevations above 150 m. Note that tensile stresses are still increasing after 12 years in most of the dam body. Again, it can be concluded from the analysis that the higher the location, the greater the risk of tensile damage. However, to ensure the same level of safety as for the reference case, in this situation transverse contraction joints should be provided every 70-90 m above elevation 150 m at least, and not above elevation 182 as in the actual design of the dam.

Figure 14 shows contour plots for the evolution of the tensile ratio in the body of the dam during the 10 first years after dam completion. All the snapshots correspond to the temperature distribution in winter (June). The corresponding years are: (a) 1989, (b) 1990, (c) 1991, (d) 1994 and (e) 1999. This has to be compared with Figure 9 to evaluate the influence of the interruption in the construction programme. Again, it can be observed how thermally induced tensile stresses progressively develop as the overall temperature decreases. Now, the higher risk of tensile cracking occurs in the upper middle part of the dam, between elevations 160-180 m. The risk of cracking in the middle part of the dam continues to grow even ten years after completion. Note also how in the last figure, the elevation at which the interruption took place is clearly visible.

Slowing of the construction process

Finally, the complete stress analysis is repeated considering that the placing interval is doubled to be 96 hs. RCC placing begins in April 1988 and finishes in December 1989. The spillway is cast in H220 from January to February 1990. Therefore, the placing speed can be estimated as $V = 10$ cm/day. The relative placing speed is $\bar{V} = V/H = 1.31 \text{ x } 10^{-3}$ 1/day $= 0.48$ 1/year, where H is the dam height.

Figure 15 shows the temperature evolution for interior points corresponding to lifts placed with 2 months interval between them. The corresponding (placing month) elevations are: (4) 130 m, (5) 135 m, (7) 141 m,

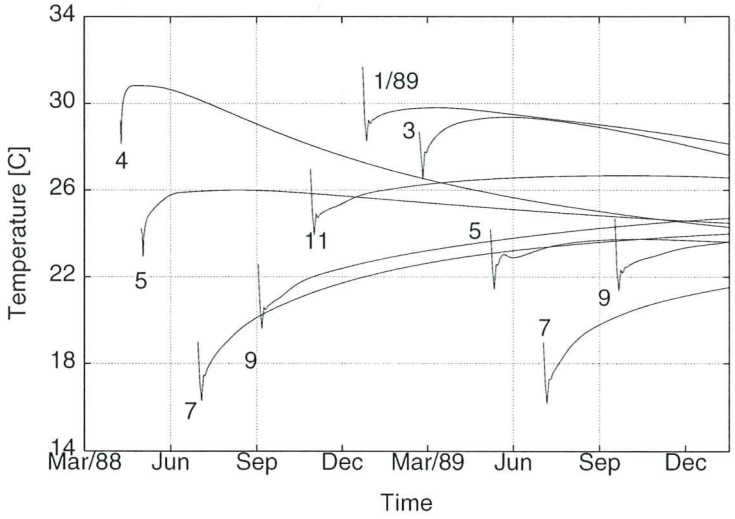

Figure 15: Temperature evolution for different elevations slowing the construction process.

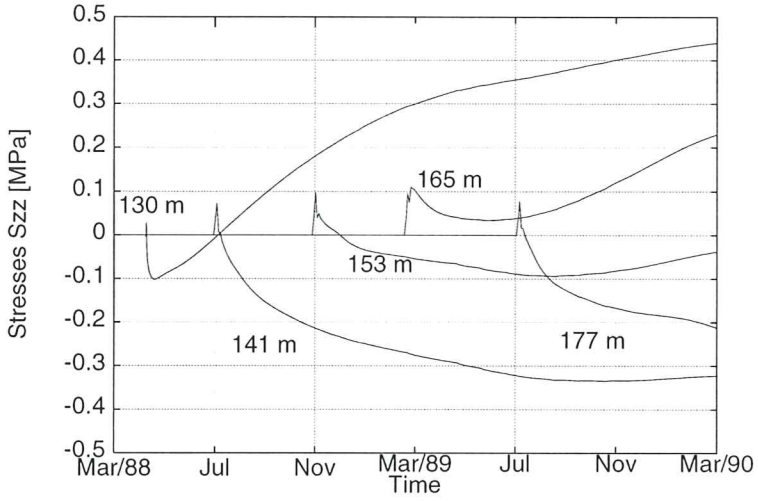

Figure 16: Short term stress evolution for different elevations slowing the construction process.

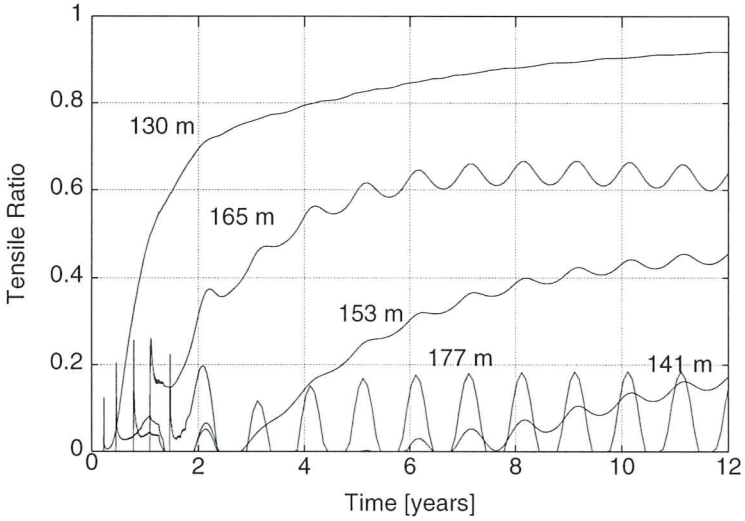

Figure 17: Long term tensile ratio evolution for different elevations slowing the construction process.

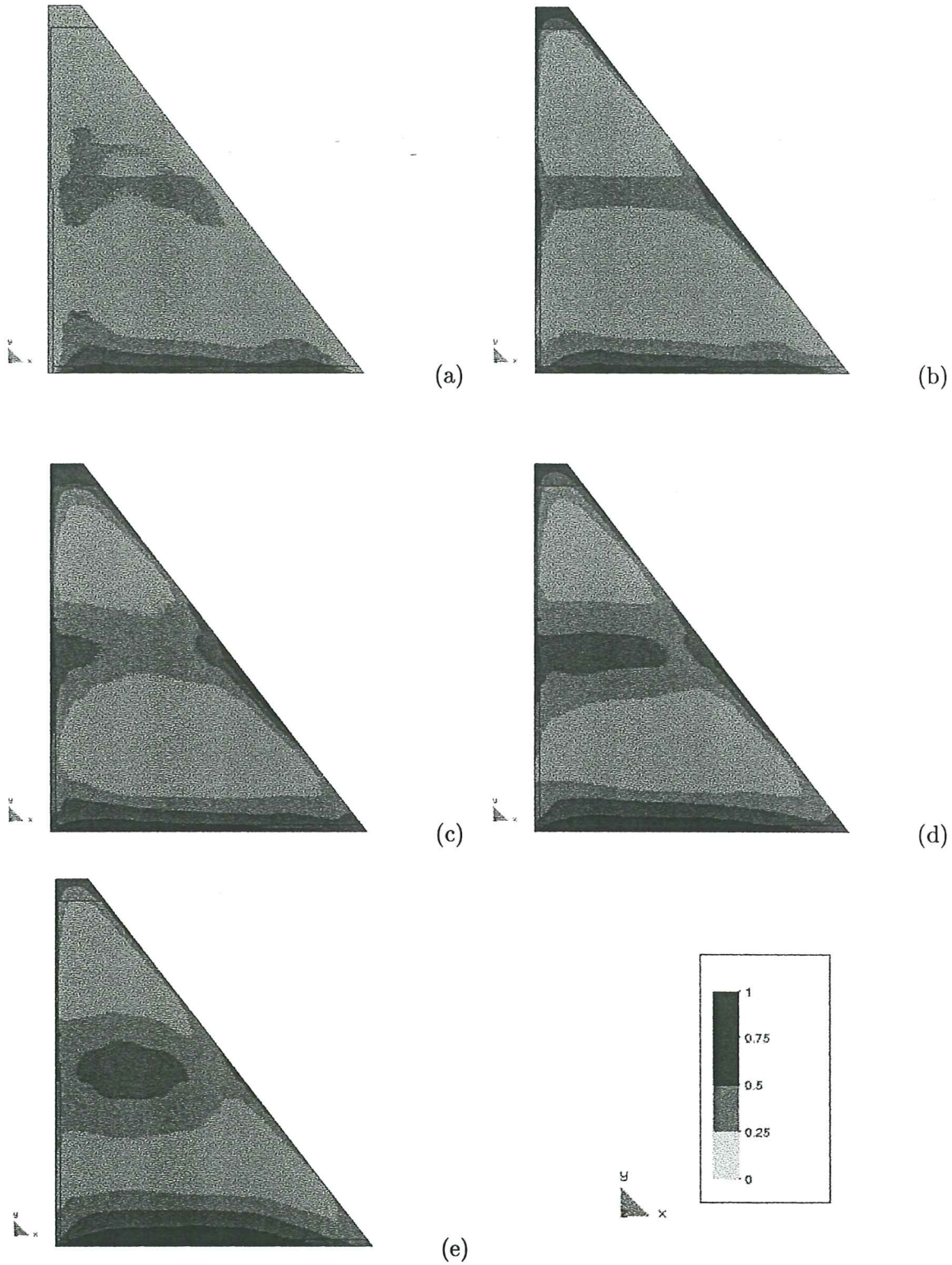

Figure 18: Long term evolution of tensile ratio slowing the construction process.

(9) 147 m, (11) 153 m, (1) 159 m, (3) 165 m, (5) 171 m, (7) 177 m and (9) 185 m. Higher temperature rises appear at the bottom lifts (April to June), and in the lifts placed during the austral summer (December to February). Compared to the short term temperature evolution for the reference case, it can be observed that higher temperatures are attained in the middle part of the dam, between elevations 150 m. and 170 m., while lower temperatures arise below and above these elevations. Heat conduction plays a significant role in this case; the bottom part of the dam attains higher temperatures than in the reference case due to heat flowing from the middle part and, reciprocally, the middle part begins to cool quite rapidly due to heat flowing down and upwards.

Figure 16 shows the short term longitudinal stress evolution for interior points corresponding to lifts placed with 2 months interval between them. The corresponding (placing month) elevations are: (4) 130 m, (6) 141 m, (11) 153 m, (1) 165 m and (3) 177 m. This has to be compared with Figure 2 to evaluate the influence of the slowing in the construction programme. Note how the stresses at elevation 141 m, for instance, go further into the compressive side because of the internal redistribution of temperature; also, the fast cooling in the middle part of the dam induce tensile longitudinal stresses very rapidly in this region, between elevations 150-170 m.

Figure 17 shows the long term evolution of the tensile ratio for the same elevations. This has to be compared with Figure 7 to evaluate the influence of the slowing in the construction programme. It is quite evident that the risk of cracking has increased significantly in the middle part of the dam, placed during the summer (see curves for elevations 153 m and 164 m). On the other hand, tensile stresses are reduced in the upper part of the dam, placed in colder weather than in the reference case; stress at elevation 177 m, for instance, is very much reduced, and it follows nicely the regular seasonal oscillations. To ensure the same level of safety as for the reference case, in this situation transverse contraction joints should be provided every 70-90 m above elevation 150 m at least, and not above elevation 182 as in the actual design of the dam.

Figure 18 shows contour plots for the evolution of the tensile ratio in the body of the dam during the 10 first years after dam completion. All the snapshots correspond to the temperature distribution in winter (June). The corresponding years are: (a) 1990, (b) 1991, (c) 1992, (d) 1995 and (e) 2000. This has to be compared with Figure 9 to evaluate the influence of the slowing in the construction programme. It is clear that concreting in hot weather leaves a mark in the long term mechanical behaviour of the dam. Now, the higher risk of tensile cracking occurs in the middle part of the dam, between elevations 150-170 m. The risk of cracking in the middle part of the dam is noticeable only one year after the dam completion, and it continues to grow stadily even ten years after completion.

CONCLUSIONS

This work presents a numerical procedure to simulate the stress analysis of the evolutionary construction process of roller compacted concrete dams.

The basis of the work is a coupled thermo-chemo-mechanical model for the behaviour of concrete at early ages that allows to simulate the observed phenomena of hydration, aging, damage and creep. In this second part the simulation and discussion of the mechanical aspects of the problem are presented. The proposed procedure is shown to be able to predict the evolution in time of the thermally induced tensile stresses that develop due to hydration heat released during the construction and the subsequent cooling process, in order to assess the risk of occurrence of tensile damage either at short or long term.

Firstly, a 2D finite element model of the Urugua-í RCC Dam, recently built in Argentina, is used to perform the corresponding stress analyses. This allows to obtain the stress field inside the dam at any time during the construction process, and more importantly, during the first years following the completion of the dam, while the temperature in the dam body decreases to reach the final stable distribution.

The results of the analysis show that significant tensile stresses develop in the bottom part of the dam due to the external restraint imposed by the foundation rock and also in the top part of the dam due to the internal restraint imposed by the concrete below, especially in the lifts located between elevation 180 and elevation 190, placed during the austral summer (December to February), when the ambient (and placing) temperatures are higher. The latter was correctly evaluated by the designers of Urugua-í Dam, as they provided transverse contraction joints from elevation 182 up every 70-90 m.

Also, temperature gradients due to the difference between the ambient and inside temperatures may lead to thermally induced superficial cracking in these faces, and because of this transverse contraction joints are cut in the facing of the dam every 14.24 m, 1.20 m deep and running inside the RCC.

Secondly, the analysis is repeated simulating a three months interruption of the construction process during the winter due, for instance, to inadequate weather conditions or flooding of the construction site. The impact of such eventuality is studied and the comparison with the reference case is described. It turns out that in such case transverse contraction should be cut deeper inside the dam, from elevation 160 at least, to provide the same level of safety against cracking. The risk of cracking due to the external restraint of the foundation remains high and almost unaffected.

Thirdly, the analysis is repeated under the hypothesis that the placement interval is doubled and, therefore, the construction process is completed in two years. It turns out that heat conduction during construction plays a significant role in this case; the bottom part of the dam attains higher temperatures than in the reference case due to heat flowing from the middle part and, reciprocally, the middle part begins to cool quite rapidly due to heat flowing down and upwards. Transverse contraction joints should also be cut deeper inside the dam for this case, from elevation 150 at least, to provide the same level of safety against cracking.

APPENDIX I. REFERENCES

[Bazant et al. 1997] Bazant, Z. P., Hauggard, A. B., Prasannan, S., and Ulm, F. J. (1997). Microprestress–solidification theory for concrete creep. i: Aging and drying effects. *J. Engrg. Mech., ASCE*, 123(11):1188–1194.

[Bazant and Prasannan 1989] Bazant, Z. P. and Prasannan, S. (1989). Solidification theory for concrete creep. i: Formulation. *J. Engrg. Mech., ASCE*, 115(8):1691–1703.

[Buchas and Buchas 1991] Buchas, J. and Buchas, F. (1991). Construction of urugua-í dam. In Hansen, K. D. and McLean, F. G., editors, *Proceedings of ASCE Specialty Conference on Roller Compacted Concrete 3*, pages 258–271, San Diego.

[Carol and Bazant 1993] Carol, I. and Bazant, Z. P. (1993). Viscoelasticity with aging caused by solidification of nonaging constituent. *J. Engrg. Mech., ASCE*, 119(11):2252–2269.

[Cervera et al. 1992] Cervera, M., Oliver, J., and Galindo, M. (1992). Numerical analysis of dams with extensive cracking resulting from concrete hydration: simulation of a real case. *Dam Engineering*, 3(1):1–22.

[Cervera et al. 1998] Cervera, M., Oliver, J., and Prato, T. (1998). A thermo-chemo-mechanical model for concrete. ii: Damage and creep. *Submitted to J. Engrg. Mech., ASCE.*

[Fujisawa and Nagayama 1985] Fujisawa, T. and Nagayama, I. (1985). Cause and control of cracks by thermal stress in concrete dams. In ICOLD, editor, *Proceedings of XV Congress on Large Dams*, volume 2, pages 117–143, Lausanne.

[Galindo 1993] Galindo, M. (1993). *Una metodología para el análisis numérico del comportamiento resistente no lineal de presas de hormigón bajo cargas estáticas y dinámicas (in Spanish).* PhD thesis, Technical University of Catalonia.

[Giovambattista 1995] Giovambattista, A. (1995). Urugua-í dam. thermal analysis, design criteria and performance. In IECA and CNEGP, editors, *Proceedings of the Int. Symposium on Roller Compacted Concrete Dams, Volume I: Materials, Planning and Design*, pages 309–323. Santander, Spain.

[Hirose et al. 1988] Hirose, T., Nagayama, I., Takemura, K., and Sato, H. (1988). A study on control temperature cracks in large roller compacted concrete dams. In ICOLD, editor, *Proceedings of XVI Congress on Large Dams*, volume 3, pages 119–135, San Francisco.

[Lorenzo and Calivari 1991] Lorenzo, A. C. and Calivari, S. C. (1991). Behavior of urugua-í dam. In Hansen, K. D. and McLean, F. G., editors, *Proceedings of ASCE Specialty Conference on Roller Compacted Concrete 3*, pages 272–290, San Diego.

[Widmann, 1985] Widmann, R. (1985). How to avoid thermal cracking of mass concrete. In ICOLD, editor, *Proceedings of XV Congress on Large Dams*, volume 2, pages 263–277, Lausanne.

APPENDIX II. NOTATION

The following symbols are used in this paper:

$\boldsymbol{D}, \overline{\boldsymbol{D}}$ = Constitutive tensor; Normalized *idem*
E, E_∞ = Elastic modulus, Final elastic modulus;
E^i = Elastic Modulus for Maxwell element i;
$f^\pm, f^\pm_\infty$ = Tensile/compressive strength, Final values;
$f^\pm_e$ = Elastic limit in uniaxial tests (tension/compression);
$G^+_{f\infty}$ = Final Tensile fracture energy;
$\boldsymbol{p}_j$ = Unit vector associated with principal direction j;
T, T_0 = Temperature, Initial temperature;
T_{ref} = Reference temperature;
w/c = Water/cement mass ratio;
α_T, α_ξ = Thermal and chemical expansion coefficients;
$\boldsymbol{\varepsilon}, \boldsymbol{\varepsilon}_e$ = Strain tensor, Elastic strain tensor;
$\boldsymbol{\varepsilon}^i_e, \boldsymbol{\varepsilon}^i$ = Elastic, Viscous strain tensor for Maxwell element i;
$\boldsymbol{\varepsilon}_T, \boldsymbol{\varepsilon}_\xi$ = Thermal strain tensor, Chemical strain tensor;
κ = Aging degree;
λ_E = Elastic modulus aging function;
μ = Normalized micro-prestress;
ν = Poisson's ratio;
$\boldsymbol{\sigma}, \overline{\boldsymbol{\sigma}}$ = Stress tensor, Effective stress tensor;
$\bar{\sigma}_j$ = Principal effective stress value j;
τ^i = Relaxation time for Maxwell element i;
$\tau_\mu, \tau_{\mu 0}$ = Relaxation time associated to flow term, Initial value;
$\mathbf{1}$ = Unit (second order) tensor;
$\dot{(\,)}$ = Time derivative or rate;
$(\,)\otimes(\,)$ = Tensorial product;
$(\,):(\,)$ = Doubly contracted tensorial product; and
$< >$ = Macaulay brackets.

Simulation of the Construction Process of Roller Compacted Concrete Dams. I: Temperature and Aging

Miguel Cervera,* Javier Oliver† and Tomás Prato‡

ABSTRACT

In this work a numerical procedure for the simulation of the construction process of Roller Compacted Concrete (RCC) dams is described. The basis of the work is a coupled thermo-chemo-mechanical model for the behaviour of concrete at early ages that allows to simulate the observed phenomena of hydration, aging, creep and damage. In this first part only the thermo-chemical aspects of the simulation of the construction process are presented. The proposed procedure can accurately predict the evolution in time of the hydration degree and the hydration heat production. This allows to obtain the temperature field inside the dam at any time during the construction and the following years. The evolution of the compressive and tensile strengths and elastic moduli can also be predicted in terms of the evolution of the hydration degree and the temperature conditions. Results from 2D and simplified vertical 1D models are compared and several parametric studies are carried out. The simulation and discussion of the mechanical aspects of the construction process are relegated to a companion paper that follows.

*Asst. Prof. Struc. Anal., ETS Ingenieros de Caminos, 08034 Barcelona, Spain.
†Prof. Cont. Mech., ETS Ingenieros de Caminos, 08034 Barcelona, Spain.
‡Grad. Res. Asst., ETS Ingenieros de Caminos, 08034 Barcelona, Spain.

INTRODUCTION AND MOTIVATION

During the last 30 years great effort has been made to find an alternative to embankment dams for large gravity constructions that would, on one hand, overcome the risk of failure due to overtopping or internal erosion (piping), while on the other, being economically competitive. Right now, the answer to this technological challenge are Roller Compacted Concrete (RCC) Dams. RCC is relatively lean no-slump concrete which can be spread horizontally and compacted using earthworking machinery like dozers and vibratory rollers. The first evaluations on place-in unit costs for several RCC dams built in the USA showed that these represented savings ranging from 30 to 70 % of the cost of conventional concrete dams (Schrader and Naminas 1988).

The basic concept of RCC already existed in the UK in the 1940s, where it was used as the subbase of road and airfield pavements. In 1964 the Alpe Gera Dam was built in Italy, transporting the concrete by trucks and spreading it from abutment to abutment without construction joints (Gentile 1964). The idea of using RCC in dams was first introduced in "The Optimum Gavity Dams" by Raphael in 1970. The first RCC dams were erected in the early 1980s: Shimajigawa Dam, 89 m (Japan, 1980) and Willow Creek Dam, 52 m (USA, 1982); several other constructions followed during the same decade in different countries: Copperfield Dam, 40 (Australia, 1984), Saco Dam, 56 m (Brazil, 1986), Tamagawa Dam, 100 m (Japan, 1987), Upper Stillwater Dam, 87 m (USA, 1987), Urugua-í Dam, 76 m (Argentina, 1989), etc. Nowadays, there are more than 200 RCC dams spread around the world, and about 40 more under construction (Franco 1996).

RCC dams have been the subject of two Questions in recent ICOLD Congresses. Question 57 in ICOLD 1985 was on "a new technology: rolled concrete (rollcrete)" and 13 papers were presented on the topic; Question 62 in ICOLD 1988 was on "new developments in the construction of concrete dams" and of the 43 papers were presented, 20 were on RCC dams. More recently, International Symposia on Roller Compacted Concrete Dams have been held in Beijing, China (Chinese Society of Hydroelectric Engineering 1991) and in Santander, Spain (IECA and CNEGP 1995).

RCC Dam construction has the following features:

(a) the dam body is constructed by placing concrete, in the same placing cycle, over a wide area encompassing several blocks;

(b) transverse joints are cut after the placement of concrete;

(c) no longitudinal joints are made; and

(d) pipe cooling is not (generally) used.

These features allow a high production rate, reducing the construction time. The resulting reduction in unit costs yields significant economic savings. On the other hand, to achieve such high production rate, particular attention must be devoted to design aspects such as:

(a) the distance between transverse contraction joints (typically, this distance is at least 30-45 m);

(b) reduction of the number of special elements such as galleries, drains or spill-ways; and

(c) limitation of the use of non RC concretes in the facing or elsewhere.

The main difference between RCC and conventional concrete is its low cement content and no-slump consistency. Usually, high admixture contents, e.g. fly ash, are used. Consequently, RCC hydration process is slower, its density is higher and its stiffness is lower than for ordinary concrete. On one hand, the low water content in the mixture leads to less shrinkage and, on the other, the low cement content makes that the hydration heat be considerably lower, down to three times smaller than for conventional concretes. Nevertheless, the high concreting rate used in RCC dams may lead to significant temperature rises.

This increase in temperature occurs during the first days after placing, when the stiffness of concrete is still quite low and creep (viscous) effects are significant; therefore, it usually leads to moderate, and mainly compressive, stresses. However, months later, when the stiffness has significantly increased, the concrete starts to cool down. The low conductivity of the material, differential effects due to the evolutionary construction process and convection phenomena with the enviroment may generate considerable thermal gradients. These, together with geometrical aspects and external restraints may develop relatively important tensile stresses, and thermally induced cracking may appear. This may result in structural damage even before the reservoir is filled and, in any case, it may affect significantly the durability and serviceability of massive concrete dams.

Clearly, the original motivation for the design of RCC dams was economical, and the first american constructions avoided transverse as well as longitudinal joints to achieve high production rates. However, the basic design requirement for concrete dams in to ensure their integrity, watertighness and durability. The risk of thermally induced cracks lead, after comprehensive studies, japanese designers to the conclusion that transverse joints cannot be totally eliminated. Chinese designers involved in the analysis of Three Gorge Dam at the Yangtze river (185 m) recommended several measures to avoid thermally induced cracking, including: precooling of concrete before placement, thermal insulation of the upper horizontal lift surface, thermal insulation of the upstream and downstream faces *and* artificial pipe cooling.

Fortunately, the RCC dam construction method is advantageous in thermal stress control because:

(a) the placement of thin lifts allows for heat losses by convection and radiation, and

(b) placing concrete at constant speed and with regularity helps to produce smooth temperature gradients within the dam body.

For all these reasons, the determination of the lift schedule and the basic cycle of concrete construction (pouring, curing and green-cutting) is essential for establishing the construction programme for a large RCC dam. The qualitative and quantitative assessment of the influence of major factors such as: the composition of the mix, the ambient temperature, the placing temperature, placing speed (lift thickness and placement interval) and time for starting placement must be established.

To simulate this type of phenomena a coupled thermo-chemo-mechanical model is needed to provide information on: the progress of the hydration process, the associated temperature rises, the evolution of the concrete

strength and stiffness, as well as the development of tensile stresses and the possibility of cracking during, and especially after, the construction process. Pioneering work in this area was published by Fujisawa and Nagayama (1985), Widmann (1985), Ditchley and Schrader (1988), Giesecke and Marx (1988), Hirose et al. (1988) and Yonezawa et al. (1988). More recently, several theoretical contributions and case studies have been published on the topic: Tatro and Schrader (1991), Yamazumi et al. (1995), Hinks and Copley (1995), Giobambattista (1995), Bofang Zhu and Ping Xu (1995), Ziming Zhang and Garga (1996), etc. However, a better knowledge of the thermo-chemo-mechanical behaviour of concrete at early ages is necessary to assess the results obtained in this kind of studies.

This paper presents a numerical procedure for the simulation of the construction process of Roller Compacted Concrete (RCC) dams. Firstly, a thermo-chemical model is proposed to simulate the hydration and aging processes of concrete. It can accurately predict the evolution in time of the hydration degree and the hydration heat production. The evolution of the compressive and tensile strengths and elastic moduli is related to the aging degree, accounting for the effect of the curing temperature in the evolution of these properties. Secondly, the case study of Urugua-í RCC Dam in Argentina is described. The geometrical design, material properties and construction process are outlined. Thirdly, the thermal analysis of Urugua-í RCC Dam is presented. The actual conditions and concreting schedule that ocurred during the construction of the dam are considered as the reference case. Also, results from the 2D numerical simulation are compared to simplified 1D simulations. Finally, some parametric studies are performed to establish the effect of some major variables of the construction process that may influence the temperature distribution and evolution: the placing temperature, the starting date and the placing speed.

NUMERICAL MODEL

Hydration of concrete is a very complex process which involves quite a number of chemical and physical phenomena at the microscopic level. In view of this evidence, a macroscopic description of the hydration phenomenon is adopted for engineering purposes. From this point of view, hydration of concrete is a highly exothermic and thermally activated reaction, so that a thermo-chemical model is necessary for its modellization. The thermo-chemical model used in this work is described in detail in Cervera et al. (1999), and it will only be sketched here.

Thermal Field Equation

From the first and second principles of thermodynamics the thermal field equation can be written, in its usual temperature form, as

$$C\dot{T} - \dot{Q} = R_{ext} + k_T \nabla \cdot (\nabla T) \tag{1}$$

where T is the temperature, C is the heat capacity per unit volume, $\dot{Q}$ is the rate of hydration heat liberated per unit volume, R_{ext} are the external volume heat sources, and k_T is the thermal conductivity. Note that the term due to the hydration heat rate, $\dot{Q}$, acts as an internal heat source.

Thermo-Chemical Model

The thermo-chemical model must provide an expression for the term due to the rate of hydration heat in Eq. (1).

Let us introduce a normalized variable called *hydration degree*, defined as $\xi = \chi/\bar{\chi}_\infty$, where χ is the number of moles of water combined per unit volume, and $\bar{\chi}_\infty$ is the final value of χ with an adequate water/cement ratio to ensure full hydration. In practice, this condition in not fulfilled, so $\chi_\infty < \bar{\chi}_\infty$ and, therefore, $\xi_\infty < 1$ (Bentz et al. 1998). The final degree of hydration ξ_∞ is related to the water/cement ratio of the mixture (Byfors 1980; Waller et al. 1996), and it can be estimated as a function of it (Pantazopoulo and Mills 1995).

Most authors identify the rate of heat liberation with the actual rate of hydration (Reinhard et al. 1982; Rostassy et al. 1993; Torrenti et al. 1994; de Schutter and Taerwe 1995). Note that in this case, the hydration degree can also be defined as $\xi = Q/\bar{Q}_\infty$, where $\bar{Q}_\infty$ is the final ammount of liberated heat in ideal conditions. This is equivalent to assume a linear dependency of the form

$$Q(\xi) = Q_\xi \xi \tag{2}$$

where Q_ξ is the latent heat per unit of hydration extent, here assumed a constant material property.

Because of its thermoactivated character, the evolution of the hydration degree can be defined by an Arrhenius type of expression, in the form (Ulm and Coussy 1996)

$$\dot{\xi} = \widetilde{A}_\xi(\xi) \exp\left(-\frac{E_a}{RT}\right) \geq 0 \tag{3}$$

where E_a is the activation energy of the reaction and R is the constant for ideal gases. The ratio E_a/R can be experimentally determined, and it ranges from 3000 to 8000 ^{o}K for concrete. The function $\widetilde{A}_\xi(\xi)$ is a normalized affinity that completely characterizes the macroscopic hydration kinetics for a given concrete mixture. This function can be obtained experimentally from an adiabatic calorimetric test. Here, we will use the following analytical expression for this function

$$\widetilde{A}_\xi(\xi) = \frac{k_\xi}{\eta_{\xi 0}} \left(\frac{A_{\xi 0}}{k_\xi \xi_\infty} + \xi\right) \left(\xi_\infty - \xi\right) \exp\left(-\bar{\eta}\frac{\xi}{\xi_\infty}\right) \tag{4}$$

where k_ξ, $A_{\xi 0}$, $\eta_{\xi 0}$ and $\bar{\eta}$ are material properties. Figure 1(a) shows the evolution of the temperatures obtained using the proposed thermo-chemical model in adiabatic tests for two typical RC concretes and two conventional Portland concretes. The dots represent the experimental values; the solid line represents the prediction by the model. Note that the adiabatic temperature rise, as well as the hydration rate are smaller for RCC than for conventional concrete.

During the last decades, many aging models have been proposed in which the mechanical properties of young concrete were expressed in terms of the hydration degree, or alternatively, of the maturity (Rastrup 1954; Oloukon et al. 1990). However, there is experimental evidence that the evolution of the concrete strength depends not only on the degree of hydration, but also on the kinetics of the hydration reaction (Byfors 1980; Carino 1981;

Shi and Day 1993; Wild et al. 1995; Tan and Gjorv 1996; Kim et al. 1998). nociteTG Therefore, let us introduce an aging internal variable, κ, so that

$$f^-(\kappa) = \kappa\, f_\infty^- \tag{5}$$

where f^- is the compressive strength and f_∞^- is its final value. Note that κ can be considered a normalized strength variable. Thus, it will be called here *aging degree*.

The evolution of the aging degree $\dot{\kappa}$ is defined in terms of the evolution of the hydration degree $\dot{\xi}$ and the kinetics of the hydtation reaction, in the form

$$\dot{\kappa} = (A_f \xi + B_f) \left(\frac{T_T - T}{T_T - T_{ref}}\right)^{n_T} \dot{\xi} \qquad \dot{\kappa} \geq 0 \tag{6}$$

where A_f and B_f are material constants, where T_{ref} is the reference temperature for the determination of f_∞^-, T_T represents the maximum temperature at which hardening of concrete may occur and n_T is a material property controlling the sensibility to the curing temperature.

According to most codes of practice, other mechanical properties such as the tensile strength f^+ or the elastic modulus E can be related to the compressive strength, and therefore, to the aging degree (Cervera et al. 1999), in the form

$$f^+(\kappa) = \kappa^{2/3}\, f_\infty^+ \qquad \text{and} \qquad E(\kappa) = \kappa^{1/2}\, E_\infty \tag{7}$$

where f_∞^+ and E_∞ are final values, when the hydration process is completed.

Figure 1(b) shows curves of evolution of the compressive strength obtained using the proposed thermo-chemical model in isothermal tests (at 20 ^{o}C) for two typical RC concretes and two conventional Portland concretes. The dots represent the experimental values; the solid line represents the prediction by the model. Note that the compressive strength is smaller for RC concretes, because of their low cement content. Also, the strength rate of evolution is slower, as it is related to the hydration rate.

Figure 1(c) shows curves of evolution of the compressive strength for a typical RCC in isothermal tests conducted at three different curing tempeartures: 10 ^{o}C, 20 ^{o}C (reference value) and 30 ^{o}C. The effect of the curing temperature is twofold: (a) the hydration reaction is accelerated by the increase in curing temperature; and (b) a significant loss of strength is observed with increasing curing temperature. The first effect is particularly evident at the iniatiation of the hydration process, with the activation phase being shortened as the curing temperature is increased. The second effect makes, for instance, that concrete cured at 30 ^{o}C shows a loss of attainable strength of more than 20 %, compared to the one cured at 10 ^{o}C.

Figure 1(d) shows curves of relative evolution of the normalized compressive strength, tensile strength and elastic modulus in terms of the aging degree. The functional dependencies expressed by Eq. (7) need to be experimentally confirmed. In de Schutter and Taerwe (1996) it was reported that the tensile strength develops faster than the compressive strength, but slower than the elastic modulus. Available experimental results for conventional concretes are consistent with the present proposal of 2/3 and 1/2 exponents for the evolution of the tensile strength and the elastic modulus, respectively. More experimental evidence is needed to confirm that these values can also be applied to RCC.

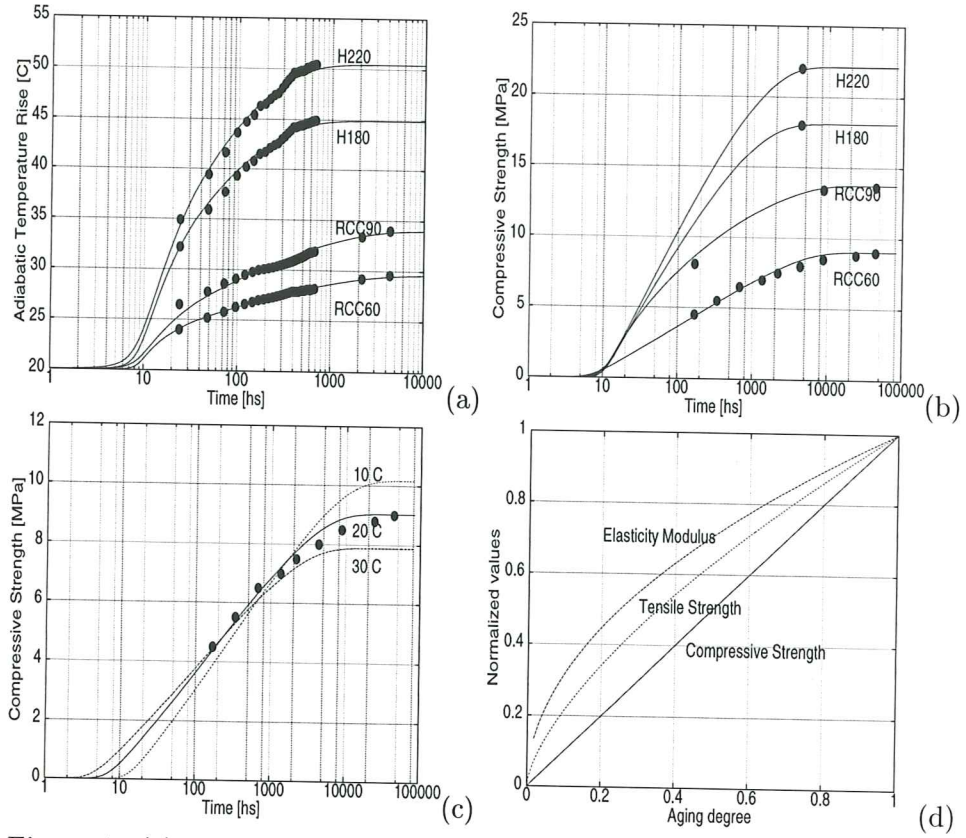

Figure 1: (a) Temperature evolution; (b) Strength evolution; (c) Effect of curing temperature; (d) Relative mechanical aging.

URUGUA-Í DAM

The Urugua-í Hydroelectric Project is located in the Province of Misiones, North East of Argentina. The dam is owned by Electricidad de Misiones SA, and it has been built at the Urugua-í river, 8 km upstream from the confluence with the Paraná river, 127 m over the sea level.

The zone has a hot, sub-tropical climate, without dry season. Its annual mean climate values are: temperature 20 ^{o}C (ranging from 11 ^{o}C in winter to 27 ^{o}C in summer), relative humidity 80 %, wind velocity 4 km/h, annual rainfall 1750 mm, annual evaporation 1168 mm.

The RCC project was approved as an alternative to the originally designed rockfill dam with concrete facing. The change was based on significant savings in time and construction costs. The project represented quite a challenge because it was the first experience of an RCC dam in Argentina while at the same time being one of the largest Rcc dams in the world at that moment. Also, the project included some outstanding features like a very low cement content in the mix and the consideration of a PVC membrane as impervious barrier.

Information on some of the design criteria used and results from the thermal analyses performed at the design stage, as well as on construction process of the dam, and its behaviour during and after its completion can be found in Giovambattista (1995), Buchas and Buchas (1991) and Lorenzo and Calivari (1991).

Geometry

The main dam is a straight RCC gravity structure, 76 m high and 676 m long. In the central part, there is a 170 m long uncontrolled spillway, with a bridge over it. Maximum width at the base is 57 m. Crest elevation is 203 m. The total volume of concrete is 600,000 m^3.

Figures 2 and 3 show a cross section and a longitudinal front view, respectively. Note that the slope of the dowstream face is 1:0.8, which is rather common in RCC dams. The development of main contraction joints is induced by the inclusion of plastic films to define pre-cut areas. They were placed in agreement with abrupt changes in the foundation or in dam geometry. The distance between the two main transverse joints is 227.25 m. Secondary pre-cut joints were placed from elevation 182 up every 70-90 m, approximately.

The foundation was built in conventional Portland concrete (CPC). Upstream facing consists of precast reinforced concrete panels anchored in the mass of the dam, a continuous 2 mm PVC membrane and conventional Portland concrete (CPC) 0.50-0.90 m thick. Facing concrete has contraction joints every 14.24 m in the spillway and 20.20 m elsewhere. These jointd are 1.20 m deep and run into the RCC.

Material Properties

Four different types of concrete were used in the dam:

- the foundation was built in CPC with a cement content of 180 kg/m^3 (H180),
- the upstream facing and the spillway crest was built in CPC with a cement content of 220 kg/m^3 (H220),
- the body of the dam was built in RCC with a low cement content of 60 kg/m^3 (RCC60), but
- the interface between the dam and the foundation (0.80 m high) was builtin RCC with a cement content of 90 kg/m^3 (RCC90).

All RCC and CPC were made with Portland cement similar to Type II ASTM, without pozzolanic admixtures. Table 1 summarizes the relevant material properties for the four types of concrete.

Properties	H180	H220	RCC60	RCC90	Rock
w/c	0.50	0.50	1.60	1.00	—
$\rho\ [Kg/m^3]$	2,440	2,400	2,500	2,500	2,700
$C\ [10^{-6} J/m^3\,{}^oC]$	2.35	1.95	2.49	2.44	2.37
$k_T\ [J/m\,hs\,{}^oC]$	6,807	6,807	6,987	6,109	7,740
$\alpha_T\ [10^6]$	6.0	8.0	7.40	8.33	—
$Q_\xi\ [10^{-7} J/m^3]$	7.79	9.50	2.57	3.97	—
$f_\infty^-\,[MPa]$	18.0	22.0	9.0	13.6	50.0
$f_\infty^+\,[MPa]$	2.0	2.2	0.875	1.36	5.0
$E_\infty\,[GPa]$	31.0	38.0	14.0	22.0	30.0

Table 1: Material Properties for Urugua-í Dam.

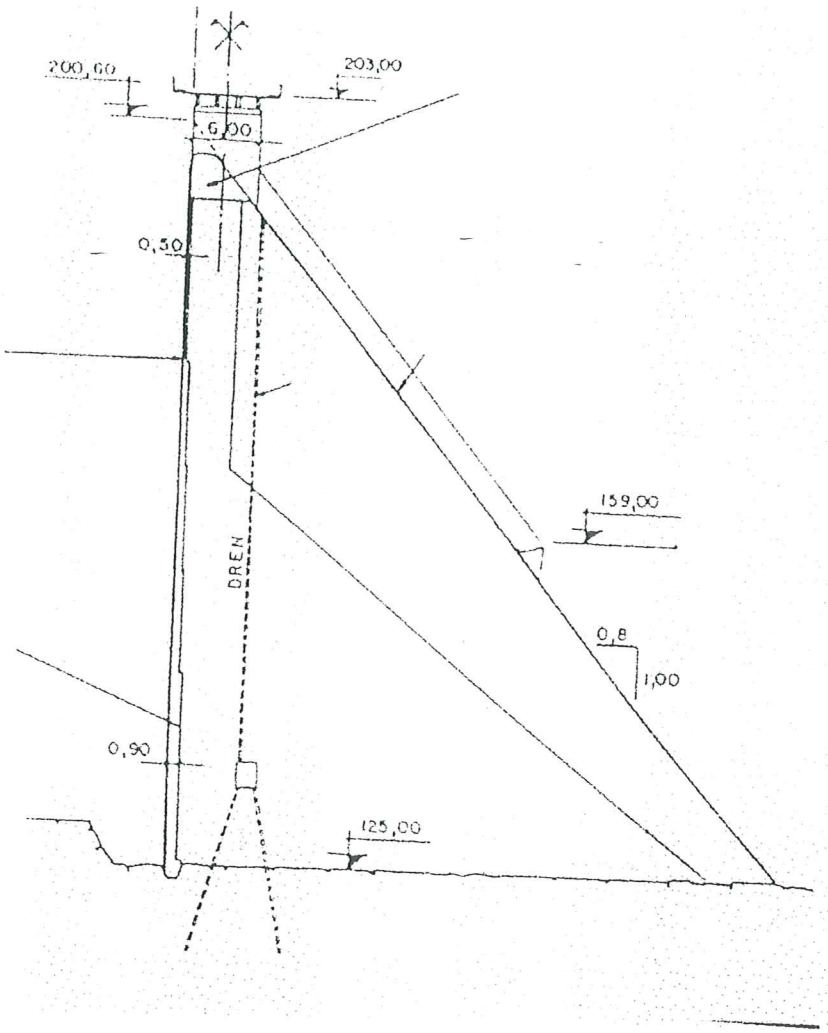

Figure 2: Cross section of Urugua-í Dam.

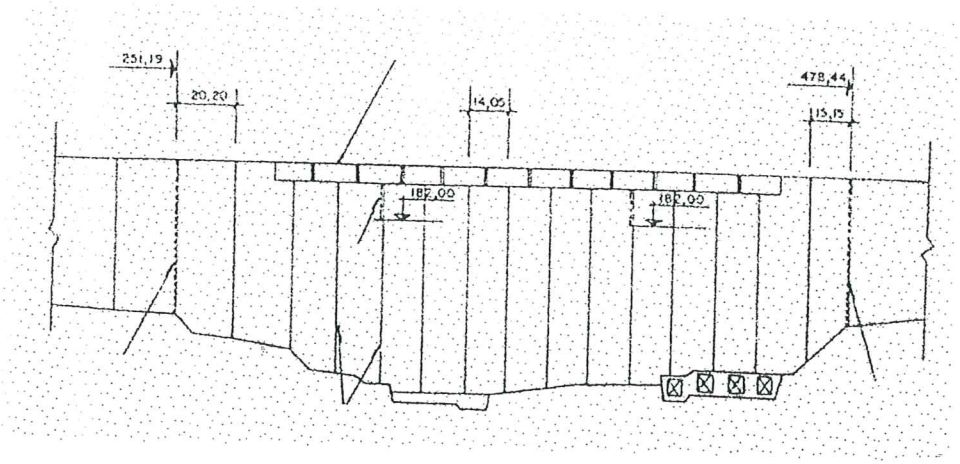

Figure 3: Longitudinal front view of Urugua-í Dam.

Figure 1(a) shows the evolution of the temperatures obtained using the proposed thermo-chemical model in adiabatic tests for the four types of concrete. Figure 1(b) shows curves of evolution of the compressive strength obtained using the proposed thermo-chemical model in isothermal tests for the four types of concrete. The dots represent the experimental values; the solid line represents the prediction by the model.

Construction Process

Concreting of the foundation and the shear key began in January 1988 and was completed in March of the same year. RCC placing began in April 1988 and finished in March 1989. Therefore, it can be considered that the constrution of the body of the dam took one year, approximately. The reservoir filling started in December 1989 and reached the spillway level in July 1990.

The dam was built with 40 cm thick lifts. The placement interval between lifts was 48 hs, approximately (up to elevation 191). Therefore, the placing speed can be estimated as $V = 20$ cm/day. The relative placing speed is $\bar{V} = V/H = 2.63$ x 10^{-3} 1/day $= 0.96$ 1/year, where H is the dam height.

Table 2 summarizes the main features of the construction process.

Height	76 m
Length	676 m
Base width	57 m
Concrete Volume	600,000 m^3
Lift thickness	40 cm
Placing speed	20 cm/day
Relative placing speed	0.96 1/year
Starting date	April 1988
Completion date	March 1989

Table 2: Main features of Urugua-í Dam.

THERMAL ANALYSIS

In this Section, results from thermal analyses performed on a numerical model of Urugua-í RCC Dam are presented. Firstly, results from the 2D basic case, simulating the real construction process of the dam are discussed. Secondly, results from simplified 1D vertical simulations are presented in order to assess the validity of these type of calculations. Finally, some parametric studies are performed to establish the effect of some major variables of the construction process that may have an influence in the temperature distribution and evolution: the placing temperature, the starting date and the placing speed.

Numerical Model

The numerical model used for the 2D thermal analyses consists of a finite element discretization of the central cross section of the dam. The mesh

represents the body of the dam (from elevation 125 to elevation 189), plus the foundation (from elevation 115 to elevation 125) and some surrounding foundation rock (down to elevation 90). The dam is formed by 157 RCC lifts 0.40 m thick. The upstream facing and the spillway crest, both cast in H220 concrete are also included in the model.

Table 3 summarizes the material properties used for in the numerical simulation.

Properties	H180	H220	RCC60	RCC90
w/c	0.50	0.50	1.60	1.00
ξ_∞	0.75	0.75	0.93	0.86
$k_\xi/\eta_{\xi 0}\ [x10^{-8}1/hs]$	0.25	0.2	0.35	0.35
$\overline{\eta}$	7.0	7.0	8.5	8.5
$A_{\xi 0}/k_\xi x10^4$	1.0	1.0	1.0	1.0
$E_a/R\,[^oK]$	5,000	5,000	5,000	5,000
$Q_\xi\ [10^{-7}J/m^3]$	7.79	9.50	2.57	3.97
ξ_{set}	0.2	0.2	0.2	0.2
A_f	1.51	1.51	1.16	0.45
B_f	0.19	0.19	0.0	0.92
$f_\infty^-\,[MPa]$	18.0	22.0	9.0	13.6
$T_T\,[^oC]$	100	100	100	100
$T_{ref}\,[^oC]$	20	20	20	20
n_T	0.0	0.5	1.0	1.0

Table 3: Material Properties for Numerical Simulations.

The numerical model used allows to simulate the actual evolutionary construction process of the dam. To this end, the finite elements corresponding to the different concrete lifts are progressively activated at the times corresponding to their respective placing in the dam.

Concreting of the foundation and the shear key starts on January 15 and finishes on March 16. This is assumed to consist of 8 layers placed one per week. The placing of the dam starts on April 4, 23 days after the foundation is finished. Placing of the RCC concrete is simulated by assuming a constant placing interval of 2 days; therefore, lifts are activated one at the time, every 2 days. A break of 15 days is kept in the second half of December during the Christmas holidays.

The initial temperature of the activated elements is automatically set equal to the corresponding placing temperature. For the reference simulation case the placing temperature of each lift is taken as equal to the ambient temperature corresponding to the placing date + 5 ^{o}C. This increase in the placing temperature is assumed to be due to the stocking conditions and the manipulation operations performed during the production process of the concrete. The initial temperature of the foundation rock is assumed to vary linearly from the ambient temperature at the surface (elevation 125) to 10 ^{o}C at the bottom of the model (elevation 90).

During the construction of the dam, temperature at the boundaries in contact with the air is automatically set equal to the ambient temperature at the corresponding date. After the completion of the dam, the analysis is continued for the subsequent eleven years, to be able to follow the evolution on the temperatures during the cooling process. To this end, the ambient

temperature is automatically adjusted to follow the average cyclic seasonal thermal variation in the area. The reservoir was filled in July 1990, and from that time on the temperature in the water and therefore, at the upstream wall, is assumed to vary linearly between the ambient temperature at the surface and the upper layer of rock at the bottom of the reservoir.

Numerical 2D Simulation

In the 2D model, every lift is discretized into 25 elements across and 2 elements thick, thus resulting in 7,850 elements in the dam body. The mesh is finer near the up and dowstream faces to represent the CPC facing and to capture the boundary thermal effects. The total number of elements in the mesh is 9,500 including the foundation.

The time step used in the analysis during the construction of the dam is 12 hs, so that once a lift is activated four time steps pass before a new lift is placed above. During this time the temperature of the newly placed concrete varies according to the ambient temperature on top and the temperature of the concrete already placed below. During these two days the concrete reaches a significant hydration and aging degree before another lift is placed on top. An automatic subincrementation technique is used within the time step to accurately integrate the evolution of the hydration and aging degrees, Eqs. (3) and (6), at these extremely early ages.

Figure 4 compares the computed and in situ measured temperature evolution for two points located at elevation 130 m and distances 2,00 m and 22,00 m from the upstream face, respectively. The ambient temperature throughout the year is also plotted. This elevation corresponds to the lower lifts in the body of the dam (RCC60), placed in April directly over the finished foundation. Agreement between the predicted curves and measured temperatures is remarkable. Note that the point located closer to the upstream wall reaches a slighly higher temperature just after being placed. This is due to its proximity to the upsteam facing, made of H220, and with a higher hydration heat. Note also that this point is quite sensitive to the variation of the ambient temperature. On the other hand, the innermost point is much more isolated by the surrounding concrete. No horizontal heat flux occurs in the interior of the dam. The very smooth temperature decrease that occurs there is due to heat conduction in the vertical direction towards the upper surface and towars the foundation and the rock below.

Figure 5 shows the temperature evolution for interior points corresponding to lifts placed with 1 month interval between them. The corresponding (placing month) elevations are: (4) 129 m, (5) 135 m, (6) 141 m, (7) 147 m, (8) 153 m, (9) 159 m, (10) 165 m, (11) 171 m, (12) 177 m, (1) 179 m and (2) 185 m. Higher temperature rises appear at the bottom lifts (April to July), because of the heat comming from the hydration of the H180 concrete in the foundation and in the lifts placed during the austral summer (December to February), between elevations 180 and 190. Note the temperature drop that occurs for the lifts placed in December because of the concreting break during Christmas. The temperature is still rising in most of the dam after completion, and more steeply in those lifts placed during winter (July to August). This is because heat conduction between vertically adjoining lifts continues for a long period of time after placement. The bottom lay-

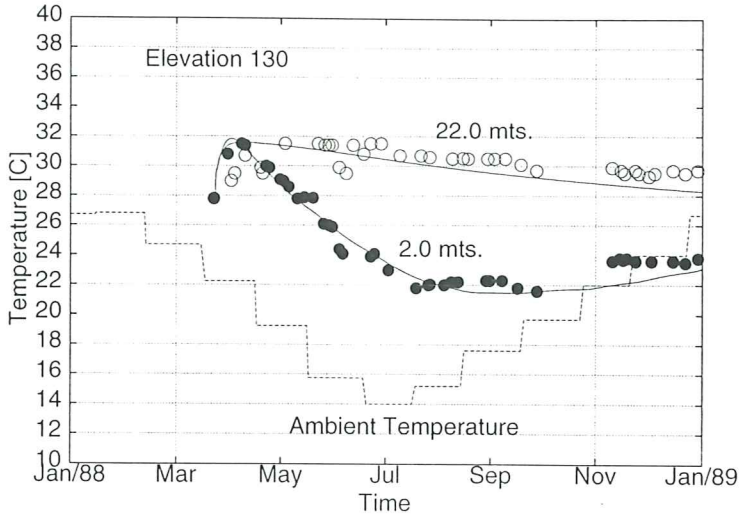

Figure 4: Temperature evolution in the dam.

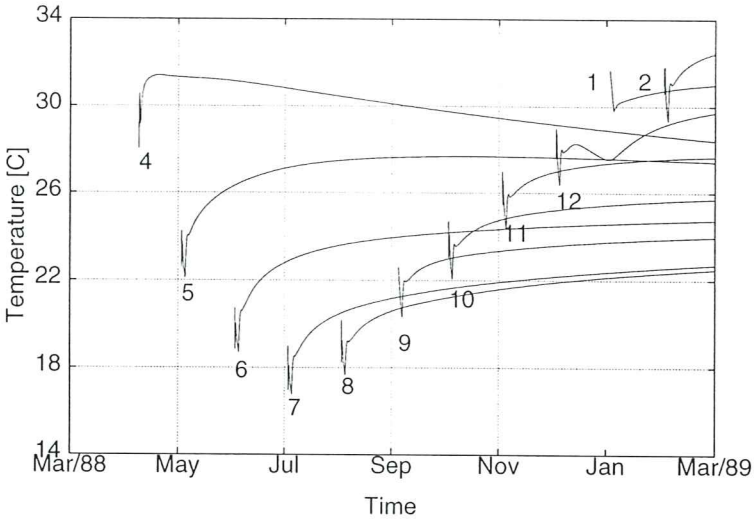

Figure 5: Temperature evolution for different elevations.

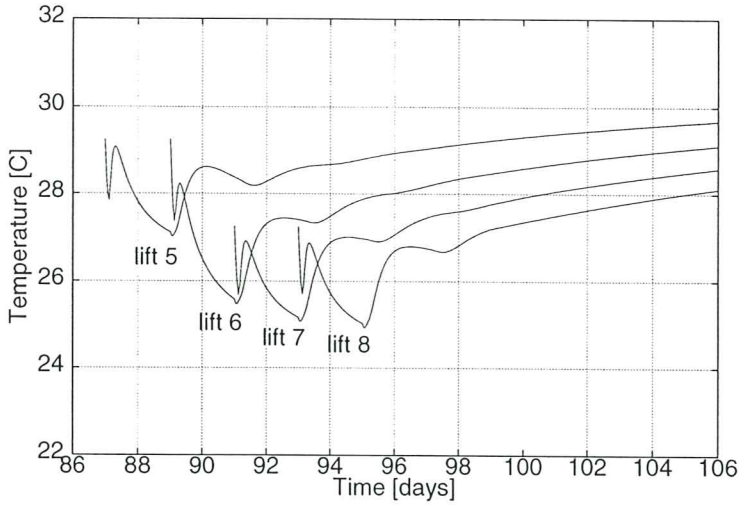

Figure 6: Temperature evolution for four consecutive lifts.

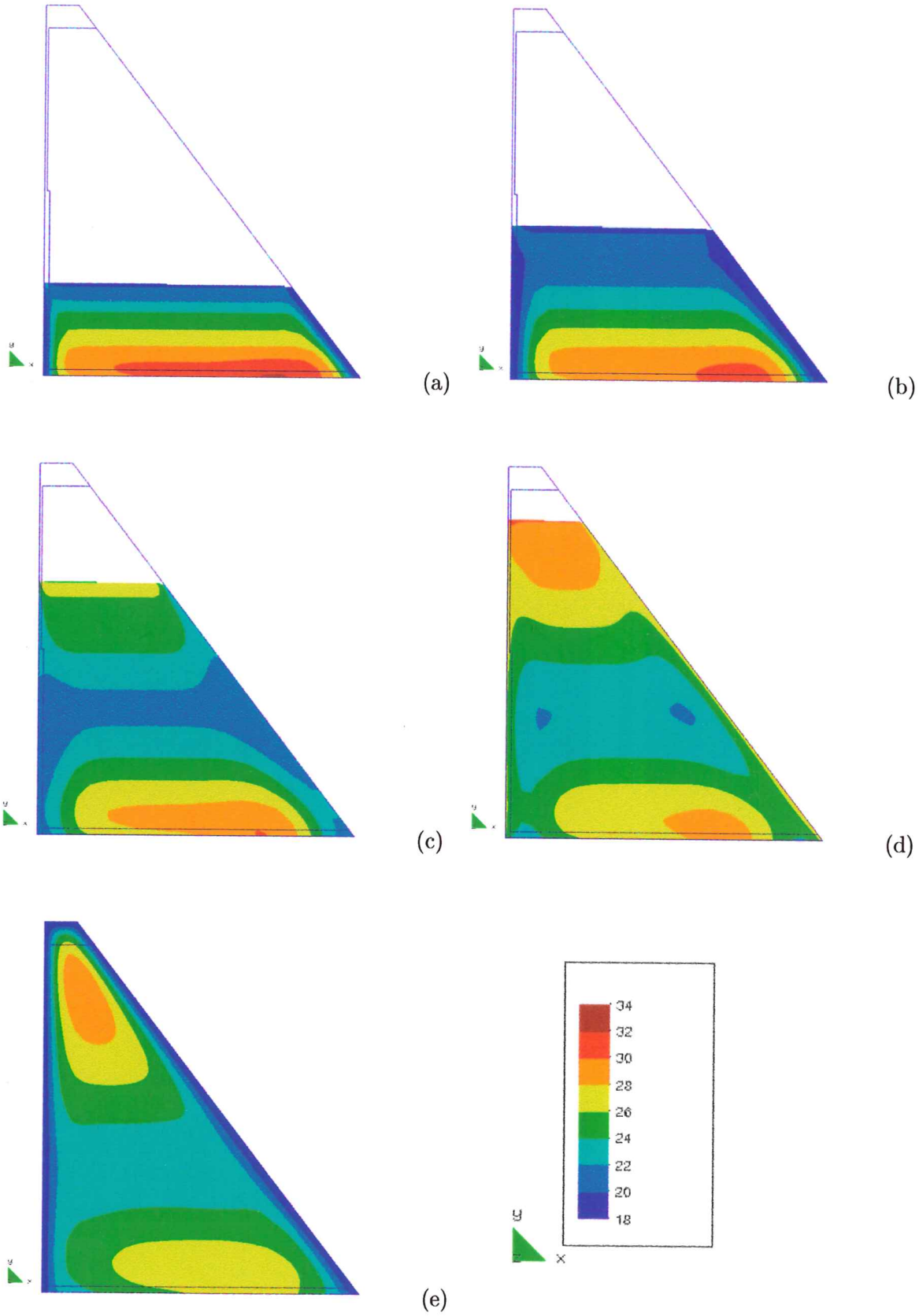

Figure 7: Short term evolution of temperatures.

ers start to cool shortly after being placed because of the heat conduction towards the foundation rock.

Figure 6 shows a detail of the temperature evolution for lifts 5, 6, 7 and 8 just after their placement (during the end of April and the beginning of May). Note how the temperature initially drops because of the difference between the placing and the ambient temperatures (+ 5 ^{o}C). Shortly after, it starts to rise due to the heat released during hydration and heat flux comming from below; a first peak temperature is attained due to the heat lost through the upper surface; temperature continues to rise again as soon as the upper lift is placed, due to vertical heat conduction; with the placing of a new lift, the cycle is repeated, every time with a smaller amplitude due to the increasing distance of the concrete to the upper exterior surface. It must be noted that this very short term oscillations in the temperature would be amplified for thinner lifts or larger placing intervals, that is, for lower production rates; on the contrary, they would be reduced for thicker lifts or shorter placing intervals, that is, for higher production rates. In any case, the temperature drop due to natural surface cooling does not influence significantly the overall evolution of temperature in the dam. Forced surface cooling may be used for temperature control, but it is not as effective as precooling of the concrete and it may lead to superficial cracking due to the forced temperature gradients (Fujisawa and Nagayama 1985).

Figure 7 shows contour plots for the evolution of the temperatures in the body of the dam during the construction process (1 year). The corresponding month–elevations are: (a) June/88 146 m, (b) August/88 157 m, (c) November/88 175 m, (d) February/89 187 m and (e) June/89 196 m. As mentioned above, the higher temperatures correspond to the foundation and those lifts located immediately over it, because of the higher hydration heat of concrete used there, and to the lifts located between elevation 180 and elevation 190, placed during the austral summer (December to February), when the ambient (and placing) temperatures are higher. Note also how the ambient temperature varies according to the seasonal oscillation. Due to the low thermal conductivity of concrete, temperature gradients due to the difference between the ambient and inside temperatures are evident, although they are limited to a distance of about 2 m from the exterior faces. These temperature gradients may lead to thermally induced superficial cracking in these faces, and because of this transverse contraction joints are cut in the facing every 14.24 m, 1.20 m deep and running inside the RCC.

Figure 8 shows contour plots for the distribution of the compressive and tensile strength after 1 year, at the time of the completion of the construction. Note that the strength distribution is not homegeneous, because of the different curing conditions ocurred at different locations. Higher strength is attained for concrete placed during the winter, at lower temperatures, at mid-height of the dam, while lower strength is attained for concrete placed during the summer, at higher temperatures, at the bottom and top parts of the dam. The distributions of compressive and tensile strengths are similar but not identical because of their different dependence on the aging degree, Eqs. 5 and 7. The prediction of the actual distribution of tensile strength is important for the evaluation of the risk of cracking due to thermal straining.

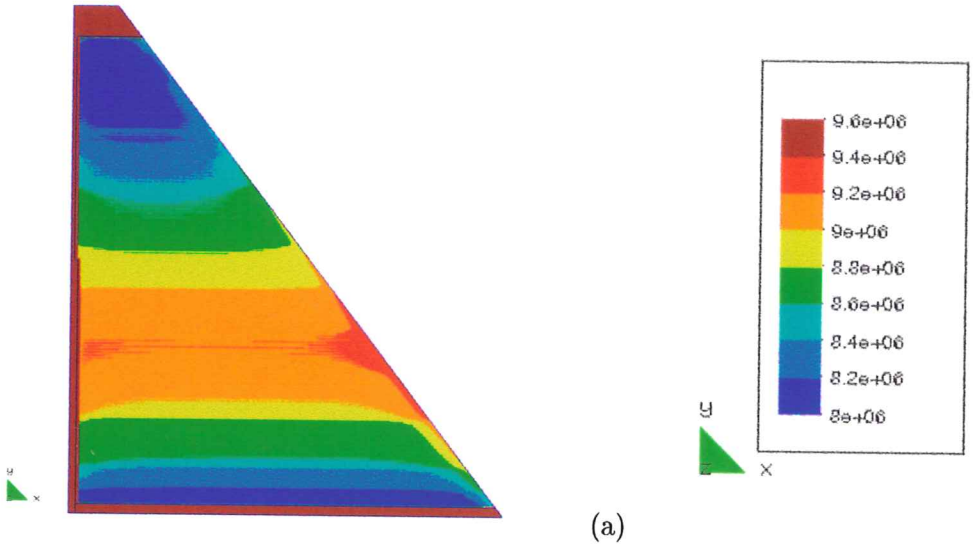

(a)

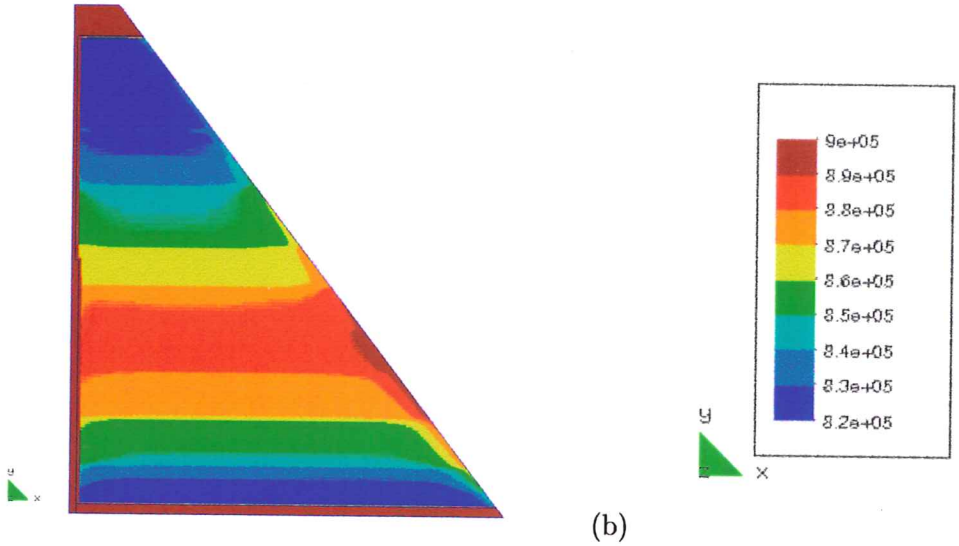

(b)

Figure 8: Distribution of : (a) Compressive strength; (b) Tensile strength, at the completion of the dam (1 year).

Figure 9 shows the long term temperature evolution for three interior points located at elevations: (a) 153 m, (b) 165 m and (c) 177 m described in figure 5. The thermal analysis is run now for 11 years after the dam completion. It is clear that the temperature in the interior of the dam decreases progressively, as the heat generated during the hydration process is released through the up and downstream faces. The final stable temperature in the interior of the dam will be approximately equal to the mean annual temperature (20 ^{o}C). The temperature drop is faster for the upper elevations, both because they were placed in summer and because they are more exposed to the ambient temperature. This temperature drop may lead to thermal induced cracking in the interior of the dam; therefore the necessity of placing transverse contraction joints from elevation 182 up every 70-90 m. Note also that the seasonal oscillation of the ambient temperature is only noted for the point located at higher elevations, while the bottom part of the dam body is virtually unaffected by it.

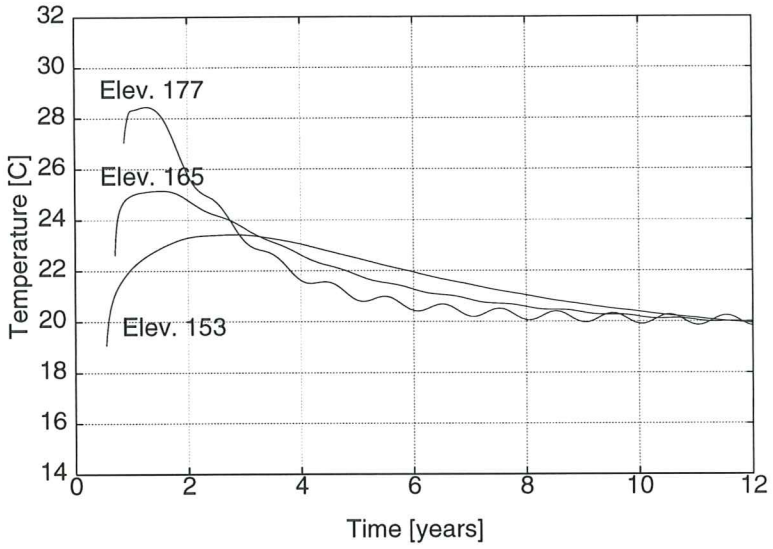

Figure 9: Long term temperature evolution for different elevations.

Figure 10 shows contour plots for the evolution of the temperatures in the body of the dam for the 10 first years after dam completion. All the snapshots correspond to the temperature distribution in winter (June). The corresponding years are: (a) 1989, (b) 1990, (c) 1991, (d) 1994 and (e) 1999. Note how the overall temperature is progressively lower, as heat is dissipated to the enviroment and, to a minor extend, to the foundation rock. The cooling is faster in the upper part of the dam, where the outer surfaces are closer. The upper 'hot spot' has completely vanished in two years. The lower 'hot spot' is still visible after five years although temperature has already drop more than 5 ^{o}C. It has also 'migrated' upwards due to heat flux towards cooler parts of the dam body. After 10 years the heat 'stored' during the construction process has virtually disappeared. The dam is then in thermally stable regime, subjected only to the cyclic seasonal oscillations.

Finally, figure 11 shows contour plots for the evolution of the temperatures in the body of the dam for the eleventh year after dam completion, once the cooling process is completed. The snapshots corresponding month/year are: (a) June/2000, (b) September/2000, (c) December/2000, (d) March/2001 and (e) June/2001. The variation of the ambient temperature is observed in the downstream wall. The temperature distribution in June is typical of winter, while that in December is typical of summer. In September (spring) and March (autumn) the effect of the thermal variations in the water in the reservoir are evident in the upper part of the upstream wall.

Numerical 1D Simulation

Thermal simulations of the construction process of concrete dams are usually done using simplified 1D models, see for instance Yamazumi et al. (1995). The reason for this is that most of the concrete mass in the dam is placed too far away from the up and dowstream faces to be influenced by the heat losses through them. Therefore, a 1D vertical model in which the horizontal heat flux is prevented seems representative of the real conditions inside the dam body.

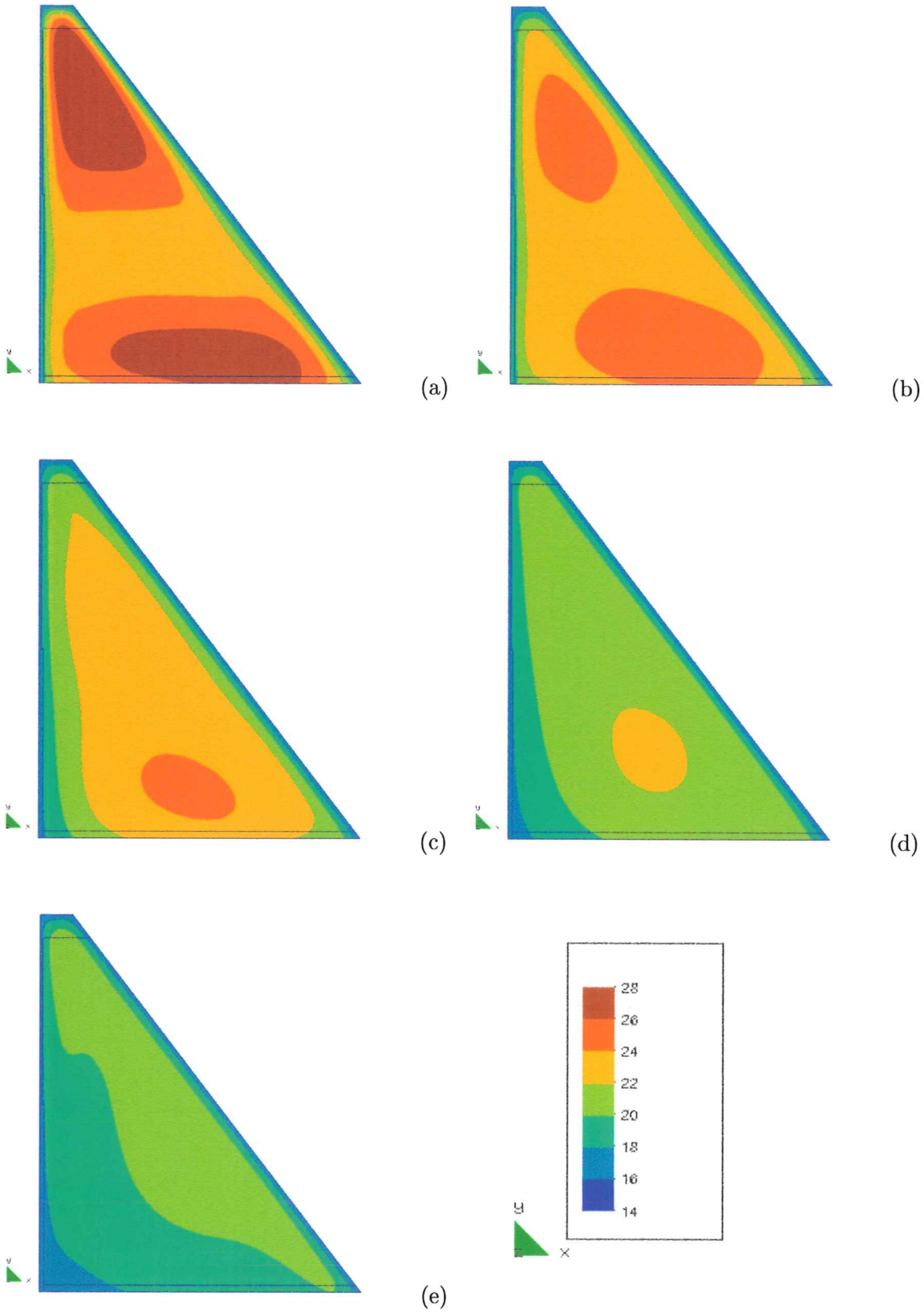

Figure 10: Long term evolution of temperatures.

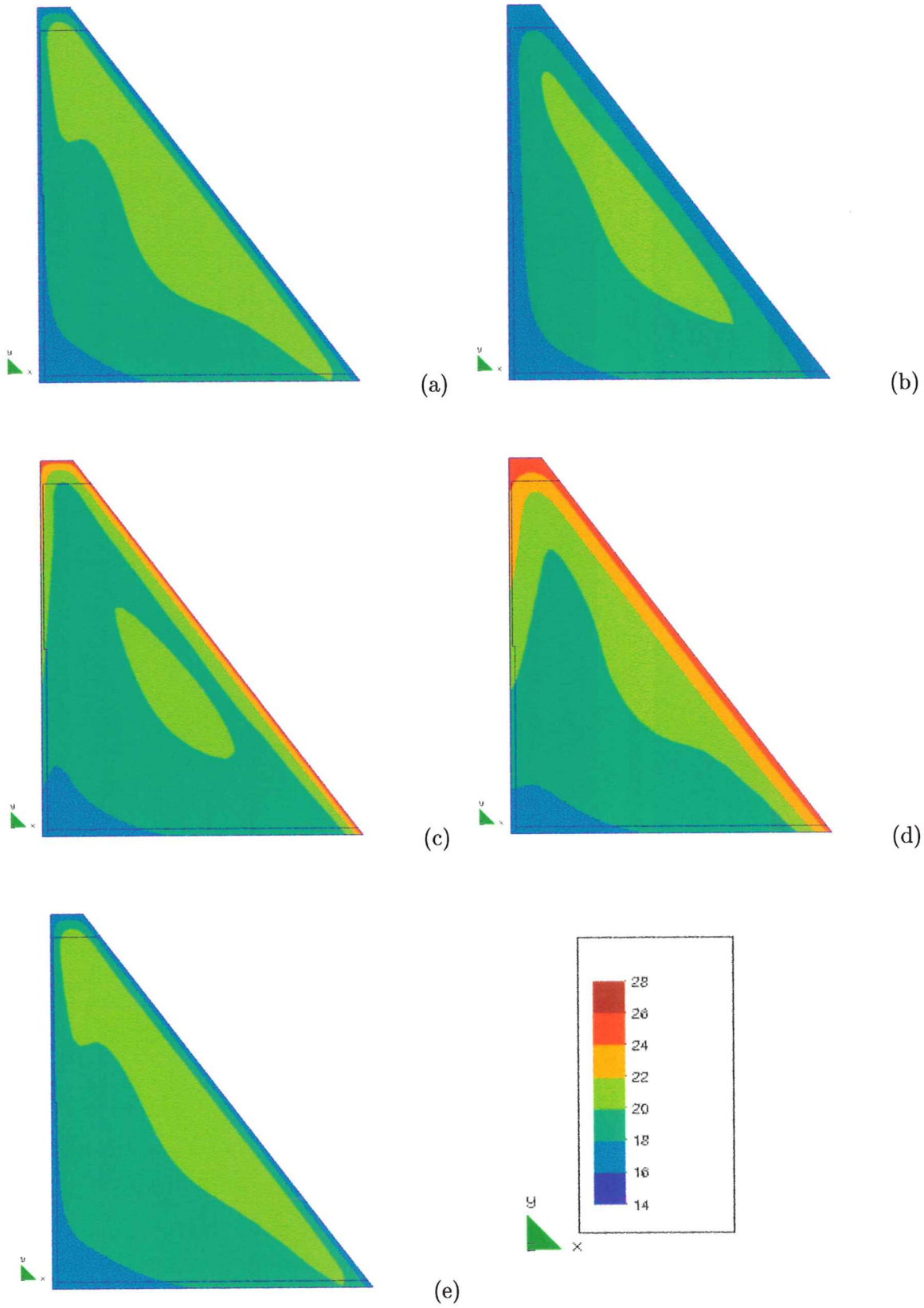

Figure 11: Seasonal thermal variation.

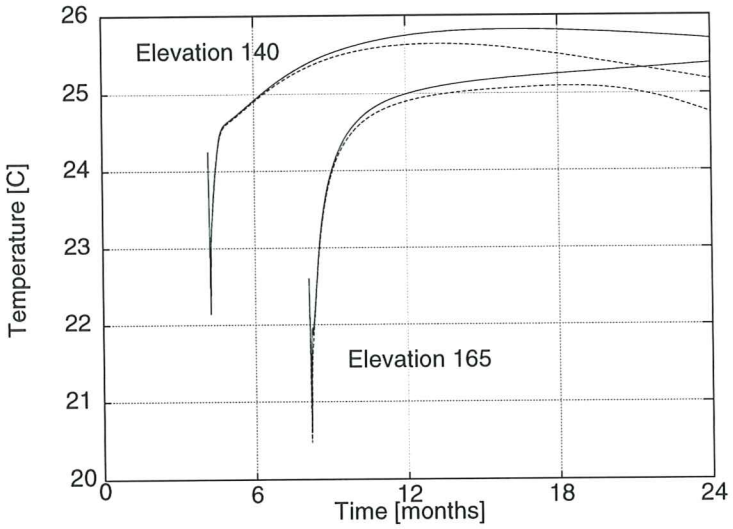

Figure 12: Long term temperature evolution for different elevations computed using 1D (solid line) and 2D (dashed line) models.

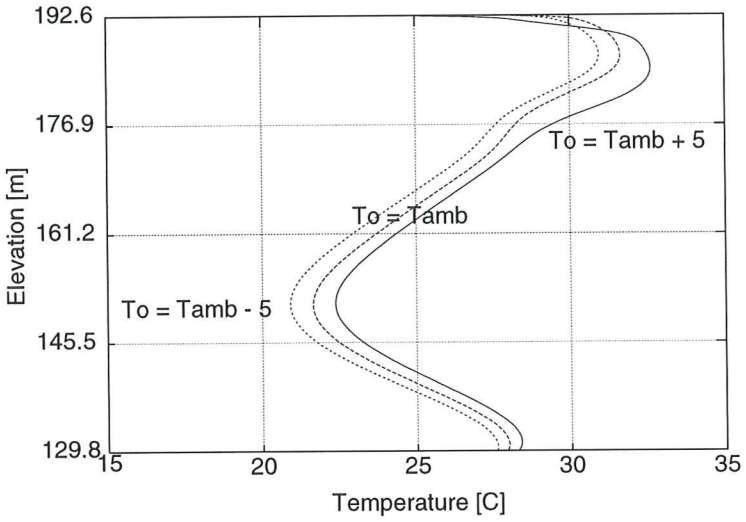

Figure 13: Influence of the Placing Temperature.

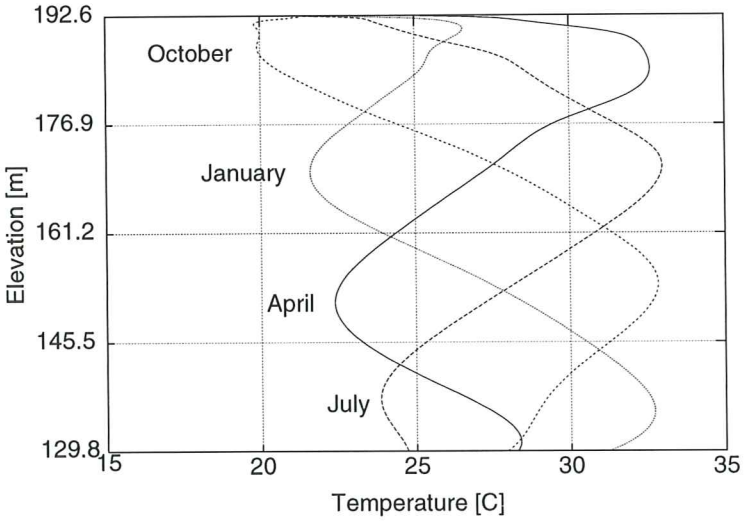

Figure 14: Influence of the Starting Date.

To validate this approach, a 1D vertical model of the Urugua-í RCC Dam is constructed, following exactly the same guidelines described for the 2D model. Therefore, the vertical size and distribution of the finite elements, the material properties, the initial and placing temperatures, as well as the overall activation strategy for the lifts are the same as described above.

Figure 12 shows the comparison between the computed evolution of temperatures using the 2D and 1D models, for two different (placing month) elevations: (a) May 140 m and (b) September 165 m. Points in the 2D model are located half way between the up and dowstream faces. The solid lines represent the 1D results, while the dashed lines represent the 2D solution.

The plot shows that results obtained using the 1D model virtually overlap with those obtained using the 2D model during the first year, that is, during the duration of the construction process. Later, the 1D model clearly underestimates the temperature drop, as it cannot represent the main thermal dissipation mechanism of the real dam: horizontal heat flux through the facing.

Thus, it can be concluded that 1D vertical thermal models can accurately predict the vertical distribution of the temperature inside the dam body during the construction process, which is in itself a very useful information. Obviosly, they cannot provide information on the thermal gradients developed near the faces of the dam, nor about the transient of the long term temperature drop until the final stable temperature distribution is reached.

Parametric Studies

Despite their simplicity, 1D vertical models can be very useful to perform parametric studies on the influence of the major variables in the construction process that may affect the final temperature distribution inside the dam, and this at an extremely low cost. In this Section some of these example simulations will be performed for the Urugua-í RCC Dam.

Influence of the Placing Temperature

In order to investigate the influence of the placing temperature of the concrete, T_0, compared to the ambient temperature at the time of placing, T_{amb}, three different cases are compared: (a) $T_0 = T_{amb} + 5\ ^o\ C$ (no precooling, reference case), (b) $T_0 = T_{amb}$ (mild precooling), and (c) $T_0 = T_{amb} - 5\ ^o\ C$ (intense precooling).

Figure 13 shows the comparison between the computed vertical distribution of temperatures for the three cases at the time of the completion of the dam. It can be seen that, although the precooling of the concrete before being placed obviously results in lower temperatures in the final distribution, the efficiency of the procedure is quite limited and it can be evaluated at about 20 % for the studied case. The reason for this can be found in figure 6 where it is evident that for the lift thickness used in Urugua-í Dam the heat flux across the exposed upper surface of the lift just being placed is enough to quickly reduce the difference between the concrete and the ambient temperatures. Precooling would obviously be more effective for: (a) thicker lifts, due to the low conductivity of concrete, or (b) faster placing speed, as this would reduce the time that a newly placed lift is exposed to the ambient temperature.

Influence of the Starting Date

In order to investigate the influence of the starting date for concreting four different cases are compared: (a) Starting in April (austral autumn, reference case), (b) Starting in July (austral winter), (c) Starting in October (austral spring), and (d) Starting in January (austral summer).

Figure 14 shows the comparison between the computed vertical distribution of temperatures at the completion of the dam for the four cases. For case (a), starting in April, highest temperatures are attained close to the foundation and near the crest. The later problem can be dealt with providing transverse joints in the upper part of the dam. For cases (b) and (c), starting in July and October, respectively, highest temperatures are attained at mid-height and, therefore, they would require much deeper transverse joints. Case (d), starting in January, is the possible worst, as highest temperatures are attained immediately above the foundation, and this would require full section transverse joints.

It is interesting to note that the maximum temperatures attained for all cases are very close, as these mainly depend on the placing and ambient temperatures and the heat released during the hydration process. However, minimum temperatures *at the completion of the dam* vary from one case to the other, as heat conduction inside the dam tends to rise the temperature of those lifts placed at lower temperatures.

Influence of the Placing Speed

In order to investigate the influence of the relative placing speed of the concrete $\bar{V} = V/H$, where H is the dam height, three different cases are compared: (a) $\bar{V} = 1.0$ 1/year (reference case), (c) $\bar{V} = 2.0$ 1/year (double speed), and (b) $\bar{V} = 0.5$ 1/year (half speed). Figure 15 shows the comparison between the computed vertical distribution of temperatures for the three cases.

Figures 15(a) and (b) show results for the reference case, where the dam is completed in a year. The black band in figure 15(a) represents the range between the ambient and the placing temperatures and, therefore, gives a graphic idea of the initial thermal conditions. The solid line in the figure shows the temperature distribition at the completion of the dam. The increase in temperature is due to the heat released during the hydration process. This distribution is compared in figure 15(b) with the dashed line representing the temperature one year after the completion of the dam. Note how the heat conduction inside the dam has already diminished the thermal gradients in the dam body, cooling the warmer parts and warming the cooler parts. Note that the complete thermal variations over the construction year are reflected in both figures.

Figures 15(c) and (d) show results for the second case, where the placing speed is doubled and the dam is completed in a half year. Now the dam is built between autumn and spring, and the hotter summer season is avoided. Note first that the difference beetween the placing and the final temperatures is larger than in the previous case. At faster placing speed the loss of hydration heat through the upper lift surfaces is smaller and the temperature rise is closer to the one measured under adiabatic conditions. Also, temperature at the bottom is higher than for the previous case

as heat conduction towars the foundation rock is just beginning after six moths. Note that after 1 year the temperature in the middle part of the dam is stiff increasing. This means that at the completion of the dam the hydration and aging process has not been completed yet.

Figures 15(e) and (f) show results for the third case, where the placing speed is halved and the dam is completed in two years. Note that the complete thermal variations over the two construction years are reflected in both figures. Heat conduction plays a significant role in this case; this is quite evident in the final distribution in the bottom half of the dam and, more so, in the distribution after one year, where the peaks in the curve have been very much diminished.

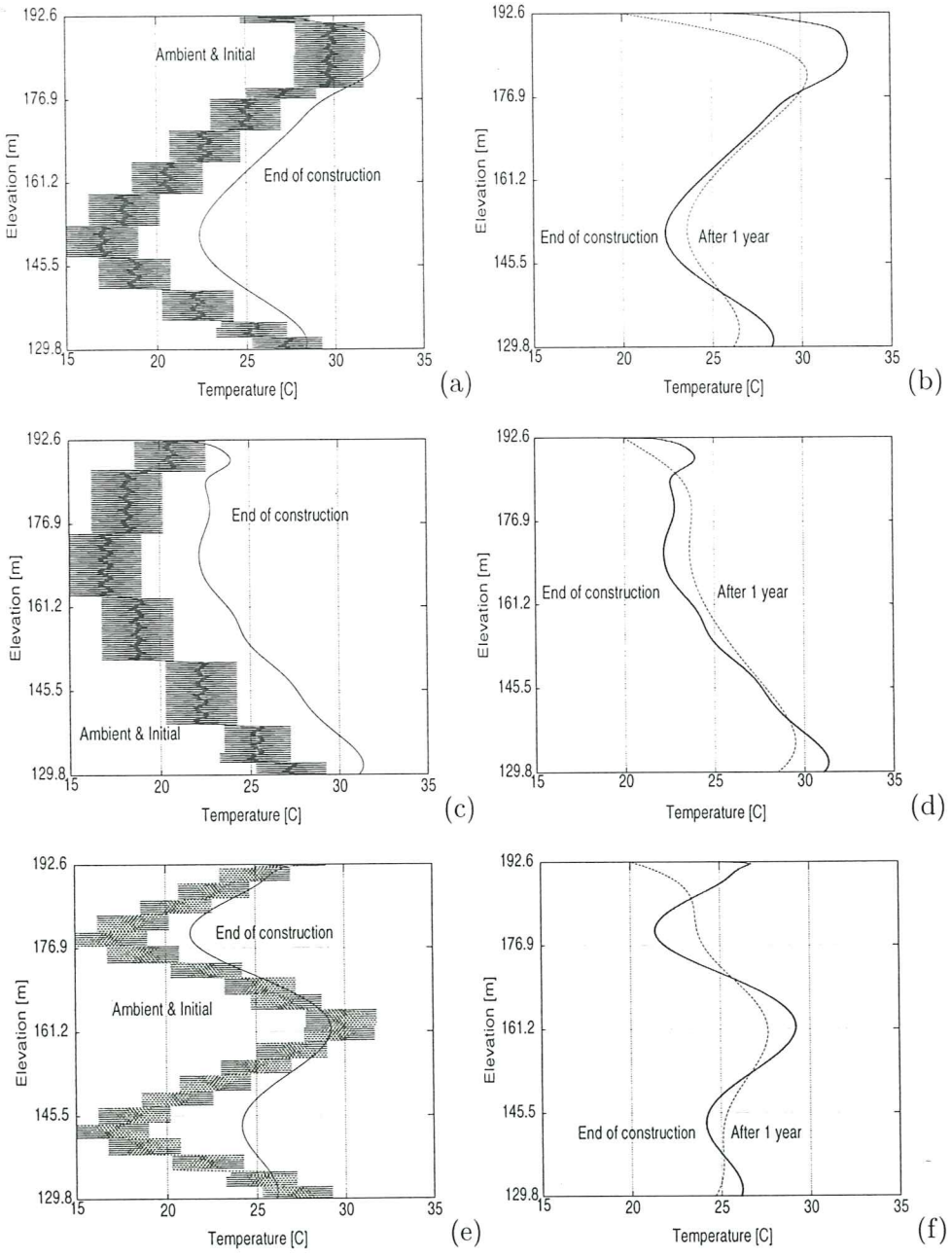

Figure 15: Influence of the Placing Speed.

CONCLUSIONS

This work presents a numerical procedure to simulate the thermal analysis of the evolutionary construction process of roller compacted concrete dams.

The basis of the work is a coupled thermo-chemo-mechanical model for the behaviour of concrete at early ages that allows to simulate the observed phenomena of hydration, aging, damage and creep. In this first part only the thermo-chemical aspects of the simulation of the construction process are presented, while the simulation and discussion of the mechanical aspects of the problem are relegated to a companion paper that follows.

The proposed procedure is shown to be able to accurately predict the evolution in time of the hydration degree and the hydration heat production. The new concept of the aging degree, different from the commonly used hydration degree or maturity concepts, is introduced. The evolution of the compressive and tensile strengths and elastic moduli can be predicted in terms of the evolution of this aging degree.

A 2D model of the Urugua-í RCC Dam, recently built in Argentina, is used to perform the corresponding thermal and aging analyses. This allows to obtain the temperature field inside the dam at any time during the construction process, and almost more importantly, during the first years following the completion of the dam, while the temperature in the dam body decreases to reach the finally stable distribution.

As expected, the higher temperatures correspond to the foundation and those lifts located immediately over it, because of the higher hydration heat of concrete used there, and to the lifts located between elevation 180 and elevation 190, placed during the austral summer (December to February), when the ambient (and placing) temperatures are higher.

The long term thermal analysis follows the drop of these higher temperatures down to the final stable distribution. The temperature drop is faster for the upper elevations, and it may lead to thermal induced cracking in the interior of the dam; therefore the necessity of placing transverse contraction joints from elevation 182 up every 70-90 m.

Temperature gradients due to the difference between the ambient and inside temperatures are limited to a distance of about 2 m from the exterior faces. These temperature gradients may lead to thermally induced superficial cracking in these faces, and because of this transverse contraction joints are cut in the facing.

Results from 2D are compared to results obtained using a simplified vertical 1D model. It can be concluded that 1D vertical thermal models can accurately predict the vertical distribution of the temperature inside the dam body during the construction process, which is in itself a very useful information. Obviosly, they cannot provide information on the thermal gradients developed near the faces of the dam, nor about the transient of the long term temperature drop until the final stable temperature distribution is reached.

Finally, some parametric studies are performed to establish the effect of some major variables of the construction process that may have an influence in the temperature distribution and evolution: the placing temperature, the starting date and the placing speed.

APPENDIX I. REFERENCES

Bentz, D. P., Waller, V., and de Larrard, F. (1998). Prediction of adiabatic temperature rise in conventional and high-performance concrets using a 3-d microstructural model. *Cement and Concrete Research*, 28(2):285–297.

Buchas, J. and Buchas, F. (1991). Construction of urugua-í dam. In Hansen, K. D. and McLean, F. G., editors, *Proceedings of ASCE Specialty Conference on Roller Compacted Concrete 3*, pages 258–271, San Diego.

Byfors, J. (1980). Plain concrete at early ages. Technical Report N. 3:80, Swedish Cement and Concrete Research Institute, Stockholm.

Carino, N. J. (1981). Temperature effects on the strength-maturity relation of mortar. Technical Report No. NBSSIR 81-2244, National Bureau of Standards, Washington, D.C.

Cervera, M., Oliver, J., and Prato, T. (1999). A thermo-chemo-mechanical model for concrete. i: Hydration and aging. *Submitted to J. Engrg. Mech., ASCE.*

Chinese Society of Hydroelectric Engineering (1991). *Proceedings of Int. Symposium on Roller Compacted Concrete Dams.* ICOLD and Chinese Electricity Council, Beijing, China.

de Schutter, G. and Taerwe, L. (1995). General hydration model for portland cement and blast furnace slag cement. *Cement and Concrete Research*, 25(3):593–604.

de Schutter, G. and Taerwe, L. (1996). Degree of hydration based description of mechanical properties of early age concrete. *Materials and Structures*, 29:335–344.

Ditchey, E. J. and Schrader, E. K. (1988). Monksville damm temperature studies. In ICOLD, editor, *Proceedings of XVI Congress on Large Dams*, volume 3, pages 379–396, San Francisco.

Franco, M. A. (1996). El hormigón compactado con rodillo (in spanish). *Cemento-Hormigón. Presas de Hormigón Compactado*, 761:747–763.

Fujisawa, T. and Nagayama, I. (1985). Cause and control of cracks by thermal stress in concrete dams. In ICOLD, editor, *Proceedings of XV Congress on Large Dams*, volume 2, pages 117–143, Lausanne.

Gentile, G. (1964). Study, preparation and placement of low cement concrete, with special regard to its use in solid gravity dams. In ICOLD, editor, *Proceedings of VIII Congress on Large Dams*, volume X, Edimburgh.

Giesecke, J. and Marx, W. (1988). Avoiding thermal cracks in concrete dams during cooling process. In ICOLD, editor, *Proceedings of XVI Congress on Large Dams*, volume 3, pages 13–31, San Francisco.

Giovambattista, A. (1995). Urugua-í dam. thermal analysis, design criteria and performance. In IECA and CNEGP, editors, *Proceedings of the Int. Symposium on Roller Compacted Concrete Dams, Volume I: Materials, Planning and Design*, pages 309–323. Santander, Spain.

Hinks, J. L. and Copley, A. F. (1995). Thermal analysis for rcc dams. In IECA and CNEGP, editors, *Proceedings of the Int. Symposium on Roller Compacted Concrete Dams, Volume I: Materials, Planning and Design*, pages 473–484. Santander, Spain.

Hirose, T., Nagayama, I., Takemura, K., and Sato, H. (1988). A study on control temperature cracks in large roller compacted concrete dams. In ICOLD, editor, *Proceedings of XVI Congress on Large Dams*, volume 3, pages 119–135, San Francisco.

ICOLD (1985). *Proceedings of XV Congress on Large Dams.* International Commission on Large Dams, Lausanne, Switzerland.

ICOLD (1988). *Proceedings of XVI Congress on Large Dams.* International Commission on Large Dams, San Francisco, USA.

IECA and CNEGP (1995). *Proceedings of Int. Symposium on Roller Compacted Concrete Dams.* Spanish Institute of Cement and its Applications & Spanish National Committee on Large Dams, Santander, Spain.

Kim, J.-K., Y, H. M., and Eo, S.-H. (1998). Compressive strength development of concrete with different curing time and temperature. *Cement and Concrete Research*, 28(12):1761–1773.

Lorenzo, A. C. and Calivari, S. C. (1991). Behavior of urugua-í dam. In Hansen, K. D. and McLean, F. G., editors, *Proceedings of ASCE Specialty Conference on Roller Compacted Concrete 3*, pages 272–290, San Diego.

Oloukon, F. A., Bourdette, E. G., and Deatherage, J. H. (1990). Early–age concrete strength prediction by maturity – another look. *ACI Materials Journal*, 87(6):565–572.

Pantazopoulo, S. J. and Mills, R. H. (1995). Microstructural aspects of the mechanical response of plain concrete. *ACI Materials Journal*, 92(6):605–616.

Raphael, J. M. (1970). *Rapid Construction of Concrete Dams*, chapter The Optimum Gravity Dams. ASCE.

Rastrup, E. (1954). Heat of hydration in concrete. *Magazine of Concrete Research*, 6(17):2–13.

Reinhardt, H. W., Blaauwendraad, J., and Jongedijk, J. (1982). Temperature development in concrete structures taking account of state dependent properties. In *Proc. Int. Conf. of Concrete at Early Ages.*

Rostassy, F. S., Gustsch, A., and Laube, M. (1993). Creep and relaxation of concrete at early ages - experiments and mathematical modelling. In Mang, H., Bicanic, N., and de Borst, R., editors, *Proc. 5th. Int.*

RILEM Symp. on Creep and Shrinkage of Concrete, pages 453–458. E & FN Spon.

Schrader, E. K. and Naminas, D. (1988). Performance of roller compacted concrete dams. In ICOLD, editor, *Proceedings of XVI Congress on Large Dams*, volume 3, pages 339–363, San Francisco.

Shi, C. and Day, R. L. (1993). Acceleration of strength gain of lime-pozzolan cements by thermal activation. *Cement and Concrete Research*, 23(4):824–832.

Tatro, S. and Schrader, E. (1991). Thermal analysis for rcc - a practical approach. In Hansen, K. D. and McLean, F. G., editors, *Proceedings of ASCE Specialty Conference on Roller Compacted Concrete 3*, pages 389–405, San Diego.

Torrenti, J. M., Ghenot, I., Laplante, P., Acker, P., and Larrand, F. (1994). Numerical simulation of temperatures ans stresses in concrete at early ages. In Bazant, Z. P. and Carol, I., editors, *Proc. Int. Conf. on Computational Modelling of Concrete Structures*, pages 559–568. Pineridge Press, Swansea, Wales.

Ulm, F. J. and Coussy, O. (1996). Strength growth as chemo–plastic hardening in early age concrete. *J. Engrg. Mech., ASCE*, 122(12):1123–1132.

Waller, V., de Larrard, F., and Roussel, P. (1996). Utilization of high-strength/high-performance concrete. In RILEM, editor, *4th Int. Symp. RILEM*, pages 415–421.

Widmann, R. (1985). How to avoid thermal cracking of mass concrete. In ICOLD, editor, *Proceedings of XV Congress on Large Dams*, volume 2, pages 263–277, Lausanne.

Wild, S., Sabir, B. B., and Khatib, J. M. (1995). Factor influencing strength development of concrete containing silica fume. *Cement and Concrete Research*, 25(7):1567–1580.

Yamazumi, A., Harita, K., Jikan, S., and Kido, K. (1995). A study of thermal control on rcd dam. In IECA and CNEGP, editors, *Proceedings of the Int. Symposium on Roller Compacted Concrete Dams, Volume I: Materials, Planning and Design*, pages 493–507. Santander, Spain.

Yonezawa, T., Takahi, K., Yomaguchi, Y., and Jikan, S. (1988). Measument and analysis of cracks caused by thermal stress in mass concrete. In ICOLD, editor, *Proceedings of XVI Congress on Large Dams*, volume 3, pages 53–79, San Francisco.

Zhang, Z. and Garga, V. K. (1996). Temperature and temperature induced stresses for rcc dams. *Dam Engineering*, 7(2):129–141.

Zhu, B. and Xu, P. (1995). Thermal stresses in roller compacted concrete gravity dams. *Dam Engineering*, 6(3):199–220.

APPENDIX II. NOTATION

The following symbols are used in this paper:

A_f, B_f = Material properties for aging evolution;
$\widetilde{A}_\xi$ = Normalized chemical affinity;
C = Heat capacity per unit volume;
E, E_∞ = Elastic modulus, Final elastic modulus;
E_a = Activation energy;
$f^\pm, f^\pm_\infty$ = Tensile/compressive strength, Final values;
k_T = Thermal conductivity;
n_T = Exponent for strength evolution;
R = Contant for ideal gases;
R_{ext} = External volume heat sources;
Q = Hydration heat per unit volume;
Q_ξ = Hydration heat per unit of hydration degree;
$\bar{Q}_\infty$ = Final ammount of liberated heat (in ideal conditions);
T, T_0 = Temperature, Initial (or placing) temperature;
T_{amb} = Ambient temperature;
T_{ref} = Reference temperature;
T_T = Maximum temperature for strength evolution;
$V, \bar{V}$ = Placing speed, Relative placing speed;
w/c = Water/cement mass ratio;
α_T = Thermal linear expansion coefficient;
χ = Hydration extent;
$\chi_\infty, \bar{\chi}_\infty$ = Final hydration extent, *idem* in ideal conditions;
$\eta_{\xi 0}$ = Reference viscosity;
$\bar{\eta}$ = Exponent for viscosity;
κ = Aging degree;
ρ = Density;
ξ = Hydration degree;
$\xi_\infty, \bar{\xi}_\infty$ = Final hydration degree, *idem* in ideal conditions;
ξ_{set} = Hydration degree at setting; and
$\dot{(\,)}$ = Time derivative or rate;

Simulation of the Construction Process of Roller Compacted Concrete Dams. II: Stress and Damage

Miguel Cervera,* Javier Oliver† and Tomás Prato‡

ABSTRACT

In this work a numerical procedure for the simulation of the construction process of Roller Compacted Concrete (RCC) dams is described. The basis of the work is a coupled thermo-chemo-mechanical model for the behaviour of concrete at early ages that allows to simulate the observed phenomena of hydration, aging, creep and damage. In this second part the formulation and assessment of the mechanical aspects of the model are presented. Long term effects are included by incorporating a creep model inspired in the Microprestress-Solidification Theory, which naturally accounts for the aging effects. Tensile damage is also considered, via a damage model formulated in a normalized format, so that the phenomenon of aging is included. This allows to obtain the stress field inside the dam at any time during the construction and the following years, in order to assess the risk of occurrence of tensile damage. Results from a real case study are compared to alternative studies considering different construction schedules.

*Asst. Prof. Struc. Anal., ETS Ingenieros de Caminos, 08034 Barcelona, Spain.
†Prof. Cont. Mech., ETS Ingenieros de Caminos, 08034 Barcelona, Spain.
‡Grad. Res. Asst., ETS Ingenieros de Caminos, 08034 Barcelona, Spain.

INTRODUCTION AND MOTIVATION

The basic design requirement for concrete dams in to ensure their integrity, watertighness and durability. Therefore, any new procedure for dam construction must contemplate and adopt measures against the risk of cracking, and particularly, against thermally induced cracking. This is also the case for RCC dams, where to achieve the high production rates that make them economically profitable, longitudinal joints are totally avoided, pipe cooling is not suitable, and even transverse joints must be reduced to the minimum. Because of this, the technological specifications for massive concrete dams differ from those used for slim structures in one essential point: heat generation and the resulting thermal stresses are decisive, rather than attaining a high initial strength.

One of the main features of RCC is that its low cement content makes its hydration heat be considerably low, down to three times smaller than for conventional concretes. Nevertheless, the high concreting rate used in RCC dams may lead to significant temperature rises (see Part I). This increase in temperature occurs during the first days after placing, when the stiffness of concrete is still quite low and creep (viscous) effects are significant; therefore, it usually leads to moderate, and mainly compressive, stresses. This means that, in general, the temperature distribution at the moment of completion of the dam may be considered as virtually free from thermally induced tensile stresses.

However, months later, when the hydration process has finished, no more hydration heat is produced and the stiffness has significantly increased, the concrete starts to cool down. The temperature in the body of the dam drops from the (almost) maximum values attained at the completion of the construction process, to a finally stable distribution that will consist of seasonal oscillations around the mean annual temperature.

The drop in the temperature at a point is inevitably accompanied by a volume reduction. If this volume change is restricted by the surrounding concrete or the foundation rock, thermally induced stresses will develop and may lead to cracking. Therefore, the cause of thermal stresses and cracking is not the temperature change in itself, but the spatial restriction for free thermal shrinkage.

The main causes for volume change restriction are:

(a) the non uniform temperature distribution due to the evolutionary construction process,

(b) thermal gradients near the faces of the dam due to convection phenomena with the enviroment,

(c) external geometrical and thermal restraints such as the foundation rock.

(d) design geometrical aspects such as the distance between transverse joints, and

Therefore, the investigation of the risk of cracking due to thermal variation must distinguish two main different patterns:

(a) Cracking in the interior of the dam body due to the cooling process from the non uniform distribution of maximum temperatures down to

the mean annual temperature. This cooling process may take several years after the completion of the dam;

(b) Cracking near the surface as a consequence of the thermal gradient in concrete. This gradient increases, for instance, with the fast cooling of the ambient temperature. This process may become the critical problem during the first weeks after concreting.

Internal cracks due to the long term cooling process must be carefully considered during the design and construction process. For RCC dams the qualitative and quantitative assessment of the influence of major factors such as the composition of the mix, the ambient temperature, the placing temperature, placing speed (lift thickness and placement interval) and time for starting placement must be established.

On the other hand, surface cracks are difficult to avoid without the use of, for instance, heat-insulating formwork. They are usually only several milimeters deep, but they have an influence on the watertightness and durability of the concrete surface and specific measures against water penetration, such as the inclusion of PVC membranes, have to be considered. Moreover, they may progress later into deeper temperature cracks due to long term temperature drop, affecting the stability of the dam, and they should be prevented.

This paper presents a numerical procedure for the simulation of the construction process of Roller Compacted Concrete (RCC) dams.

Firstly, a mechanical model is proposed to predict the evolution of the thermally induced stresses in concrete at early ages. The reference model is based on the theory of Continuum Damage Mechanics and it incorporates two separate scalar internal variables to represent damage both under tension and compression conditions. The damage model is reformulated in a suitable normalized format so that it can incorporate the phenomenon of aging. Long term mechanical behaviour is considered by incorporating a creep model inspired in the recently proposed Microprestress-Solidification Theory.

Secondly, the case study of Urugua-í RCC Dam in Argentina is discussed. The dam is a straight RCC gravity structure, 76 m high and 676 m long. Crest elevation is 203 m. The actual conditions and concreting schedule that ocurred during the construction of the dam between January 1988 and March 1989 are considered as the reference case. The stress analysis during the construction and the first eleven years of service life of the dam is carried out. Results concerning the short term, long term and stable regime are shown to assess the safety of the design and the risk of tensile cracking.

Thirdly, alternative studies considering different construction schedules are performed to their effect on the safety assessment of the dam. An interruption of the construction process during the winter months due, for instance, to inadequate weather conditions or flooding of the construction site, is considered. Also, a slower placing speed taking two years instead of one to complete the dam is also discussed. It is concluded that any of these two eventualities would increase the risk of tensile cracking, and full section transverse contraction joints should be provided to ensure the same level of safety as for the reference case.

NUMERICAL MODEL

The mechanical model used in this work is described in detail in Cervera et al. (1999), and it will only be sketched here. The assessment of the model and numerical simulations of available experiments regarding the mechanical behaviour of concrete at early ages can also be found in that reference.

Microprestress-Solidification Theory

Figure 1 shows a schematic representation of the viscoelastic rheological model used to represent the long term mechanical behaviour of concrete; it consists of a Maxwell chain model that can be described in terms of the elastic moduli, E^i, and the dashpot viscosities, η^i, of the $i = 1, ..., N$ Maxwell elements of the chain. It is also helpful to consider the elastic moduli, E^i, and the relaxation times of the dashpots, defined as $\tau^i = \eta^i / E^i$, as an alternative characterization of the chain. It is convenient to take $\tau^1 = \infty$ in the series expansion, so that E^1 can be considered as the *asymptotic* elastic modulus of concrete.

In the framework of aging models the general case of such a rheological model would consist of independently varying elastic moduli and dashpot viscosities. However, it is usual to restrict the model to the consideration of proportional varying elastic moduli and constant relaxation times (Carol and Bazant 1993). In the following we will assume that during the aging process all the elastic moduli vary proportionally to the aging function defined by the aging model (see Part I), $E^i(\kappa) = \lambda_E(\kappa)\, E^i_\infty$ (where κ is the aging degree, E^i_∞ are values at the end of the hydration process, and $E_\infty = \sum_{i=1}^N E^i_\infty$), and that the relaxation times, τ^i, remain constant. It was shown in Carol and Bazant (1993) that this is equivalent to the model arising from Solidification Theory (Bazant and Prasannan 1989) with a non-aging Maxwell chain for the basic constituent. The total stress sustained by the Maxwell chain is easily computed as

$$\boldsymbol{\sigma} = \sum_{i=1}^{N} \boldsymbol{\sigma}^i \tag{1}$$

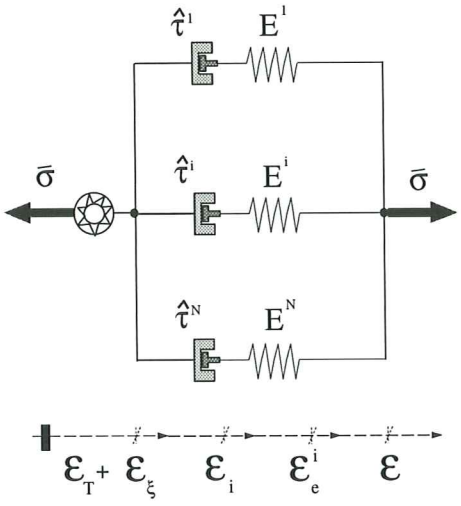

Figure 1: Rheological model for long term behaviour.

Choosing the stress in each Maxwell element of the chain, $\boldsymbol{\sigma}^i$, as internal variables, it was shown there that the first order differential equations governing the evolution of these variables are

$$\dot{\boldsymbol{\sigma}}^i + \frac{\boldsymbol{\sigma}^i}{\tau^i} = \lambda_E(\kappa) E^i_\infty \overline{\boldsymbol{D}}\, \dot{\boldsymbol{\varepsilon}} \quad \text{for} \quad i = 1, ..., N \tag{2}$$

where tensor entities are used as the multidimensional counterparts of the scalar ones used for uniaxial models; $\boldsymbol{\varepsilon}$ is the total strain tensor and the non-dimensional tensor $\overline{\boldsymbol{D}} = (1/E)\boldsymbol{D}$ has been used, being $\boldsymbol{D}$ the usual linear–elastic constitutive tensor.

The proposed model (and the underlying Solidification Theory) cannot be the final solution of the long term aging because the duration of creep for a fixed load decreases significantly with an increasing age at loading even after many years, while the hydration degree essentially stops before one year of age. In Bazant et al. (1997) a physical model is formulated to obtain the viscosity of the flow dashpot as a function of the tensile micro-prestress carried by the bonds and bridges crossing the gel pores in the hardened cement gel. The long term creep is assumed to originate from viscous shear slips between the opposite walls of micropores in which the bonds that transmit the micro-prestress break and reform. Let us define μ as a variable that can be regarded as the normalized value of the micro-prestress. If humidity effects are not considered the evolution of this normalized micro-prestress can be defined as

$$\mu(t) = \frac{1}{1 + c_{\mu 0}\, t} \tag{3}$$

Let us *define* the relaxation time of the flow term as

$$\tau_\mu = \frac{\tau_{\mu 0}}{\lambda_E(\kappa)\, \mu(t)} \tag{4}$$

where $\tau_{\mu 0}$ is a material property. Note that as time increases, the micro-prestress decreases, and so the viscosity of the flow term increases. Eventually, the micro-prestress will vanish, the viscosity will tend to infinity and the flow term will become inactive.

Now, Eq. (2) has to be modified to include the effect of the nonlinear flow term:

$$\dot{\boldsymbol{\sigma}}^i + \Big(\frac{1}{\tau^i} + \frac{1}{\tau_\mu}\Big)\, \boldsymbol{\sigma}^i = E^i(\kappa)\, \overline{\boldsymbol{D}}\, \dot{\boldsymbol{\varepsilon}} \quad \text{for} \quad i = 1, ..., N \tag{5}$$

Alternatively, the viscous strain in each Maxwell element, $\boldsymbol{\varepsilon}^{\boldsymbol{i}}$, rather than the stress, $\boldsymbol{\sigma}^{\boldsymbol{i}}$, can be selected as internal variables. The relationship between them is

$$\boldsymbol{\sigma}^i = E^i(\kappa)\, \overline{\boldsymbol{D}} : (\boldsymbol{\varepsilon} - \boldsymbol{\varepsilon}^i) \tag{6}$$

Substitution of Eq. (6) into Eq. (5) leads to the obtention of the evolution law for the viscous strains in the form

$$\dot{\boldsymbol{\varepsilon}}^i = \Big(\frac{1}{\tau^i} + \frac{1}{\tau_\mu} + \frac{1}{\tau_a}\Big)(\boldsymbol{\varepsilon} - \boldsymbol{\varepsilon}^i) = \frac{1}{\hat{\tau}^i}(\boldsymbol{\varepsilon} - \boldsymbol{\varepsilon}^i) \qquad \text{for} \quad i = 1, ..., N \tag{7}$$

with $\tau_a(\kappa) = \lambda_E / \dot{\lambda}_E$ representing the aging effect on the elastic modulus. Details on the numerical integration of Eq. (7) are given in Cervera and al.

(1992) and Galindo (1993). Note that even if τ^i and τ_μ are sufficiently large, there would be some viscous straining as long as the aging progresses and the elastic modulus varies ($\dot{\lambda}_E \neq 0$). As time increases, the rate of hydration decreases, and so the viscosity due to aging increases. Eventually, $\tau_a(t = \infty) = \infty$ and the model would revert to a standard Maxwell viscoelastic arrangement.

Aging Viscoelasticity and Damage

Finally, let us consider the coupling of the viscoelastic model described above with the aging damage model described in Cervera et al (1999), as well as including the relevant thermal and chemical couplings.

The basic hypothesis is that the stress sustained by the Maxwell chain is the effective (undamaged) stress, rather than the total stress. This idea is based on the concept that it is the effective stress the one acting on the effective (undamaged) solid concrete, while the total stress acts on the whole (damaged) solid.

Let us begin by defining the effective stresses and the elastic strains for one element of the Maxwell chain as:

$$\overline{\boldsymbol{\sigma}}^i \left(\boldsymbol{\varepsilon}_e^i, \kappa\right) = E^i(\kappa)\, \overline{\boldsymbol{D}} : \boldsymbol{\varepsilon}_e^i \tag{8}$$

with

$$\boldsymbol{\varepsilon}_e^i(\boldsymbol{\varepsilon}, \boldsymbol{\varepsilon}^i, T, \xi) = \boldsymbol{\varepsilon} - \boldsymbol{\varepsilon}_T - \boldsymbol{\varepsilon}_\xi - \boldsymbol{\varepsilon}^i \tag{9}$$

where T is the temperature and ξ is the hydration degree. Note that the thermal, $\boldsymbol{\varepsilon}_T = \alpha_T\,(T - T_{ref})\ \mathbf{1}$, and chemical, $\boldsymbol{\varepsilon}_\xi = \alpha_\xi \xi\, \mathbf{1}$, volumetric strains affect all the elements in the same way, but the viscous strain tensor, $\boldsymbol{\varepsilon}^i$, is different for each Maxwell element. The reference temperature T_{ref} can be taken as equal to the temperature reached at the end of the setting phase (when the hydration degree reaches the percolation threshold, $\xi = \xi_{set}$), so that the thermal stressing initiates then.

Let us also define the stress split for each element, as

$$\overline{\boldsymbol{\sigma}}^{i+} = \sum_{j=1}^{3} < \overline{\sigma}_j^i > \boldsymbol{p}_j^i \otimes \boldsymbol{p}_j^i \qquad \text{and} \qquad \overline{\boldsymbol{\sigma}}^{i-} = \overline{\boldsymbol{\sigma}}^i - \overline{\boldsymbol{\sigma}}^{i+} \tag{10}$$

where $\overline{\sigma}_j^i$ denotes the *j–th* principal stress value from tensor $\overline{\boldsymbol{\sigma}}^i$, $\boldsymbol{p}_j^i$ represents the unit vector associated with its respective principal direction and the symbol $\otimes$ denotes the tensorial product. The symbols $< . >$ are the Macaulay brackets.

The total stress sustained by the Maxwell chain is obtained in the form:

$$\begin{aligned} \boldsymbol{\sigma} &= (1 - d^+) \sum_{i=1}^{N} \overline{\boldsymbol{\sigma}}^{i+} + (1 - d^-) \sum_{i=1}^{N} \overline{\boldsymbol{\sigma}}^{i-} \\ &= (1 - d^+)\, \overline{\boldsymbol{\sigma}}^+ + (1 - d^-)\, \overline{\boldsymbol{\sigma}}^- \end{aligned} \tag{11}$$

where the damage indices under tension and compression, d^+ and d^- respectively, have been introduced. These indices are monotonically increasing functions of the corresponding tensile and compressive effective stresses such that they vary in the range $0 \leq d^+(\overline{\boldsymbol{\sigma}}^+)\,, d^-(\overline{\boldsymbol{\sigma}}^-) \leq 1$.

The detailed description of the procedures followed for the characterization and evolution of the damage indices is given in Cervera et al. (1999).

URUGUA-Í DAM

The Urugua-í Hydroelectric Project is located in the Province of Misiones, North East of Argentina. The main dam is a straight RCC gravity structure, 76 m high and 676 m long. Maximum width at the base is 57 m. Crest elevation is 203 m. Details about the design and location of the joints are given in Part I and in Giobambattista (1995), Buchas and Buchas (1991) and Lorenzo and Calivari (1991).

Four different types of concrete were used in the dam:

- the foundation was built in CPC with a cement content of 180 kg/m^3 (H180),
- the upstream facing and the spillway crest was built in CPC with a cement content of 220 kg/m^3 (H220),
- the body of the dam was built in RCC with a cement content of 60 kg/m^3 (RCC60), but
- the interface between the dam and the foundation (0.80 m high) was builtin RCC with a cement content of 90 kg/m^3 (RCC90).

All RCC and CPC were made with Portland cement similar to Type II ASTM, without pozzolanic admixtures. Table 1 summarizes the relevant material properties for the four types of concrete.

STRESS ANALYSIS

In this Section, results from thermally induced stress analyses performed on a numerical model of Urugua-í RCC Dam are presented. Firstly, results from the reference case study, simulating the real construction process of the dam are discussed. This will provide an accurate assessment of the dam design and the actual short and long term safety conditions of the construction. Secondly, the analysis is repeated simulating a three months interruption of the construction process during the winter. The impact of such eventuality is studied and the comparison with the reference case is described. Thirdly, the analysis is repeated under the hypothesis that the placement interval is doubled and, therefore, the construction process is completed in two years. Again, results are compared to those from the reference case.

Properties	H180	H220	RCC60	RCC90	Rock
w/c	0.50	0.50	1.60	1.00	—
$\rho\ [Kg/m^3]$	2,440	2,400	2,500	2,500	2,700
$C\ [10^{-6} J/m^3\,{}^oC]$	2.35	1.95	2.49	2.44	2.37
$k_T\ [J/m\,hs\,{}^oC]$	6,807	6,807	6,987	6,109	7,740
$\alpha_T\ [10^6]$	6.0	8.0	7.40	8.33	—
$Q_\xi\ [10^{-7} J/m^3]$	7.79	9.50	2.57	3.97	—
$f_\infty^-\,[MPa]$	18.0	22.0	9.0	13.6	50.0
$f_\infty^+\,[MPa]$	2.0	2.2	0.875	1.36	5.0
$E_\infty\,[GPa]$	31.0	38.0	14.0	22.0	30.0

Table 1: Material Properties for Urugua-í Dam.

Numerical Model

The numerical model used for the stress analyses is identical to the one used in Part I for the 2D thermal analyses; it consists of a finite element discretization of the central cross section of the dam. The mesh represents the body of the dam (from elevation 125 to elevation 189), plus the foundation (from elevation 115 to elevation 125) and some surrounding foundation rock (down to elevation 90). The dam is formed by 157 RCC lifts 0.40 m thick. The upstream facing and the spillway crest, both cast in H220 concrete are also included in the model. In the 2D model, every lift is discretized into 25 elements across and 2 elements thick, thus resulting in 7,850 elements in the dam body. The mesh is finer near the up and dowstream faces to represent the CPC facing and to capture the boundary thermal effects. The total number of elements in the mesh is 9,500 including the foundation.

The material properties used to simulate the hydration and aging processes were listed in Part I. Table 2 summarizes the additional mechanical material properties used for in the numerical simulation for the stress analyses. They refer to the constitutive modelling of creep and tensile damage.

Properties	H180	H220	RCC60	RCC90
w/c	0.50	0.50	1.60	1.00
N	2	2	2	2
$E^1 : E^2$	3:1	3:1	3:1	3:1
$\tau^1\,[hs]$	∞	∞	∞	∞
$\tau^2\,[hs]$	15	15	75	75
$\tau_{\mu 0}\,[hs]$	600	700	1,000	1,000
$c_{\mu 0}\,[x10^{-3}1/hs]$	5.0	6.0	2.0	2.0
r_e^+	1.0	1.0	1.0	1.0
r_p^+	1.0	1.0	1.0	1.0
$G_{f\infty}^+\,[N/m]$	300	300	300	300

Table 2: Material Properties for Numerical Simulations.

The numerical model used allows to simulate the actual evolutionary construction process of the dam. To this end, the finite elements corresponding to the different concrete lifts are progressively activated at the times corresponding to their respective placing in the dam.

The initial temperature of the activated elements is automatically set equal to the corresponding placing temperature. For the reference simulation case the placing temperature of each lift is taken as equal to the ambient temperature corresponding to the placing date + 5 ^{o}C. The initial temperature of the foundation rock is assumed to vary linearly from the ambient temperature at the surface (elevation 125) to 10 ^{o}C at the bottom of the model (elevation 90). During the construction of the dam, temperature at the boundaries in contact with the air is automatically set equal to the ambient temperature at the corresponding date. After the completion of the dam, the analysis is continued for the subsequent eleven years, to be able to follow the evolution on the stresses during the cooling process. To this end, the ambient temperature is automatically adjusted to follow the average cyclic seasonal thermal variation in the area. The reservoir was

filled in July 1990, and from that time on the temperature in the water and therefore, at the upstream wall, is assumed to vary linearly between the ambient temperature at the surface and the upper layer of rock at the bottom of the reservoir.

Reference case study

The reference case study corresponds to the real concreting programme followed in the construction process of the Urugua-í RCC Dam. Concreting of the foundation began in January 1988 and was completed in March of the same year. RCC placing began in April 1988 and finished in March 1989. Therefore, it can be considered that the constrution of the body of the dam took one year, approximately. The dam was built with 40 cm thick lifts. The placement interval between lifts was 48 hs, approximately (up to elevation 191). Therefore, the placing speed can be estimated as $V = 20$ cm/day. The relative placing speed is $\bar{V} = V/H = 2.63$ x 10^{-3} 1/day = 0.96 1/year, where H is the dam height.

Figure 2 shows the short term longitudinal stress evolution for interior points corresponding to lifts placed with 2 months interval between them. The corresponding (placing month) elevations are: (4) 130 m, (6) 141 m, (8) 153 m, (10) 165 m and (12) 177 m. As the placing temperature is assumed above the ambient temperature (+ 5 ^{o}C), the lifts start to cool after being placed and they go into tension because of the restriction to deform imposed by the lifts below. However, the stress turns into compresion shortly afterwards, as the concrete starts to warm because of the release of the hydration heat and the heat flux coming from the surrounding concrete. This lasts until the concrete begins to cool again after the hydration process is finished and the heat in the dam is released towards the enviroment and the foundation rock. Note that lifts placed at the bottom of the dam begin to cool fairly early after their placement, and they are subjected to tension almost from the beginning (self-weight not considered).

Figure 3 shows a detail of the short term stress evolution for lifts 5, 6, 7 and 8 just after their placement (during the end of April and the beginning of May). Note how immediately after being placed the lifts are under tension because of the difference between the placing and the ambient temperatures (+ 5 ^{o}C) and heat is lost through the upper surface. Shortly after, a peak in the stress is reached as soon as the upper lift is placed and the temperature begins to rise again due to vertical heat conduction; as heat continues to be released through the upper surface a second peak is reached, now in compression; with the placing of a new lift, the cycle is repeated, every time with a smaller amplitude due to the increasing distance of the concrete to the upper exterior surface. It must be noted that this very short term oscillations in the stress would be amplified for thinner lifts or larger placing intervals, that is, for lower production rates; on the contrary, they would be reduced for thicker lifts or shorter placing intervals, that is, for higher production rates. Eight days after the placing of a lift, the stresses are clearly on the compression side as can be seen both in figures 2 and 3.

Figure 4 shows the short term evolution of the tensile strength for lifts 5, 6, 7 and 8. Note how the strength develops faster than the tensile stresses and, therefore, there is no risk of tensile cracking at this very early stage.

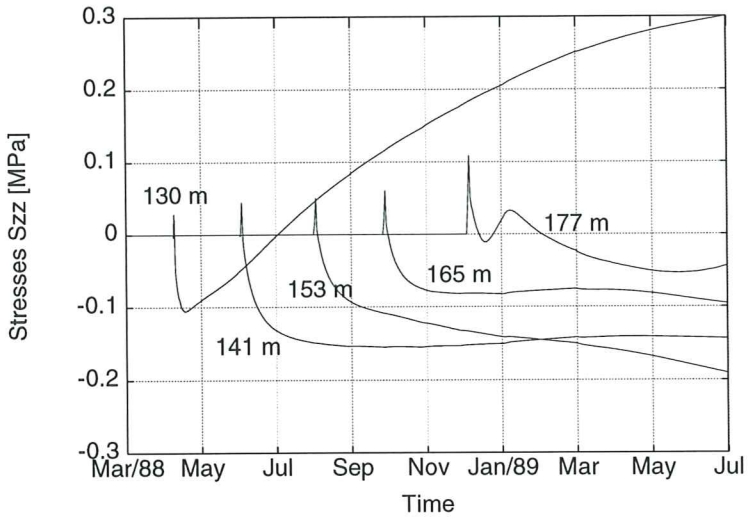

Figure 2: Short term stress evolution for different elevations.

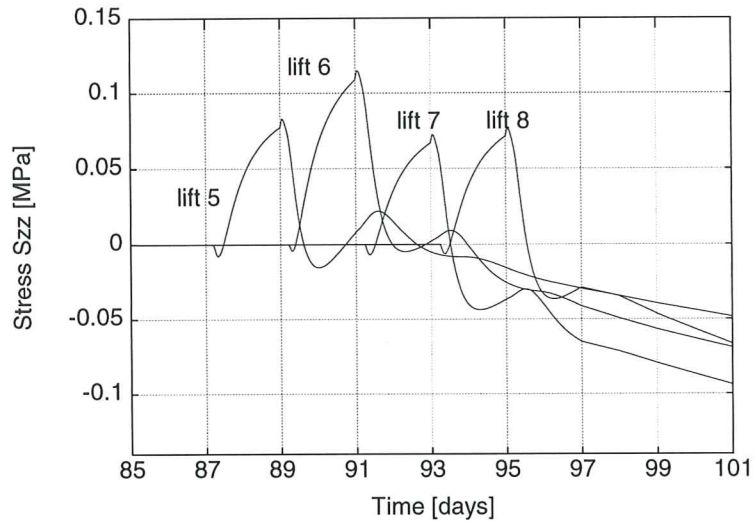

Figure 3: Short term stress evolution for four consecutive lifts.

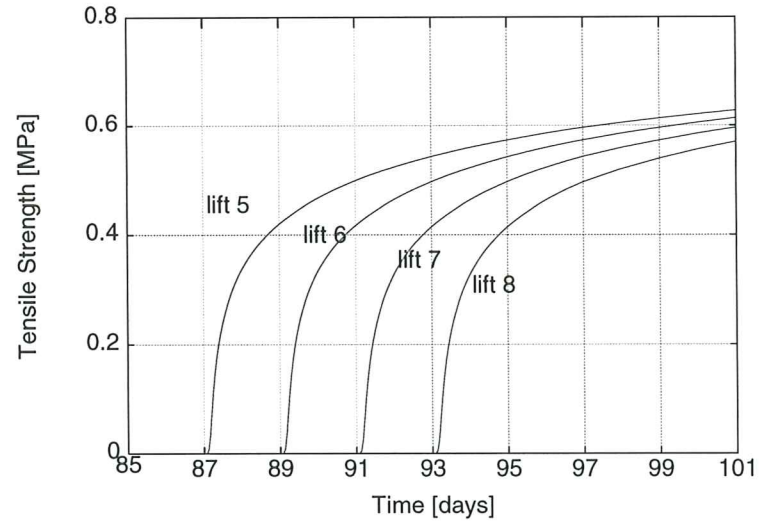

Figure 4: Short term strength evolution for four consecutive lifts.

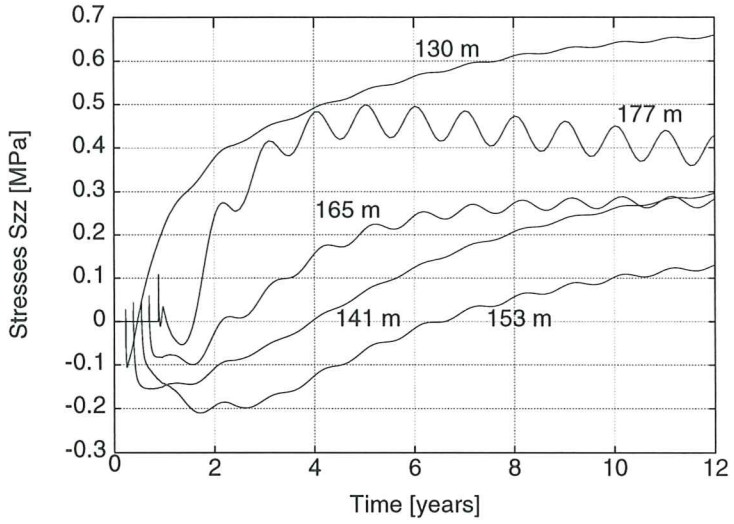

Figure 5: Long term stress evolution for different elevations.

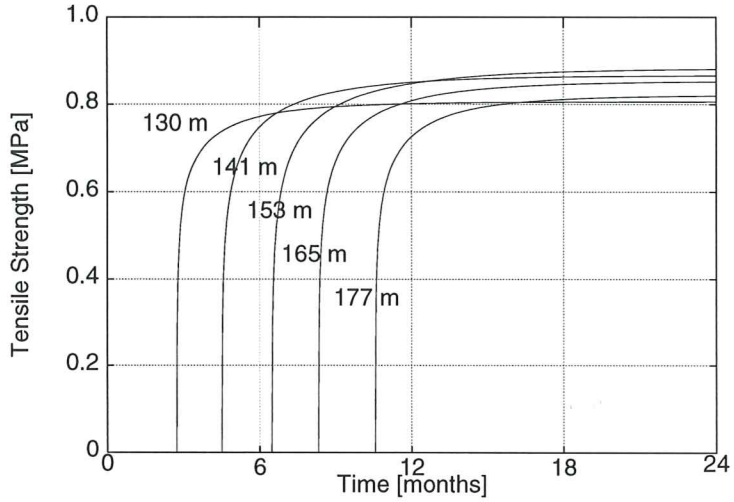

Figure 6: Long term strength evolution for different elevations.

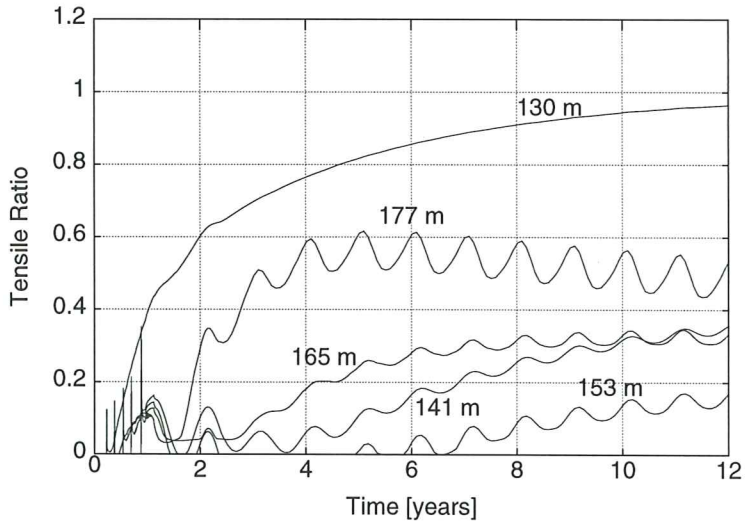

Figure 7: Long term tensile ratio evolution for different elevations.

Figure 5 shows the long term stress evolution for the same interior points described in figure 2. The stress analysis is run now for 11 years after the dam completion. During this period the temperature in the interior of the dam decreases progressively, as the heat generated during the hydration process is released through the up and downstream faces. The final stable temperature in the interior of the dam will be approximately equal to the mean annual temperature (20 ^{o}C). As the temperature drops, the longitudinal stress in concrete turns progresively from compression to tension. This phenomenon is faster for the upper elevations, both because they were placed in summer and because they are more exposed to the ambient temperature. However, the bottom lifts also go into tension very quickly because of the loss of heat towards the foundation rock. Note also that the seasonal oscillation of the ambient temperature is only noted in the stresses for the points located at higher elevations, while the bottom part of the dam body is virtually unaffected by it.

The evolution of the long term tensile stresses must be compared with the development of the tensile strength, depicted in figure 6, in order to assess the risk of cracking. Note that different tensile strengths are attained at the different elevations, due to the influence of temperature in the aging process. Figure 7 combines both results by showing the evolution of the tensile ratio, defined as the ratio of (the norm of) the tensile stresses over the current tensile strength. The closer this value is to unity, the greater is the risk of the onset of tensile damage. In general, it can be concluded from the analysis that the higher the location, the greater the risk of tensile damage. This was correctly evaluated by the designers of Urugua-í Dam, and they provided transverse contraction joints from elevation 182 up every 70-90 m. However, the present analysis also shows significant risk of tensile cracking in the long term in the contact area between the dam and the foundation. This risk is well recognised in the literature and it is usually referred to as *cracking by external restraint*. In fact, the stress analysis performed for Miyagase RCC Dam, reported by Hirose et al. (1988), found that the maximum risk of cracking occurred when the concrete just above the foundation rock was placed in summer. Nevertheless, it must be remarked that, due to Poisson's effect, the compressive vertical stresses due to self-weight, will also lead to compressive longitudinal stresses that largely reduce the risk of tensile cracking in this bottom area.

Figure 8 shows contour plots for the evolution of the tensile ratio in the body of the dam during the construction process (1 year). The corresponding month–elevations are: (a) June/88 146 m, (b) August/88 157 m, (c) November/88 175 m, (d) February/89 187 m and (e) June/89 196 m. As mentioned above, the developed stresses in the dam interior are initially compressive because they are due to the increase of temperature due to the hydration heat; they turn into tension some months after the concrete is placed, when the release of heat is completed and the concrete has started to cool. During this first year tensile stresses develop mainly in the lower part of the dam, because of external restraint caused by the foundation, and at the upstream and downstream faces, because of the enviromental thermal variations. Due to the low thermal conductivity of concrete, temperature gradients due to the difference between the ambient and inside temperatures are limited to a distance of about 2 m from the exterior faces. In

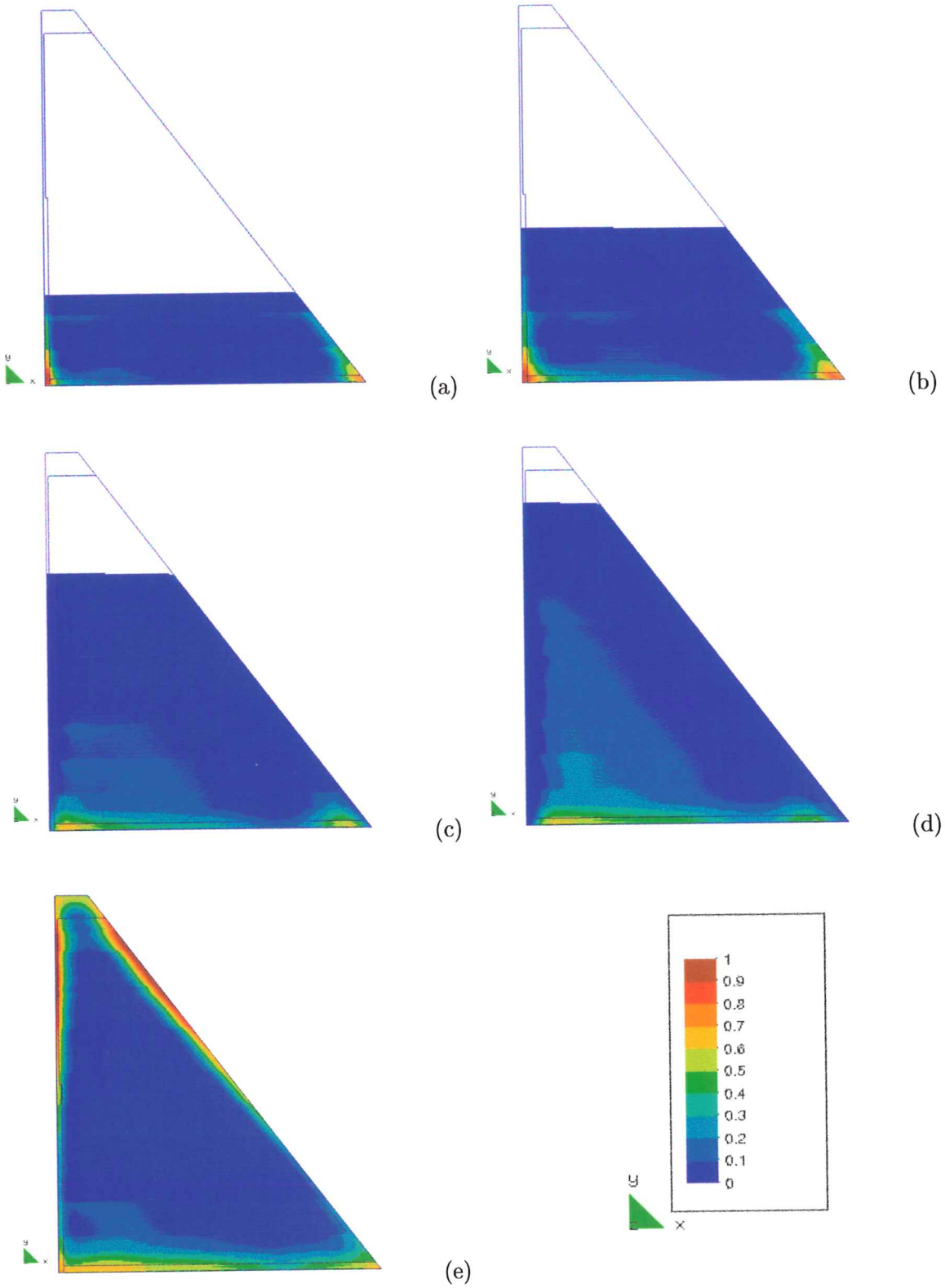

Figure 8: Short term evolution of tensile ratio.

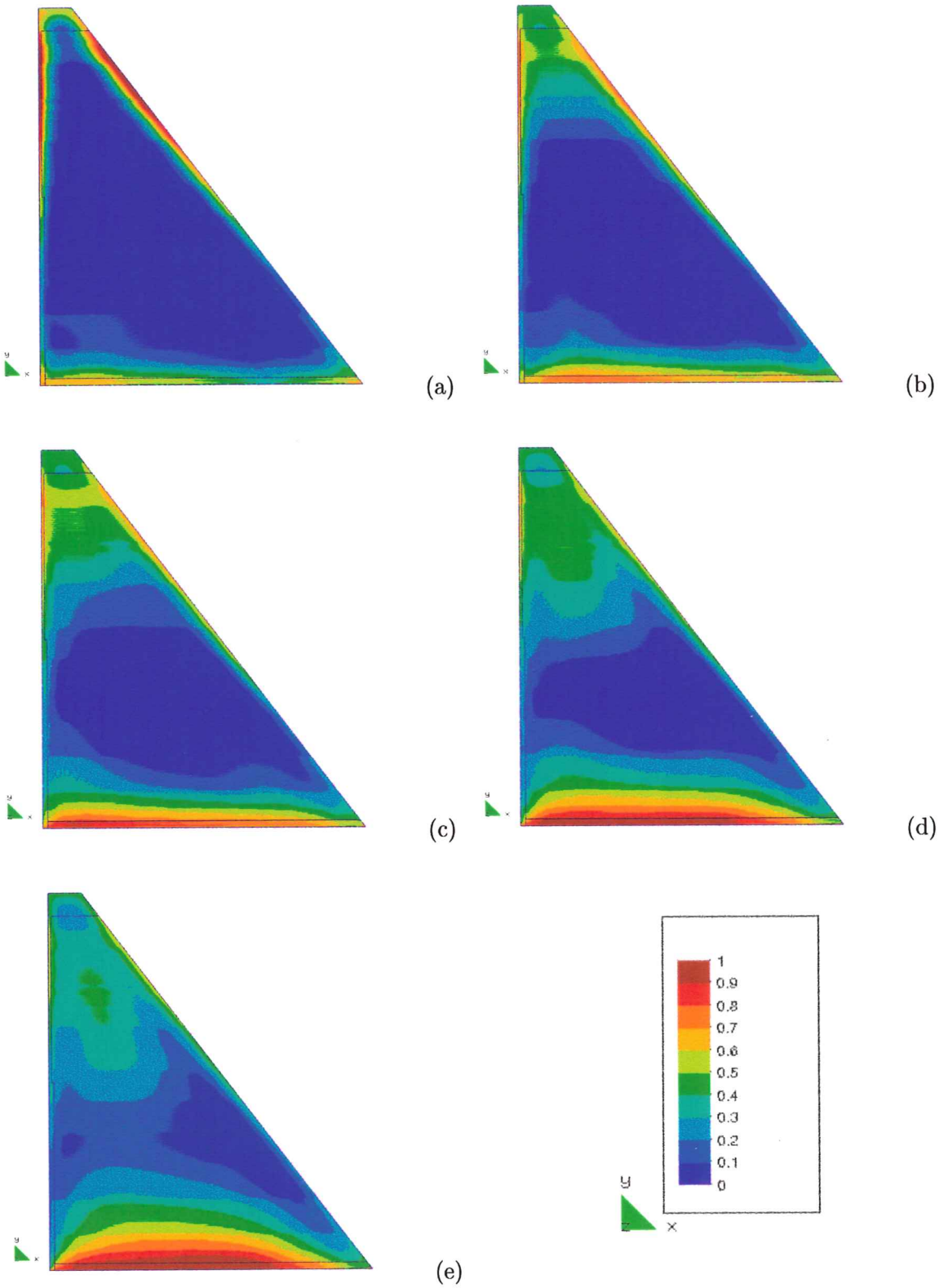

Figure 9: Long term evolution of tensile ratio.

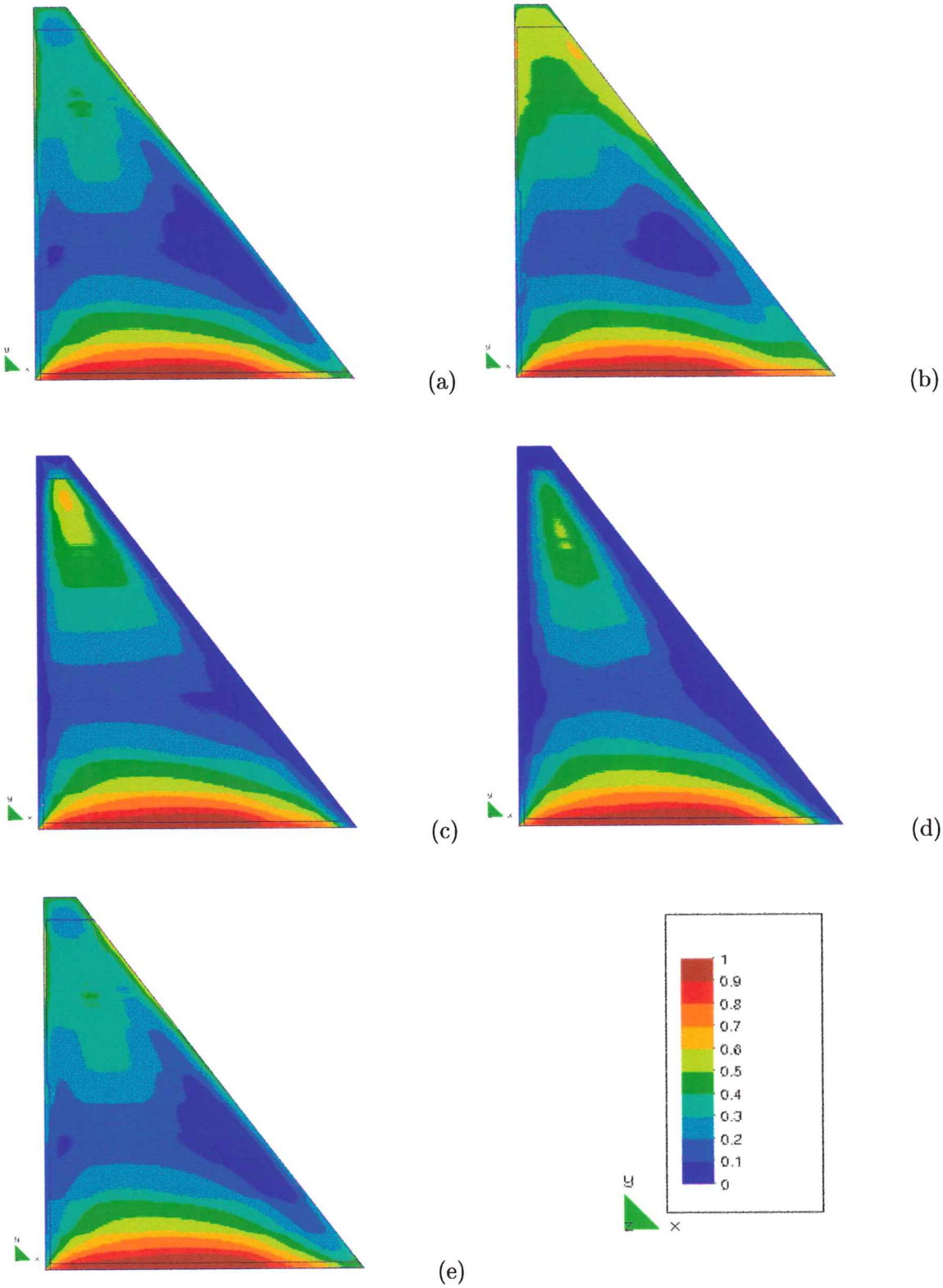

Figure 10: Seasonal evolution of the tensile ratio.

order to avoid superficial cracking induced by these temperature gradients transverse contraction joints are cut in the facing of the dam every 14.24 m, 1.20 m deep and running inside the RCC.

Figure 9 shows contour plots for the evolution of the tensile ratio in the body of the dam during the 10 first years after dam completion. All the snapshots correspond to the temperature distribution in winter (June). The corresponding years are: (a) 1989, (b) 1990, (c) 1991, (d) 1994 and (e) 1999. Note how as the overall temperature in the dam decreases, thermally induced tensile stresses progressively develop. In the upper part of the dam they are due to the internal restraint provided by the warmer concrete below; in the lower part of the dam free volume changes are restricted both by the warmer concrete above and the cooler foundation rock below. It is clear in the figure that the risk of cracking in the upper part of the dam develops in the first two years after completion.

After 10 years the heat 'stored' during the construction process has virtually disappeared. The dam is then in a thermally stable regime, subjected only to the cyclic seasonal oscillations. Figure 10 shows contour plots for the evolution of the tensile ratio in the body of the dam for the eleventh year after dam completion, once the cooling process is completed. The snapshots corresponding month/year are: (a) June/2000, (b) September/2000, (c) December/2000, (d) March/2001 and (e) June/2001. The stress distribution in June is typical of winter, while that in December is typical of summer. The September (spring) and March (autumn) distributions are typical transition distribution between the former. Due to the thermal inertia of the concrete maximum tensile stresses in the upper part of the dam appear in spring, after the cold winter conditions.

Interruption of the construction process

The complete stress analysis is repeated now considering that an interruption of the construction process during the winter months due, for instance, to inadequate weather conditions or flooding of the construction site, occurs. Thus, the concreting schedule from January 1988 until the end of June is followed as for the reference case, then it is stopped during July, August and September and resumed at the same placing speed from the beginning of October until the end of June 1999.

Figure 11 shows the temperature evolution for interior points corresponding to lifts placed with 1 month interval between them. The corresponding (placing month) elevations are: (4) 130 m, (5) 135 m, (6) 141 m, (10) 147 m, (11) 153 m, (12) 159 m, (1) 165 m, (2) 171 m, (3) 177 m, (4) 181 m and (5) 185 m. Higher temperature rises appear at the bottom lifts (April to June), because of the heat coming from the hydration of the H180 concrete in the foundation and in the lifts placed during the austral summer (December to February). The temperature is still rising in most of the dam after completion, particularly in those lifts placed immediatety before and after the winter interruption (June and October). The bottom layers, however, start to cool shortly after being placed because of the heat conduction towards the founding rock. Compared to the short term temperature evolution for the reference case, it can be observed that higher temperatures are attained in the middle part of the dam, between eleva-

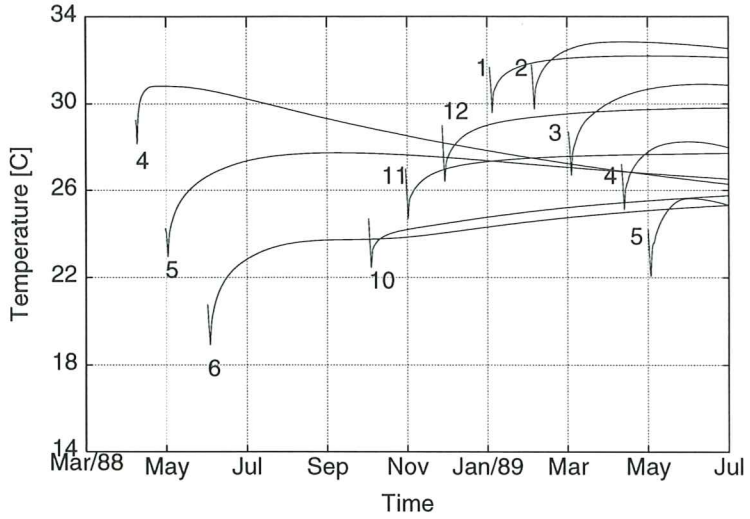

Figure 11: Temperature evolution for different elevations with 3 months interruption.

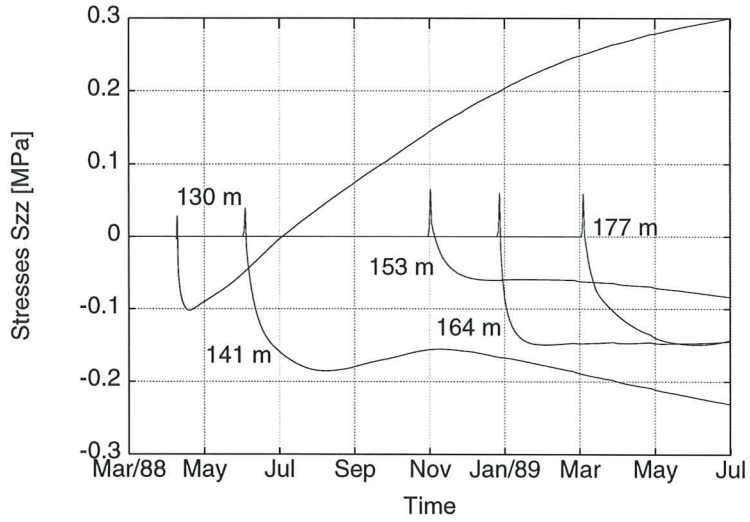

Figure 12: Short term stress evolution for different elevations with 3 months interruption.

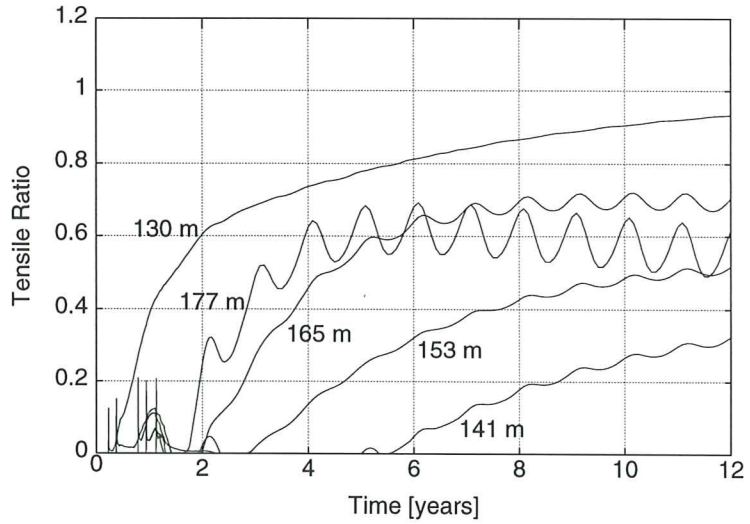

Figure 13: Long term tensile ratio evolution for different elevations with 3 months interruption.

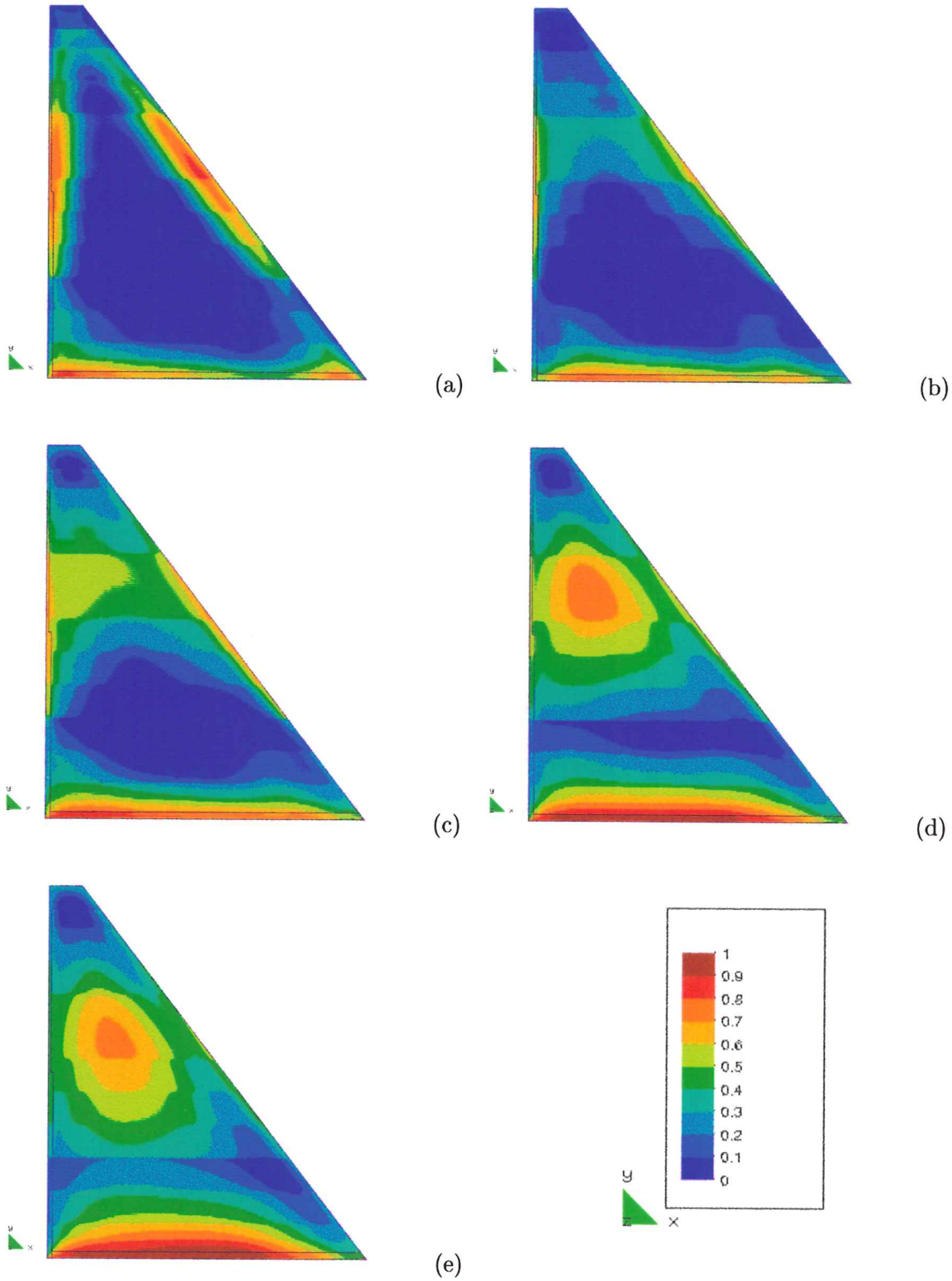

Figure 14: Long term evolution of tensile ratio with 3 months interruption.

tions 150 m. and 170 m., while lower temperatures arise above the latter elevation.

Figure 12 shows the short term longitudinal stress evolution for interior points corresponding to lifts placed with 2 months interval between them. The corresponding (placing month) elevations are: (4) 130 m, (6) 141 m, (11) 153 m, (1) 165 m and (3) 177 m. This has to be compared with Figure 2 to evaluate the influence of the interruption in the construction programme. As most of the concrete in dam is still warming at this early age, most of the longitudinal stresses are still compressive. Only at the bottom the thermally induced stresses turn rapidly into tension, very much in the same fashion as for the reference case. Note the effect of the three months interruption in the evolution of the stress at elevation 141 m: a peak is reached in compression because of the heat lost through the upper surface during the interruption, but compressive stresses continue to grow after the construction is resumed and heat continues to flow downwards from the new lifts placed above.

Figure 13 shows the long term evolution of the tensile ratio for the same elevations. This has to be compared with Figure 7 to evaluate the influence of the interruption in the construction programme. It is quite evident that the risk of cracking has increased significantly, particularly for elevations above 150 m. Note that tensile stresses are still increasing after 12 years in most of the dam body. Again, it can be concluded from the analysis that the higher the location, the greater the risk of tensile damage. However, to ensure the same level of safety as for the reference case, in this situation transverse contraction joints should be provided every 70-90 m above elevation 150 m at least, and not above elevation 182 as in the actual design of the dam.

Figure 14 shows contour plots for the evolution of the tensile ratio in the body of the dam during the 10 first years after dam completion. All the snapshots correspond to the temperature distribution in winter (June). The corresponding years are: (a) 1989, (b) 1990, (c) 1991, (d) 1994 and (e) 1999. This has to be compared with Figure 9 to evaluate the influence of the interruption in the construction programme. Again, it can be observed how thermally induced tensile stresses progressively develop as the overall temperature decreases. Now, the higher risk of tensile cracking occurs in the upper middle part of the dam, between elevations 160-180 m. The risk of cracking in the middle part of the dam continues to grow even ten years after completion. Note also how in the last figure, the elevation at which the interruption took place is clearly visible.

Slowing of the construction process

Finally, the complete stress analysis is repeated considering that the placing interval is doubled to be 96 hs. RCC placing begins in April 1988 and finishes in December 1989. The spillway is cast in H220 from January to February 1990. Therefore, the placing speed can be estimated as $V = 10$ cm/day. The relative placing speed is $\bar{V} = V/H = 1.31$ x 10^{-3} 1/day $= 0.48$ 1/year, where H is the dam height.

Figure 15 shows the temperature evolution for interior points corresponding to lifts placed with 2 months interval between them. The corresponding (placing month) elevations are: (4) 130 m, (5) 135 m, (7) 141 m,

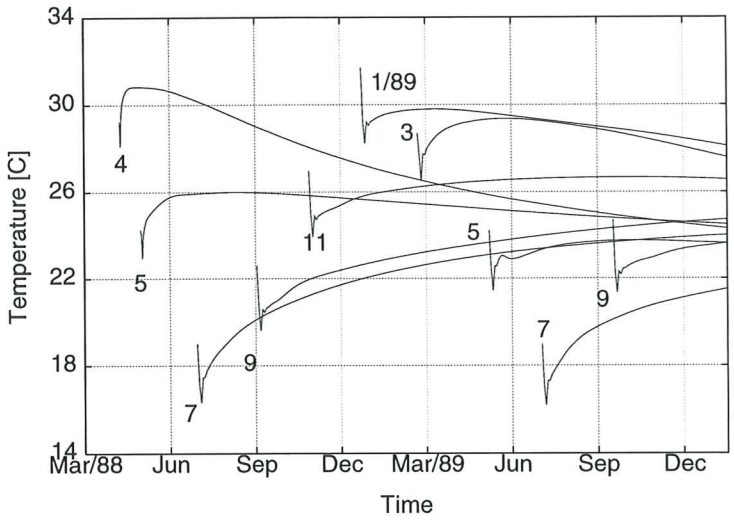

Figure 15: Temperature evolution for different elevations slowing the construction process.

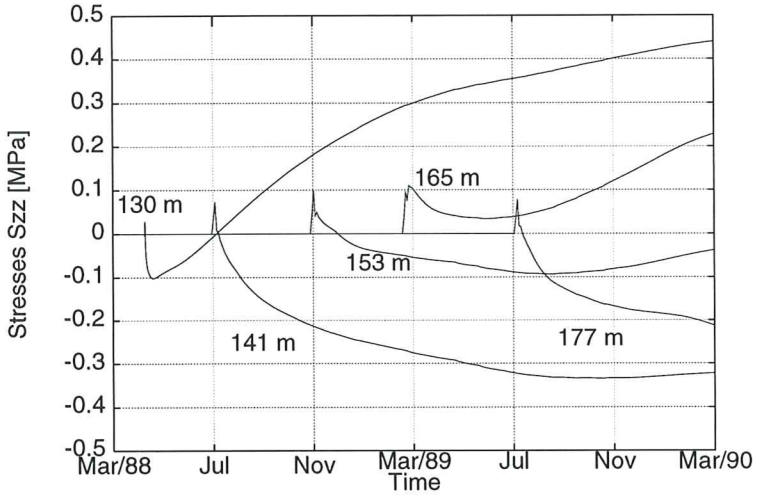

Figure 16: Short term stress evolution for different elevations slowing the construction process.

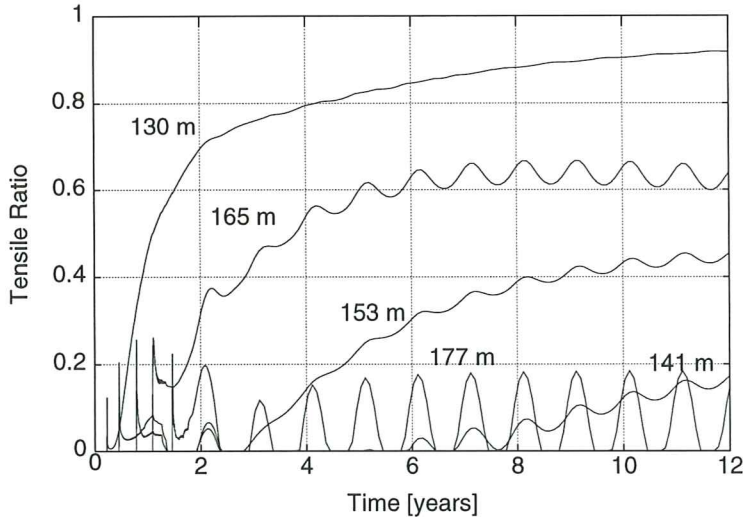

Figure 17: Long term tensile ratio evolution for different elevations slowing the construction process.

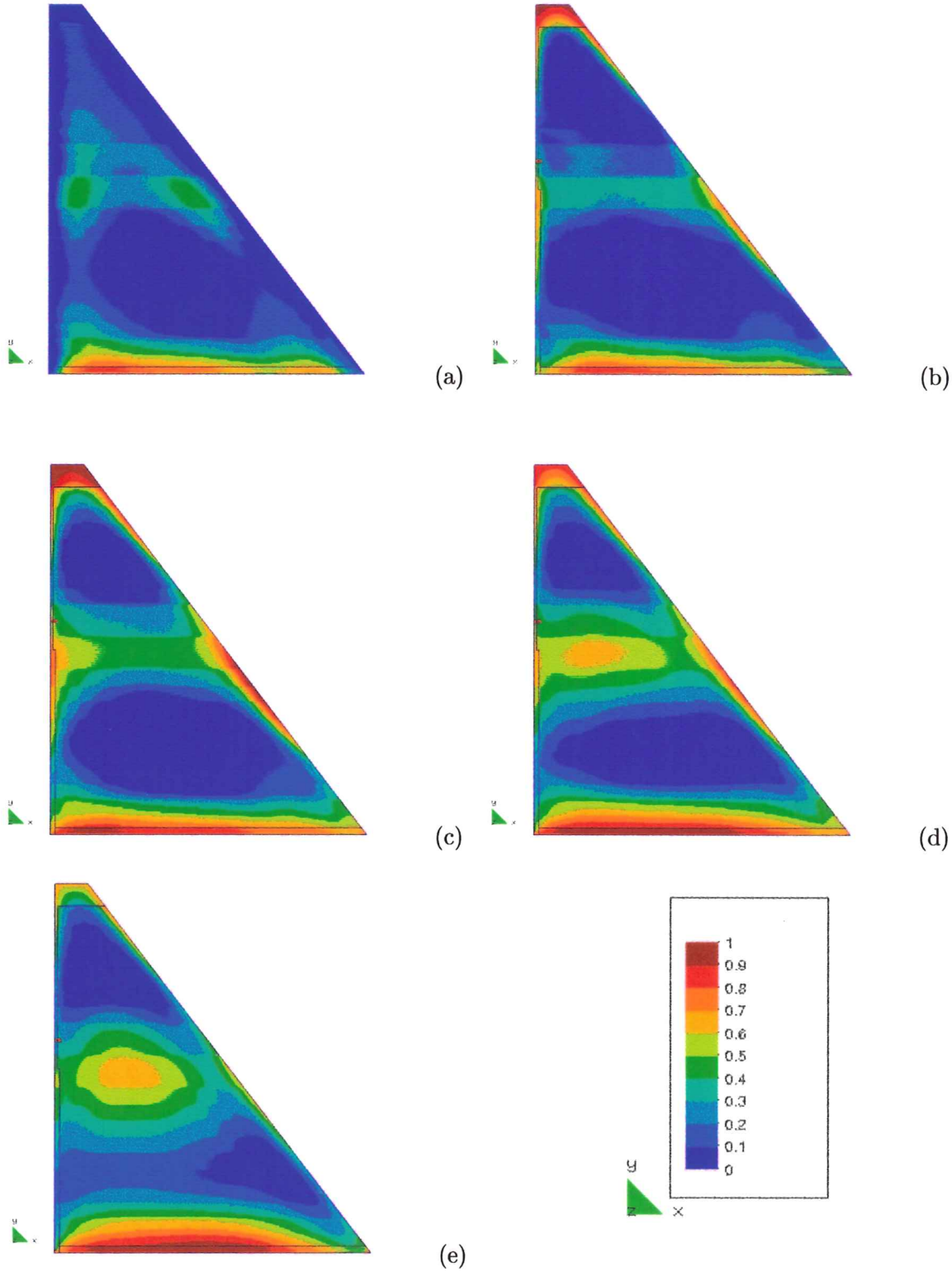

Figure 18: Long term evolution of tensile ratio slowing the construction process.

(9) 147 m, (11) 153 m, (1) 159 m, (3) 165 m, (5) 171 m, (7) 177 m and (9) 185 m. Higher temperature rises appear at the bottom lifts (April to June), and in the lifts placed during the austral summer (December to February). Compared to the short term temperature evolution for the reference case, it can be observed that higher temperatures are attained in the middle part of the dam, between elevations 150 m. and 170 m., while lower temperatures arise below and above these elevations. Heat conduction plays a significant role in this case; the bottom part of the dam attains higher temperatures than in the reference case due to heat flowing from the middle part and, reciprocally, the middle part begins to cool quite rapidly due to heat flowing down and upwards.

Figure 16 shows the short term longitudinal stress evolution for interior points corresponding to lifts placed with 2 months interval between them. The corresponding (placing month) elevations are: (4) 130 m, (6) 141 m, (11) 153 m, (1) 165 m and (3) 177 m. This has to be compared with Figure 2 to evaluate the influence of the slowing in the construction programme. Note how the stresses at elevation 141 m, for instance, go further into the compressive side because of the internal redistribution of temperature; also, the fast cooling in the middle part of the dam induce tensile longitudinal stresses very rapidly in this region, between elevations 150-170 m.

Figure 17 shows the long term evolution of the tensile ratio for the same elevations. This has to be compared with Figure 7 to evaluate the influence of the slowing in the construction programme. It is quite evident that the risk of cracking has increased significantly in the middle part of the dam, placed during the summer (see curves for elevations 153 m and 164 m). On the other hand, tensile stresses are reduced in the upper part of the dam, placed in colder weather than in the reference case; stress at elevation 177 m, for instance, is very much reduced, and it follows nicely the regular seasonal oscillations. To ensure the same level of safety as for the reference case, in this situation transverse contraction joints should be provided every 70-90 m above elevation 150 m at least, and not above elevation 182 as in the actual design of the dam.

Figure 18 shows contour plots for the evolution of the tensile ratio in the body of the dam during the 10 first years after dam completion. All the snapshots correspond to the temperature distribution in winter (June). The corresponding years are: (a) 1990, (b) 1991, (c) 1992, (d) 1995 and (e) 2000. This has to be compared with Figure 9 to evaluate the influence of the slowing in the construction programme. It is clear that concreting in hot weather leaves a mark in the long term mechanical behaviour of the dam. Now, the higher risk of tensile cracking occurs in the middle part of the dam, between elevations 150-170 m. The risk of cracking in the middle part of the dam is noticeable only one year after the dam completion, and it continues to grow stadily even ten years after completion.

CONCLUSIONS

This work presents a numerical procedure to simulate the stress analysis of the evolutionary construction process of roller compacted concrete dams.

The basis of the work is a coupled thermo-chemo-mechanical model for the behaviour of concrete at early ages that allows to simulate the observed phenomena of hydration, aging, damage and creep. In this second part the simulation and discussion of the mechanical aspects of the problem are presented. The proposed procedure is shown to be able to predict the evolution in time of the thermally induced tensile stresses that develop due to hydration heat released during the construction and the subsequent cooling process, in order to assess the risk of occurrence of tensile damage either at short or long term.

Firstly, a 2D finite element model of the Urugua-í RCC Dam, recently built in Argentina, is used to perform the corresponding stress analyses. This allows to obtain the stress field inside the dam at any time during the construction process, and more importantly, during the first years following the completion of the dam, while the temperature in the dam body decreases to reach the final stable distribution.

The results of the analysis show that significant tensile stresses develop in the bottom part of the dam due to the external restraint imposed by the foundation rock and also in the top part of the dam due to the internal restraint imposed by the concrete below, especially in the lifts located between elevation 180 and elevation 190, placed during the austral summer (December to February), when the ambient (and placing) temperatures are higher. The latter was correctly evaluated by the designers of Urugua-í Dam, as they provided transverse contraction joints from elevation 182 up every 70-90 m.

Also, temperature gradients due to the difference between the ambient and inside temperatures may lead to thermally induced superficial cracking in these faces, and because of this transverse contraction joints are cut in the facing of the dam every 14.24 m, 1.20 m deep and running inside the RCC.

Secondly, the analysis is repeated simulating a three months interruption of the construction process during the winter due, for instance, to inadequate weather conditions or flooding of the construction site. The impact of such eventuality is studied and the comparison with the reference case is described. It turns out that in such case transverse contraction should be cut deeper inside the dam, from elevation 160 at least, to provide the same level of safety against cracking. The risk of cracking due to the external restraint of the foundation remains high and almost unaffected.

Thirdly, the analysis is repeated under the hypothesis that the placement interval is doubled and, therefore, the construction process is completed in two years. It turns out that heat conduction during construction plays a significant role in this case; the bottom part of the dam attains higher temperatures than in the reference case due to heat flowing from the middle part and, reciprocally, the middle part begins to cool quite rapidly due to heat flowing down and upwards. Transverse contraction joints should also be cut deeper inside the dam for this case, from elevation 150 at least, to provide the same level of safety against cracking.

APPENDIX I. REFERENCES

Bazant, Z. P., Hauggard, A. B., Prasannan, S., and Ulm, F. J. (1997). Microprestress–solidification theory for concrete creep. i: Aging and drying effects. *J. Engrg. Mech., ASCE*, 123(11):1188–1194.

Bazant, Z. P. and Prasannan, S. (1989). Solidification theory for concrete creep. i: Formulation. *J. Engrg. Mech., ASCE*, 115(8):1691–1703.

Buchas, J. and Buchas, F. (1991). Construction of urugua-í dam. In Hansen, K. D. and McLean, F. G., editors, *Proceedings of ASCE Specialty Conference on Roller Compacted Concrete 3*, pages 258–271, San Diego.

Carol, I. and Bazant, Z. P. (1993). Viscoelasticity with aging caused by solidification of nonaging constituent. *J. Engrg. Mech., ASCE*, 119(11):2252–2269.

Cervera, M., Oliver, J., and Galindo, M. (1992). Numerical analysis of dams with extensive cracking resulting from concrete hydration: simulation of a real case. *Dam Engineering*, 3(1):1–22.

Cervera, M., Oliver, J., and Prato, T. (1999). A thermo-chemo-mechanical model for concrete. ii: Damage and creep. *Submitted to J. Engrg. Mech., ASCE.*

Fujisawa, T. and Nagayama, I. (1985). Cause and control of cracks by thermal stress in concrete dams. In ICOLD, editor, *Proceedings of XV Congress on Large Dams*, volume 2, pages 117–143, Lausanne.

Galindo, M. (1993). *Una metodología para el análisis numérico del comportamiento resistente no lineal de presas de hormigón bajo cargas estáticas y dinámicas (in Spanish).* PhD thesis, Technical University of Catalonia.

Giovambattista, A. (1995). Urugua-í dam. thermal analysis, design criteria and performance. In IECA and CNEGP, editors, *Proceedings of the Int. Symposium on Roller Compacted Concrete Dams, Volume I: Materials, Planning and Design*, pages 309–323. Santander, Spain.

Hirose, T., Nagayama, I., Takemura, K., and Sato, H. (1988). A study on control temperature cracks in large roller compacted concrete dams. In ICOLD, editor, *Proceedings of XVI Congress on Large Dams*, volume 3, pages 119–135, San Francisco.

Lorenzo, A. C. and Calivari, S. C. (1991). Behavior of urugua-í dam. In Hansen, K. D. and McLean, F. G., editors, *Proceedings of ASCE Specialty Conference on Roller Compacted Concrete 3*, pages 272–290, San Diego.

Widmann, R. (1985). How to avoid thermal cracking of mass concrete. In ICOLD, editor, *Proceedings of XV Congress on Large Dams*, volume 2, pages 263–277, Lausanne.

APPENDIX II. NOTATION

The following symbols are used in this paper:

$\boldsymbol{D}, \overline{\boldsymbol{D}}$ = Constitutive tensor; Normalized *idem*
E, E_∞ = Elastic modulus, Final elastic modulus;
E^i = Elastic Modulus for Maxwell element i;
$f^\pm, f^\pm_\infty$ = Tensile/compressive strength, Final values;
$f^\pm_e$ = Elastic limit in uniaxial tests (tension/compression);
$G^+_{f\infty}$ = Final Tensile fracture energy;
$\boldsymbol{p}_j$ = Unit vector associated with principal direction j;
T, T_0 = Temperature, Initial temperature;
T_{ref} = Reference temperature;
w/c = Water/cement mass ratio;
α_T, α_ξ = Thermal and chemical expansion coefficients;
$\boldsymbol{\varepsilon}, \boldsymbol{\varepsilon}_e$ = Strain tensor, Elastic strain tensor;
$\boldsymbol{\varepsilon}^i_e, \boldsymbol{\varepsilon}^i$ = Elastic, Viscous strain tensor for Maxwell element i;
$\boldsymbol{\varepsilon}_T, \boldsymbol{\varepsilon}_\xi$ = Thermal strain tensor, Chemical strain tensor;
κ = Aging degree;
λ_E = Elastic modulus aging function;
μ = Normalized micro-prestress;
ν = Poisson's ratio;
$\boldsymbol{\sigma}, \overline{\boldsymbol{\sigma}}$ = Stress tensor, Effective stress tensor;
$\bar{\sigma}_j$ = Principal effective stress value j;
τ^i = Relaxation time for Maxwell element i;
$\tau_\mu, \tau_{\mu 0}$ = Relaxation time associated to flow term, Initial value;
$\mathbf{1}$ = Unit (second order) tensor;
$\dot{(\,)}$ = Time derivative or rate;
$(\,)\otimes(\,)$ = Tensorial product;
$(\,):(\,)$ = Doubly contracted tensorial product; and
$< >$ = Macaulay brackets.